

出國報告（出國類別：進修）

赴美國邁阿密大學進修機械工程碩士 心得報告

服務機關：國防部軍備局生產製造中心第二〇二廠
姓名職稱：廖沂陞少校
派訓國家：美國
出國時間：110年8月13日至112年8月4日
報告日期：112年10月2日

摘要

本次進修奉國防部 110 年 8 月 3 日國人培育字第 1100170621 號令核定赴美國邁阿密大學 (Miami University) 進修機械工程碩士班。進修期程自 110 年 8 月 13 日至 112 年 8 月 12 日止，另因疫情影響修訂出國日期自 110 年 8 月 13 日至 110 年 8 月 25 日，在臺期間採視訊方式上課，並於 112 年 7 月 30 日完成全數課程，於臺灣時間 8 月 4 日返臺，並於當日返回原單位軍備局第二 0 二 廠報到，於國防部核定文令律定修業期限 8 月 12 日前回國，在學 2 年進修期間內取得碩士學位。

本案心得報告所述均屬於公開性質，未涉及機密資料，內容主要記述於美國進修 2 年期間之研究及學習心得，本報告概分為：目的、進修過程、心得與建議及參考資料來源等項次，碩士期間主要修業課目計「斷裂力學」、「熱傳學」、「動力系統控制」、「應用非線性動力學」、「高級振動學」、「工程分析」、「化學工程熱力學」、「概率論」、「數位信號處理」及「工程傳遞現象」等 10 門課目，研究項目為「通過可編成晶格結構制定機械行為」，該研究旨在理解不同晶格結構組成和配置之結構力學，通過計算模擬和實驗測試，進行不同晶格結構之設計，並研究其對於不同材料強度、剛性、彈性、塑性變形和破壞行為之影響，研究成果可用於優化現有裝備，以增強強度和剛性、提高防護力與抗衝擊力，並同時降低整體重量。

目錄

壹、目的.....	3
貳、進修過程.....	3
參、心得與建議.....	18
肆、參考資料.....	20
伍、附件.....	21

壹、目的

本次進修奉國防部 110 年 8 月 3 日國人培育字第 1100170621 號令核定赴美國邁阿密大學（Miami University）進修機械工程系碩士班。進修期程自 110 年 8 月 13 日至 112 年 8 月 12 日止，另因疫情影響修訂出國日期自 110 年 8 月 13 日至 110 年 8 月 25 日，在臺期間採視訊方式上課，並於 112 年 7 月 30 日完成全數課程，於臺灣時間 8 月 4 日返臺，並於當日返回原單位軍備局第二 0 二 廠報到，於國防部核定文令律定修業期限 8 月 12 日前回國，在學 2 年進修期間內取得碩士學位

本報告係依「行政院及所屬各機關出國報告綜合處理要點」相關規定撰擬，旨在提供進修經驗及論文研究心得予相關人員參考運用。

貳、進修過程

一、學校簡介

邁阿密大學（Miami University）位於美國俄亥俄州牛津（Oxford, Ohio），該校創立於西元 1809 年（如圖 1-2），為全美第十間公立學校，並為原始公立常春藤盟校（Original Public Ivies）之一，公立常春藤盟校係指學校豐富教育資源與環境可與常春藤盟校（Ivy League）匹敵，但學費卻僅為公立收費。此外，邁阿密大學坐落之城市，牛津，屬於大學城性質，其氣候舒適且四季分明，各式商鋪及店家大多是為了學校學生而設立，距離俄亥俄州第 3 大城市辛辛那提（Cincinnati）僅約一小時車程，整體生活機能完善，警力充沛、治安及風情純樸，除了本州居民為主的學生，更廣收各國國際學生，學術研究及學習氣氛良好。



圖 1. 美國邁阿密大學校徽



圖 2. 美國邁阿密大學校園

二、修業規定：

職進修系所為機械工程所（Mechanical Engineering - Master of Science），依邁阿密大學機械工程所律定之研究生畢業要求，主要區分為研究選項及課程強化選項等兩種修課方式取得碩士學位，對於為研究選項要求為須完成 32 學分（專業

課程至少 15 學分，選修課程至少 9 學分，研究生研討會至少 6 學分及研究學分至少 6 學分)，而課程強化選項則須完成 34 學分（專業課程至少 18 學分，選修課程至少 12 學分，研究生研討會至少 3 學分及研究學分至少 3 學分），兩者除修課外均須完成學術研究報告撰擬及通過口試方可獲取碩士學位

學業成績評等 GPA 區分由 A+至 F 等第，換算對應成績為 A+: 4.0、A: 4.0、A-: 3.7、B+: 3.3、B: 3.0、B-: 2.7、C+: 2.3、C: 2.0、C-: 1.7、D+: 1.3、D: 1.0、D-: 0.7、F: 0，其中研究生課業要求為每學期平均分數須高於 B（換算百分比分數約為 80/100）。

三、課程介紹

邁阿密大學機械工程所為幫助學生具備高水平機械工程之工程實踐能力，該學位課程方向主要為數學建模、動力系統控制、熱流體系統、材料力學和機械行為等核心課程，以及科學、工程和數學課程等周邊課程，學生可以各自研究及實際需求，依照修業規定之學分配額進行修課；另為加強自身英語能力，職於在學期間加選進階英語課程（2 學分）以強化自身學術寫作及口說能力，職最終修畢 36 學分、平均 GPA3.72（A-），相關修業課程摘述如后：

(一)進階英語課程

主要為銜接非英語母語國家之國際學生研究所所需之語言能力，該課程旨在強化學生對於學術文章之閱讀及強化學生對於學術研究演講之口說能力，透過每節課分組討論與寫作作業或定期報告等內容，培養學生具備學術文章撰擬及演說之能力。

(二)修業課程介紹

1、 斷裂力學 (Fracture Mechanics)

斷裂力學是一門研究材料斷裂行為的學科，該課程介紹了結構材料中存在裂紋時的力學。主要關注線性彈性斷裂力學 (LEFM)，包括能量釋放率、裂紋阻力、裂紋穩定性/不穩定性和斷裂韌性測試等主題。強調理論和應用問題解決，具有材料工程的視角。該課程還介紹了非線性斷裂力學的基礎，包括彈塑性斷裂力學 (EPFM) 和時間依賴斷裂力學 (TDFM) 的概念。這些主題包括 J 積分、J-阻力曲線、C*積分和 C_t 等。通過學習斷裂力學，可深入了解材料的斷裂行為，於研發及優化系統時，需確保所使用的材料能夠承受高壓力和振動負載，同時保持其完整性和可靠性，以預測和防止潛在斷裂問題。

2、 熱傳學 (Heat Transfer)

該課強調熱傳遞的作用，學習穩態和非穩態傳導，以及層流、紊流、沸騰和冷凝對流熱傳。還包括輻射熱傳、熱交換器、蒸發器和傳熱單元的研究。藉由了解熱傳遞原理可以幫助優化系統散熱設計，確保其在高溫環境下穩定運行。同時，熱傳遞亦對於冷卻系統設計至關重要，以確保系統在長時間使用時不會過熱

3、 動力系統控制 (Control of Dynamic Systems)

動力系統控制是一門研究如何控制和調節具有時間變化之系統，該課程深入研究動態系統的反饋控制的理論、設計和分析。將電路和計算機輔助實驗的問題解決技術和概念融入到可編程邏輯控制系統的設計和構建中，並應用於現代製造系統中。課程中亦介紹實驗室練習和短期設計項目中應用的設

計方法論。透過學習動態系統控制，可以了解如何開發出先進的控制算法和策略，以提高系統的準確性、穩定性和響應能力。

非線性動力學主要是研究非線性系統行為，該課程研究動態系統的非線性動力學，並應用相關的一維和二維流動/映射、分岔、相平面動力學、穩定性和控制。課程中將運用物理學、生物學、化學和工程學等領域的應用案例。對於較極端環境之系統所產生之機械行為均為非線性行為，如振動、共振、非線性反饋，學習應用非線性動力學可以幫助理解和預測這些系統的複雜行為，並開發出更有效之控制和設計策略，這對於提高系統穩定性、安全性和性能非常重要，可更容易理解及控制系統，並提高其性能和可靠性。

4、高級振動學（Advanced Vibration）

該課程探討振動及其應用中的高級研究和計算主題。主題包括離散和連續振動系統的建模和響應、主動和被動振動控制、估計振動系統響應的計算方法，以及振動領域的研究問題，裝備系統振動問題是需要關注和解決之重要課題。透過學習高級振動學，使我們能夠研究和分析系統振動行為，預測和減少振動引起的損壞及疲勞，並開發有效振動控制策略，這對於提高系統之精確度、耐久性和運行穩定性至關重要。

5、工程分析（Engineering Analysis）

工程分析課程涉及化學工程和機械工程相關系統之數學模型構建和解決應用問題之分析考慮，分析方法將包括穩態和非穩態狀態工程問題的建模。透過工程分析，可於生產和研發過程中使用數學和科學方法來評估和預測兵器系統性能、可靠性和安全性。這包括使用數值模擬和仿真技術，分析和優

化系統的結構、材料、力學行為和性能，工程分析知應用能夠幫助制定更好的設計和製造決策，從而提高系統效能及品質。

6、化學工程熱力學（Chemical Engineering Thermodynamics）

化學工程熱力學為研究能量轉換和傳遞之學科，該課程以相和化學平衡為重點，進階研究熱力學關係和應用，研究理想和非理想單成分和多成分系統之性質，其包含理想和非理想相平衡、相圖、平衡閃蒸分離器之設計，使用狀態方程研究相平衡，研究化學平衡，以及可行反應平衡之最佳條件。於系統開發方面具有廣泛應用，對於製造和研發系統時，需要深入了解熱力學原理，以確保燃燒和能量傳輸的有效性和效率。透過學習該課程，可優化能源系統設計，提高燃燒效率、節能減排，同時確保系統可持續運行。

7、概率論（Probability）

該課程重點介紹概率理論發展，並強調概率如何與統計推斷相關。主題包括基礎概率、計數規則、貝葉斯定理、分佈函數、隨機變量和隨機變量函數期望值和變異數、動差生成函數、動差、特殊隨機變量概率模型、聯合分布、最大概然估計、無偏性、隨機變量函數分布、卡方分布、T 分布、F 分布及樣本均值和變異數抽樣分布等，於生產和研發過程中，概率論應用是為了評估和預測不確定性事件發生概率。系統運作涉及到多種因素和變數，包括材料性能、工程參數、環境條件等等。通過學習概率論，可以用統計方法來分析不確定因素，並進行風險評估和可靠性分析。這有助於制定有效風險管理策略，確保系統在各種條件下正常運行和安全性。

8、數位信號處理（Digital Signal Processing）

該課程旨在探討連續時間和離散時間信號之間的關係以及離散時間信號的處理。主題包括取樣理論、信號表示、量化噪聲、數字信號的轉換和處理及數字濾波器結構和設計等。數位信號處理在可應用於機電整合類系統的感測、信號處理和通信方面。透過該課程，可研究和開發數位信號處理技術，以提取和分析感測器收集數位信號，並進行數據壓縮、篩選、增強和分析。這對於改善系統感知能力、數據處理效率和通信可靠性至關重要。

9、工程傳遞現象（Transport Phenomena in Engineering）

該課程主要探討熱量、物質和動量傳遞的原理和機制，發展廣義的傳遞方程式、宏觀和微觀平衡及熱量和物質同時傳遞，並包括質量、熱量和動量傳遞間之類比關係，工程中的傳輸現象涉及到物質、能量和動量於系統中之傳輸和轉移，這包括了流體力學、熱傳學和質傳學等領域應用。透過學習該課程，可深入了解系統流體流動、熱傳導和質量傳輸過程，從而優化設計和性能，對於改進裝備系統之冷卻能力、燃料供應和液體噴射等方面至關重要。

四、研究內容

(一)導論（Introduction）

晶格結構（Lattice Structure）是一種由相互連接的支撐構件定義的細胞結構類型，其創建了多孔結構，由於其輕量及高強度的特性，近年在多個領域引起廣泛關注，借助積層製造（Additive Manufacturing）技術，晶格結構可高效地設計和製造，通過不同的設計，其可展現截然不同的特性及特點，比如改善強度重量比、高能量吸收能力及熱膨脹縮小等，此外，晶格結構允許依照使用者需求進行定制，以符合實際設計或使用需求。儘管晶格結構具有顯

著的機械特性，囿於其生產難度高及複雜的結構，且不同的幾何形狀及材料均會大幅影響最終的機械行為，最大的挑戰在於結構需在保持輕量化同時具備相應強度，這一設計及測試過程相當耗費時間及成本，導致其迄今仍難以被廣泛的量產應用。

目前對於晶格結構準確預測機械行為和行為存在幾個挑戰，其中一個主要挑戰是其複雜的幾何形狀，傳統的模擬難以建模且機械性質難以預測，晶格結構的行為可能高度非線性，難以預測其對不同加載條件的響應，且晶格結構的機械性質高度依賴於組成材料和製造過程，這會導致最終機械性質的顯著差異。另一個挑戰是晶格結構通常是根據特定性能（如剛度、強度或能量吸收）設計，這使得難以比較不同設計結果，且該結構製造過程具有高度變化性，導致幾何形狀、孔隙率和其他基本性質的差異。對於晶格結構，現有方法無法完全預測不同材料在不同條件下的複雜行為，且晶格結構通常用於較大變形或極端加載條件下的應用，這會進一步複雜其行為，這些問題使得將晶格結構應用到主流製造流程中變得困難。透過不同材料和不同幾何形狀晶格結構的模擬及實驗，實現優化結構設計之過程，這將使設計過程變得較不耗時和嚴苛，並使其更易應用於常見產品。另外，制定晶格結構的標準測試方法和設計指南將有助於確保其品質和可靠性，並使開發者更容易採用該技術。因此，研究晶格結構的基本性質並制定標準化協議對於應用到主流製造流程中至關重要，最終將帶來改善的產品性能和成本效益。此研究旨在通過各種方式，包括獲取實驗數據、編程機械行為、促進更廣泛的接受以及推動標準化，為晶格結構的發展和應用作出貢獻。透過探索及建立晶格結構

的基本性質可以促進其廣泛應用到主流製造流程中。

(二)晶格結構設計及材料 (Lattice Structure Designing and Materials)

1、晶格結構設計

晶格結構係透過基本單元細胞結構所組成，本研究主要使用三種基本單元細胞結構，分別為十字立方體 (Cross-Cubic)、體心立方體 (Body-Centered Cubic) 及八面立方體 (Octahedron)，及四種由前述三種單元細胞結構所衍生之複雜結構 (如圖 3)，組成 20 mm * 20 mm * 20 mm 之晶格結構 (如圖 4)，並透過 2 種不同的內部結構柱尺寸 (1 mm 及 2 mm，如圖 5-6) 及 4 種不同的材料，獲取晶格結構於不同條件下之機械性質；另外，對於模擬及實驗所需之樣品，均採用電腦輔助設計軟體 (CAD) Fusion 360 進行設計及建模作業。

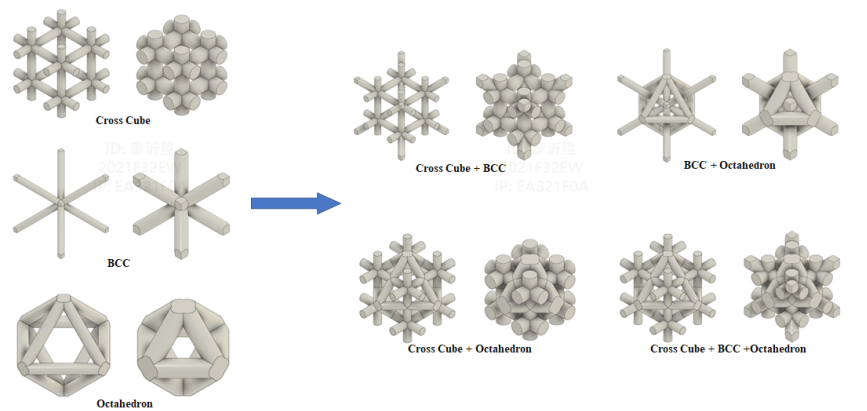


圖 3. 基本單元細胞結構示意圖

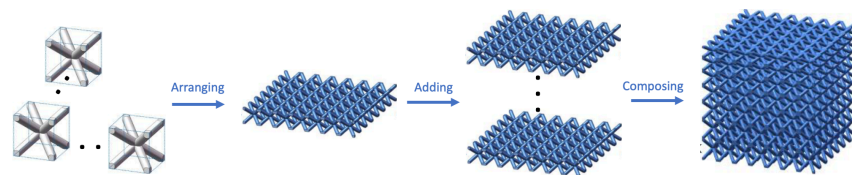


圖 4. 晶格結構組成示意圖

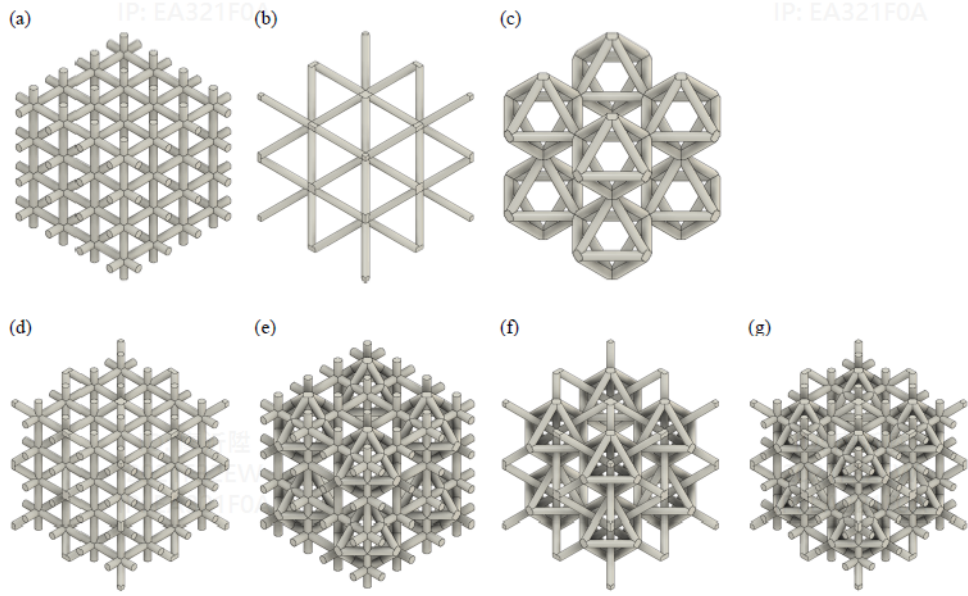


圖 5. 1mm 結構柱之晶格結構：
 (a) 十字立方體, (b) 體心立方體, (c) 八面立方體,
 (d) 十字立方體+體心立方體, (e) 十字立方體+八面立方體,
 (f) 體心立方體+八面立方體, (g) 十字立方體+體心立方體+八面立方體

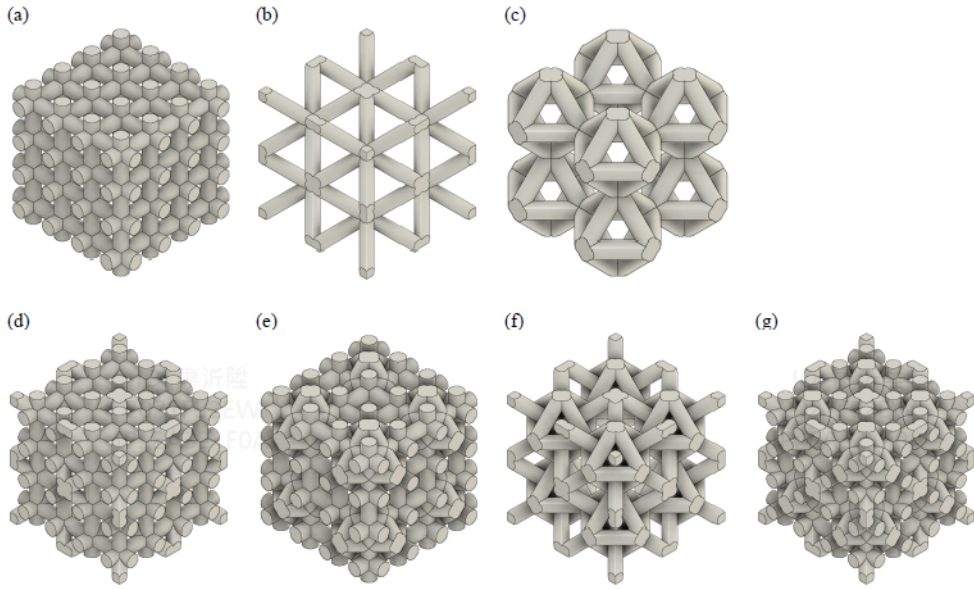


圖 6. 2mm 結構柱之晶格結構：
 (a) 十字立方體, (b) 體心立方體, (c) 八面立方體,
 (d) 十字立方體+體心立方體, (e) 十字立方體+八面立方體,
 (f) 體心立方體+八面立方體, (g) 十字立方體+體心立方體+八面立方體

2、材料選用

因應不同的積層製造方式，分別選用聚乳酸（Poly Lactic Acid, PLA）、熱塑性聚氨酯（Thermoplastic Polyurethane, TPU）及兩種光敏液體聚合物（Grey resin and Elastic 50A resin）等 4 種材料進行樣品製造，不同的材料之特性、使用方式及應用領域均有所不同，聚乳酸是可再生、可生物降解且環保的聚合物，多被應用於生物醫學和包裝等各個領域，熱塑性聚氨酯為一種熱塑性彈性體，以其卓越的韌性、柔軟性和耐用性而著稱，適用於運動器材、鞋類和醫療器械等應用，而光敏液體聚合物是用於立體光固化的一種樹脂，由於能夠在紫外線照射下固化，該樹脂相對於傳統的原材料具有一系列優勢，例如能夠以高精度和精確度製造複雜的幾何形狀。光敏液體聚合物樹脂的潛在應用範圍廣泛多樣，從陶瓷到多層結構複合材料都可使用。

(三)模擬及實驗方法（Simulation and Experiment Methods）

靜態應力模擬，也稱為靜態分析，是一種模擬方法，它確定了在給定載荷或一組載荷下結構的應力和變形。Fusion 360 的靜態應力模擬利用有限元分析（FEA）算法將結構分解為較小的元素，然後分析這些元素在施加载荷下的形變和應力。模擬結果提供了對結構行為的全面了解，可以用來識別潛在的故障點，優化設計以提高強度和減輕重量，並改善整體性能。Fusion 360 的靜態應力模擬軟體所需參數計有楊氏模數（Young's Modulus）、泊松比（Poisson's Ratio）、剪切模數（Shear Modulus）、密度（Density）、屈服強度（Yield Strength）和抗拉強度（Tensile Strength）等，然而，這些參數可能會根據各種因素而變化，例如生產方法、強化後處理，以及不同品牌型號材料

等均會影響，此外，有限元分析（FEA）中的靜態應力模擬所獲得的線性結果是基於受分析的試件為均勻完美材料的假設，因此在載荷下呈線性行為並遵循虎克定律（Hooke's Law），材料所受應力的大小與它所經歷的應變量成正比，從而產生線性應力-應變（Stress-Strain）關係。此一模擬結果雖可以用來預測材料在不同載荷條件下的行為，但如果所施加的載荷足夠大，以至於引起塑性變形或屈服，那麼線性假設就不再適用，必須通過實驗來確定塑性極限，以進行更準確的分析。

為進一步獲得實際機械行為及塑性極限，INSTRON 5867 被用來執行壓縮測試，該機器具有最大軸向負荷能力為 30 千牛頓，其操作由一個控制器和一台配備軟件的計算機管理，以提供系統的完全控制，在測試過程中可以實現載荷或位移控制，在測試過程中，樣本受到恆定的壓縮位移速率 0.15 mm/s 的作用，並同時記錄載荷活塞的位置，直到樣本完全破裂或壓縮達到 15mm 為止；此外，因測試試件係採用積層製造方式製作，與模擬時不同，需另行考慮積層方向與受力方向（垂直或水平），故實際測試時需依一併測試不同積層方向之機械行為。

(四)模擬及實驗結果（Simulation and Experiment Results）

在模擬壓縮測試中，目標是確定材料在受到壓縮載荷下的行為。該測試通常涉及對材料施加壓縮力，直到它變形或破裂。為了模擬這個測試，鋁板模組被添加到測試模型的頂部和底部表面，以模擬壓縮測試機的測試夾具，這個設置是為了模擬能夠對上部鋁板施加壓縮力並測量受測材料變形的壓縮測試機，且下部鋁板固定在原地，以防止在測試過程中出現任何移動。如圖

7 所示，靜態應力模擬的線性結果的斜率表示被分析材料的剛度或彈性模量，這是衡量材料在給定載荷下會形變多少的重要參數，可用來設計和優化工程結構，以達到最大的強度和可靠性。

而壓縮測試是材料科學和工程中常用的一種方法，用於評估試樣在壓縮載荷下的機械行為。該測試涉及對試樣施加壓縮力，直到它變形或失效，以分析試樣對不同壓縮載荷的反應。測試過程中試樣的機械行為有助於了解其性能，如強度、剛度和變形特性，並確定其適用於各種應用和行業標準的程度。如圖 8 所示，在壓縮測試過程中，試樣通常會經歷彈性變形、屈服、塑性變形和斷裂等階段。在彈性變形階段，應力-應變曲線預期將大致呈線性，遵循虎克定律，直到達到屈服點。屈服點標誌著從彈性到塑性變形的過渡，這是材料在永久變形發生之前能夠承受的最大應力的關鍵性質。隨著材料受到越來越高的壓縮載荷，屈服階段中，它開始表現出可逆的塑性變形，不再遵循虎克定律，應力-應變曲線開始彎曲，並在某一負荷下平穩，這就是屈服強度。之後，隨著負荷繼續增加，材料開始經歷不可逆的塑性變形，負荷-延伸曲線進入塑性變形階段。在塑性變形階段，材料經歷顯著的變形，應力-應變曲線是非線性的，此時材料繼續變形，直到最終失效或緻密化發生。

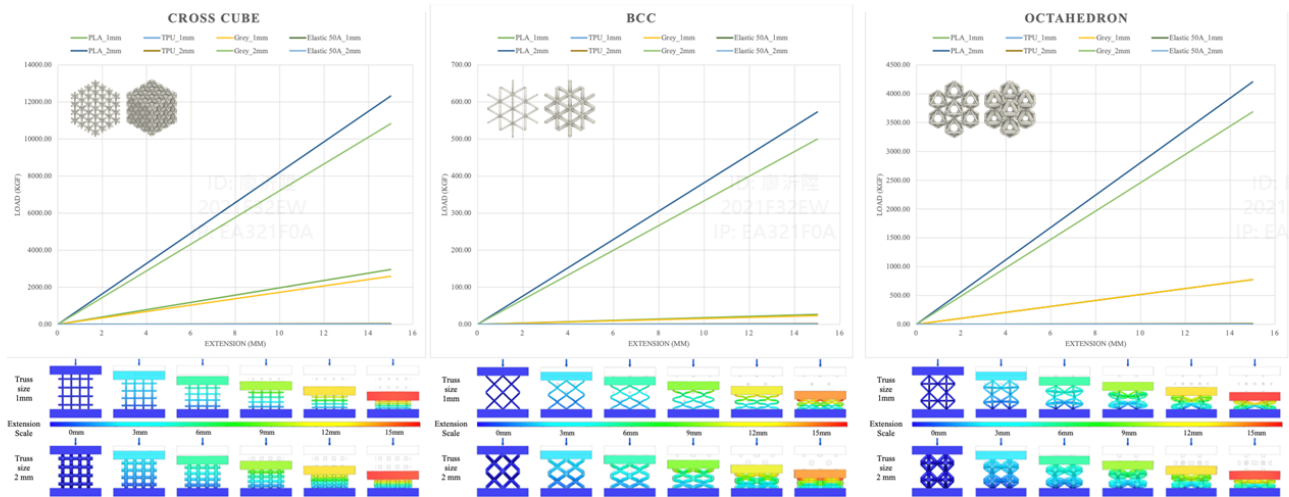


圖 7. 模擬結果示意圖

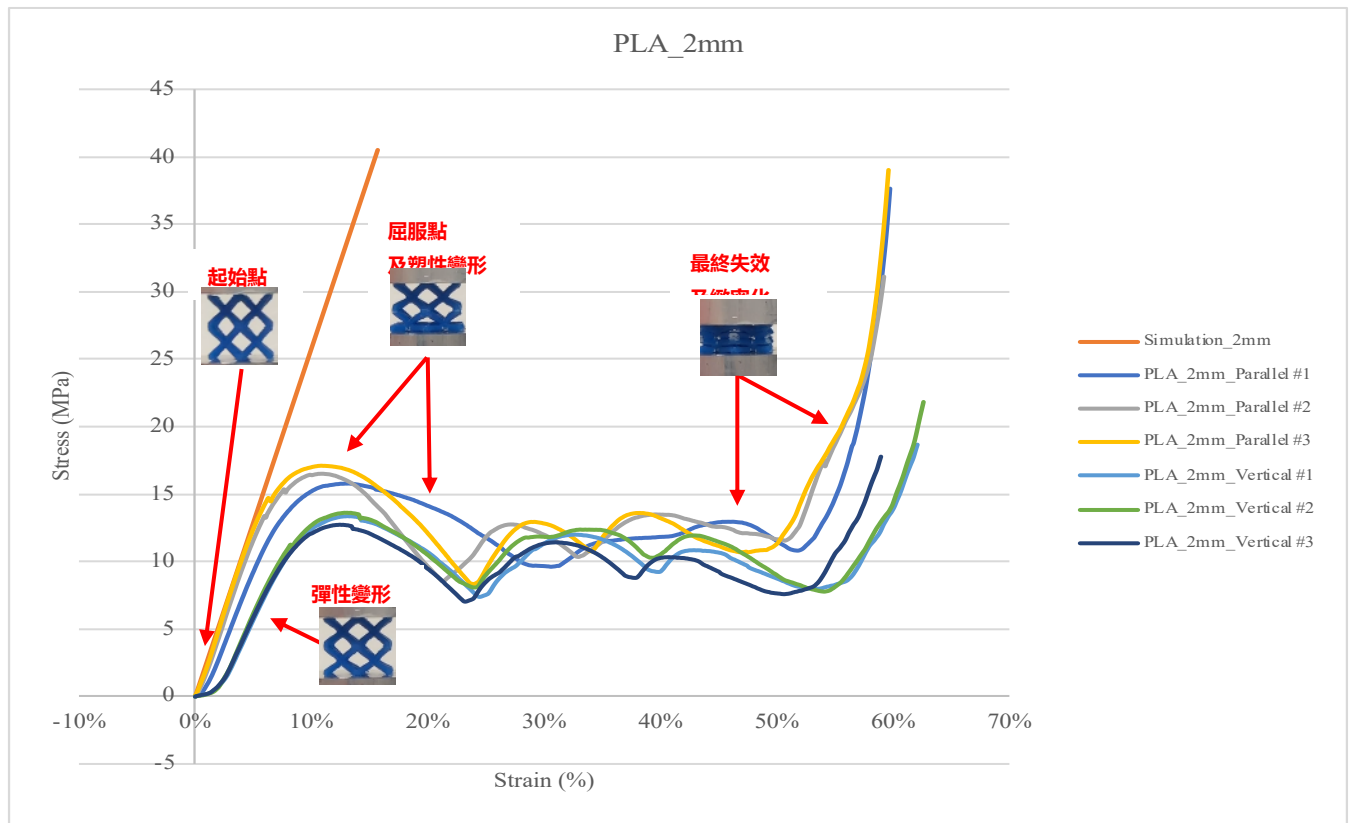


圖 8. 實驗結果示意圖

(五)研究成果及未來規劃 (Conclusion and Future Work)

晶格結構研究和積層製造技術方面的進展已經促成了具有卓越機械性能的輕量結構開發，通過不同材料、密度及各種晶格結構設計的實驗數據，並根據獲得的數據編程其機械行為，以進一步發展晶格結構。此外，了解晶格結構的基本性質對於建立標準化協議非常重要，可有效促進晶格結構融入主流製造流程。通過優化晶格結構的設計，實現極限強度並最小化重量，可以將此技術應用於各種行業和應用中。然而，在晶格結構研究領域仍有很多需要探索的地方。未來的工作可以包括進一步研究在不同條件下不同結構配置的單層響應，並使用有限元分析來獲得有關各式晶格結構在使用過程中所受之應力和應變，並使用這些數據來編程晶格結構並制定機械行為，以及用於創建它們的材料特性。另外，亦可以涉及使用先進材料，如納米材料、複合材料和 3D 列印金屬，創建具有更優機械性能的晶格結構。而另一個重要研究方向則是開發一個全面的晶格結構性能和行為特徵數據庫，透過進一步研究在不同條件下各種結構的響應，使用數據來編程所需結構，以及製造它們的材料特性，藉此析結果並用於反向工程設計，這種方法可以創建更高效和更有效的結構，更好地滿足各種行業的需求。

總之，儘管在晶格結構研究和開發方面取得了進展，但仍有許多領域需要進一步研究。通過持續探索新材料、應用和設計方法，可以發掘該領域更大的潛力，為輕量高性能結構的新一代鋪平道路。

參、心得與建議

一、自主研究學習及自我意見表達能力

美國的教育體制和文化背景在學習上較為自由，主要講求學生在開放自由的環境下自我學習，學生須自主自發性地學習及研究，美國教育宗旨是希望學生具備自主性學習、思考及研究能力，並在遭遇困難時了解如何提出問題，藉此訓練獨立思考及溝通能力。此外，學生除本職學能外，亦須懂得團隊合作，許多課程均須要求學生與其它組員研討互動，並將各自負責的研究領域進行整合，共同合作以發表專題報告。另外，於實作課程及研究中，學生會被要求上台簡報，並表達對於問題的想法，及如何克服所遇到的難關。在討論過程中，教授及台下學生均相當重視個人意見的表達，美國教育不鼓勵一味接受指導，而是希望學生能夠提出質疑，並勇於發言、積極互動

二、嚴格教育規定及良好學習風氣

美國在課業方面，十分注重誠實，無論是作業、報告或是研究論文，對於「考試舞弊」或「抄襲」為零容忍。在課業上，教授均鼓勵同學間相互討論並合作，但須獨立完成各自作業，每一次線上繳交作業，均會經過第三方軟體查驗抄襲率，如果抄襲率偏高即視為抄襲。然而，雖然在教育規定上較為嚴謹，但為了營造方便學生學習的環境，除了圖書館 24 小時開放外，在校園各個角落，不論是室內或是室外，均隨處設有適合三五好友即時做為課業討論的區域，此外，研究生有專用討論室及閱覽室，在與指導教授做研究期間，指導教授會從自己教導的大學班級中，邀請對該研究領域有興趣的大學部學生，共同參與研究討論，透過彼此間的腦力激盪，共同成長，且經瞭解這些大學生參與研究通常是出自於興趣，

而非取得學分或僅僅是完成教授交付的任務，這種學習及研究的熱忱可以有效地帶動整體風氣。

三、獨立生活能力及多元文化發展

抵達新環境，首當其衝的挑戰就是生活起居的適應及不同國家法律規定及文化的不同，在食宿方面，東西方口味及租屋合約規定的不同，都有著各式各樣的文化差異，在交通方面，除換取美國駕照外，亦要適應並了解交通法規及如何訪價及買車，雖現在網路發達，多數資訊均可於出國前確認，但仍然有許多狀況需要去克服。此外，透過結交異國他鄉的朋友，可以更加深入瞭解不同的文化背景，了解不同國家間學生的學習方法、飲食起居及文化的差異，並且可以借助不同國家學生之間的長處團隊合作、並肩作戰，有不明白的課業都可以一起討論，有效提升對學習效率。

四、英文能力改善及語文能力深化

對於出國進修而言，托福考試分數必須達到要求方可申請美國學校，雖順利通過考試，然而實際應用是完全不同的情況，在與人溝通上，仍然需要學習如何有效地與同學及教授溝通；此外，除聽與說的能力外，對於學術文章的撰擬及閱讀，僅通過托福的鍛鍊是遠遠不足的，透過沉浸在學術環境中，更能深化專業文章的文法及學術文字運用的能力。綜觀世界各個語言，英語仍是最強勢且最普遍的語言，因此，透過出國進修的時機，利用課後機會努力與教授、同儕甚至是路人或店員進行交流，強化語言能力，在國外學習對於語文能力提升非常迅速，故鼓勵有想進修的同仁努力爭取出國機會，以持衡提升本國專業素養。

肆、參考資料

- 1、邁阿密大學，<https://miamioh.edu>
- 2、維基百科，<http://wikipedia>
- 3、C. Pan, Y. Han, and J. Lu, “Design and optimization of lattice structures: A review,” *Applied Sciences (Switzerland)*, vol. 10, no. 18. MDPI AG, pp. 1–36, Sep. 02, 2020. doi:10.3390/APP10186374.
- 4、A. Seharing, A. H. Azman, and S. Abdullah, “A review on integration of lightweight gradient lattice structures in additive manufacturing parts,” *Advances in Mechanical Engineering*, vol. 12, no. 6. SAGE Publications Inc., Jun. 01, 2020. doi: 10.1177/1687814020916951.
- 5、B. K. Nagesha, V. Dhinakaran, M. Varsha Shree, K. P. Manoj Kumar, D. Chalawadi, and T. Sathish, “Review on characterization and impacts of the lattice structure in additive manufacturing,” in *Materials Today: Proceedings*, Elsevier Ltd, 2020, pp. 916–919. doi: 10.1016/j.matpr.2019.08.158.
- 6、E. Castro-Aguirre, F. Iniguez-Franco, H. Samsudin, X. Fang, and R. Auras, “Poly (lactic acid) —Mass production, processing, industrial applications, and end of life,” *Advanced Drug Delivery Reviews*, vol. 107. Elsevier B.V., pp. 333–366, Dec. 15, 2016. doi: 10.1016/j.addr.2016.03.010.
- 7、S. Farah, D. G. Anderson, and R. Langer, “Physical and mechanical properties of PLA, and their functions in widespread applications — A comprehensive review,” *Advanced Drug Delivery Reviews*, vol. 107. Elsevier B.V., pp. 367–392, Dec. 15, 2016. doi: 10.1016/j.addr.2016.06.012.
- 8、Z. Li, D. Feng, B. Li, D. Xie, and Y. Mei, “FDM printed MXene/MnFe₂O₄/MWCNTs

reinforced TPU composites with 3D Voronoi structure for sensor and electromagnetic shielding applications,” Compos Sci Technol, vol. 231, Jan. 2023, doi: 10.1016/j.compscitech.2022.109803

伍、附件

- 1、研究報告
- 2、學位證書

TAILORING MECHANICAL BEHAVIORS THROUGH PROGRAMMABLE LATTICE

Research Report

Submitted By
Yi-Sheng Liao

DEPARTMENT OF MECHANICAL AND
MANUFACTURING ENGINEERING



MIAMI UNIVERSITY

COLLEGE OF ENGINEERING AND COMPUTING

Oxford, Ohio, 45056

Abstract

Lattice structures, which are composed of periodic unit cells, have gained prominence due to their superior mechanical performance and properties, such as high strength-to-weight ratio, energy absorption, and vibration resistance. In recent years, they have been widely used in various fields, including aerospace, bio-industrial, and automation. With the development of additive manufacturing technology, more complex shapes and architectures of test products and prototypes can be manufactured to fabricate end-user products. Currently, lattice structure performance analysis is typically carried out using finite element analysis (FEA) or computational fluid dynamics (CFD) software, which simulate the behavior of the lattice structure under linear loading condition. However, these simulations provide few insights into the structural integrity, deformation, and failure modes, specifically under nonlinear loading condition.

This proposed study evaluates the mechanical properties of lattice structures made from various materials and scales off truss through simulation and experimental data, while emphasizing the need to research fundamental properties and standardize manufacturing protocols. The study also highlights opportunities and challenges for lattice structures in different industries and emphasizes the need to understand their potential applications and limitations. Through using three basic structures and four structures composed of three basic structures to analyze the relationship among the structures. These seven structures tested are BCC, Octahedron, Cross-cube, two structures composed of BCC and Octahedron, two structures composed of BCC and Cross-cube, and one structure composed of Octahedron and Cross-cube. Overall, the presented tool for analyzing and understanding the lattice structure performance is essential for optimizing lattice structure design, reducing design and production costs, improving product quality, and fostering innovation in the field of additive manufacturing.

However, there is still much to be explored in the field of lattice structures research, and future work can involve further research into the behavior of individual layers under various conditions, exploring the use of advanced materials, and developing a database of lattice structures properties and performance characteristics. Ultimately, continuing research in lattice structures can unlock even greater potential for this technology and pave the way for a new generation of lightweight and high-performance structures.

Table of Contents

1	INTRODUCTION.....	1
1.1	BACKGROUND.....	1
1.2	RESEARCH MOTIVATION.....	3
1.2.1	<i>Literature Review</i>	4
1.3	CONTRIBUTIONS OF THIS WORK.....	6
1.4	ORGANIZATION OF THIS REPORT.....	7
2	EXPERIMENTAL METHODS	7
2.1	LATTICE STRUCTURE DESIGNING.....	7
2.2	FABRICATING AND MATERIALS.....	12
2.2.1	<i>3D Printer</i>	12
2.2.2	<i>Materials of 3D Printing</i>	13
2.3	SIMULATION.....	15
2.4	COMPRESSION TEST.....	16
3	RESULT.....	17
3.1	SIMULATION RESULT.....	17
3.2	COMPRESSION TEST RESULT.....	26
4	DISCUSSION	63
4.1	MECHANICAL BEHAVIOR OF LATTICE STRUCTURE.....	63
4.1.1	<i>PLA</i>	63
4.1.2	<i>TPU</i>	69
4.1.3	<i>Grey Resin</i>	74
4.1.4	<i>Elastic 50A Resin</i>	78
4.2	POTENTIAL APPLICATIONS OF PROGRAMING LATTICE STRUCTURE.....	82
5	CONCLUSION AND FUTURE WORK	83
6	REFERENCE.....	85

List of Tables

Table 1 Methodologies of Predicting the mechanical properties.....	6
Table 2 Printing parameters of FDM printer	14
Table 3 Printing parameters of SLA printer	15
Table 4 Model Volume	15
Table 5 Mechanical and Strength properties of materials	16
Table 6 Load-Extension Results of Simulation	24
Table 7 Ratio of decreasing volume of Composed Lattice Structure	24
Table 8 Ratio of Load-Extension changing of Composed Lattice Structure	25
Table 9 Ratio of increased Volume and Load-Extension from truss diameter 1mm to 2mm	25
Table 10 The maximum stress and strain data of LS in PLA	66
Table 11 The maximum stress and strain data of LS in TPU	71
Table 12 The maximum stress and strain data of LS in Grey Resin.....	75
Table 13 The maximum stress and strain data of LS in Elastic 50A Resin.....	79

List of Figures

Figure 1 Examples of lightweight geometry while maintaining a high-functional with Lattice Structures	2
Figure 2 Manufacturing process of Subtractive Manufacturing	2
Figure 3 Manufacturing process of Additive Manufacturing	3
Figure 4 10mm cubic unit cell	8
Figure 5: 1mm truss CAD model.....	9
Figure 6: 2mm truss CAD model.....	10
Figure 7 Lattice Structure formed by unit cells	11
Figure 8 2*2*2 Lattice Structure with 1 mm truss CAD model.....	11
Figure 9 2*2*2 Lattice Structure with 2 mm truss CAD model.....	12
Figure 10 Additive Manufacturing	13
Figure 11 3D printer.....	13
Figure 12 INSTRON 5867 compression/tensile machine	17
Figure 13 Simulation Model	18
Figure 14 Pure Lattice Structure	19
Figure 15 Composed Lattice Structure	20
Figure 16 Cross Cube (PLA) - Compression Test and Simulation Results	29
Figure 17 Cross Cube (TPU) - Compression Test and Simulation Results	30
Figure 18 Cross Cube (Grey Resin) - Compression Test and Simulation Results	31
Figure 19 Cross Cube (Elastic 50A Resin) - Compression Test and Simulation Results.....	32
Figure 20 BCC (PLA) - Compression Test and Simulation Result.....	34
Figure 21 BCC (TPU) - Compression Test and Simulation Result.....	35
Figure 22 BCC (Grey Resin) - Compression Test and Simulation Result	36
Figure 23 BCC (Elastic 50A Resin) - Compression Test and Simulation Result.....	37
Figure 24 Octahedron (PLA) - Compression Test and Simulation Result	39
Figure 25 Octahedron (TPU) - Compression Test and Simulation Result	40
Figure 26 Octahedron (Grey Resin) - Compression Test and Simulation Result.....	41
Figure 27 Octahedron (Elastic 50A Resin) - Compression Test and Simulation Result.....	42
Figure 28 Cross Cube + BCC (PLA) - Compression Test and Simulation Results.....	44
Figure 29 Cross Cube + BCC (TPU) - Compression Test and Simulation Results.....	45
Figure 30 Cross Cube + BCC (Grey Resin) - Compression Test and Simulation Results	46
Figure 31 Cross Cube + BCC (Elastic 50A Resin) - Compression Test and Simulation Results	47
Figure 32 Cross Cube + Octahedron (PLA) - Compression Test and Simulation Results.....	49
Figure 33 Cross Cube + Octahedron (TPU) - Compression Test and Simulation Results.....	50
Figure 34 Cross Cube + Octahedron (Grey Resin) - Compression Test and Simulation Results	51
Figure 35 Cross Cube + Octahedron (Elastic 50A Resin) - Compression Test and Simulation Results.....	52
Figure 36 BCC + Octahedron (PLA) - Compression Test and Simulation Results	54
Figure 37 BCC + Octahedron (TPU) - Compression Test and Simulation Results	55
Figure 38 BCC + Octahedron (Grey Resin) - Compression Test and Simulation Results.....	56
Figure 39 BCC + Octahedron (Elastic 50A Resin) - Compression Test and Simulation Results	57
Figure 40 Cross Cube + BCC + Octahedron (PLA) - Compression Test and Simulation Results	59

Figure 41 Cross Cube + BCC + Octahedron (TPU) - Compression Test and Simulation Results	60
Figure 42 Cross Cube + BCC + Octahedron (Grey Resin) - Compression Test and Simulation Results.....	61
Figure 43 Cross Cube + BCC + Octahedron (Elastic 50A Resin) - Compression Test and Simulation Results	62
Figure 44 LS in PLA with 1mm truss diameter.....	67
Figure 45 LS in PLA with 2mm truss diameter.....	68
Figure 46 LS in TPU with 1mm truss diameter.....	72
Figure 47 LS in TPU with 1mm truss diameter.....	73
Figure 48 LS in Grey Resin with 1 mm truss diameter	76
Figure 49 LS in Grey Resin with 2 mm truss diameter	77
Figure 50 LS in Elastic 50A Resin with 1 mm truss diameter.....	80
Figure 51 LS in Elastic 50A Resin with 2 mm truss diameter.....	81
Figure 52 The process of selecting LS.....	82

1 Introduction

1.1 Background

Additive Manufacturing (AM), or 3D printing, is constructing three-dimensional objects by layering materials based on Computer-aided design (CAD). There are various technologies in the process of AM, including Fused Deposition Modeling (FDM), Stereolithography (SLA), Selective Laser Sintering (SLS), Digital Light Processing (DLP), Selective Laser Melting (SLM), and Electron-Beam Melting (EBM) [1], [2]. With the layer-by-layer process, AM enables the production of complex geometries and shapes that are impossible to achieve through traditional manufacturing methods such as lathe machines, milling machines, and CNC. [3]. Also, AM has the advantage of reducing lead times, as the digital design can be transferred directly to the manufacturing process, reducing the need for intermediate stages and tools. Additionally, AM eliminates the need for expensive tooling, making it a cost-effective option for small-batch production [2]. Another advantage of AM is its ability to produce lighter, more robust, and more sustainable products. This is achieved by creating internal structures and optimizing material usage, reducing waste and the environmental impact of production [3].

Lattice Structures (LS), a type of cellular structure defined by their interconnected pattern of struts that create a porous, have recently gained significant attention in various fields due to their combination of lightweight and high-strength properties. With the novel technology of AM, LS is efficiently designed and manufactured nowadays. Through different and unique designs, LS has many advantages, including improved strength-to-weight ratio, high energy absorption, and reduced thermal expansion compared to solid structures [4]. Also, LS allows for the integration of functional features and the tailoring of properties to specific requirements. For instance, they can be designed to have high stiffness [5].

Furthermore, using LS can help minimize material usage and reduce waste, making them an environmentally friendly alternative to traditional solid structures [6]. Because of their fabulous mechanical properties, LS is widely used in many applications, including aerospace, automotive, biomedical engineering, and energy industries. In aerospace, LS designs lightweight, high-strength components such as fuselages, wings, and thermal protection systems [5]. In the biomedical field, LS is used to design implantable medical devices due to their biocompatibility and ability to

conform to complex shapes [6]. With the ability to create complex and customized forms, along with their structural performance, LS can also be used to create unique and aesthetically pleasing architectural designs, which has led to an increased interest in using these structures in the field of architecture [7]. LS is also being explored for energy-absorbing applications, such as shock-absorbing systems, due to their high energy-absorption capacity [8]. The examples are shown in Fig. 1.

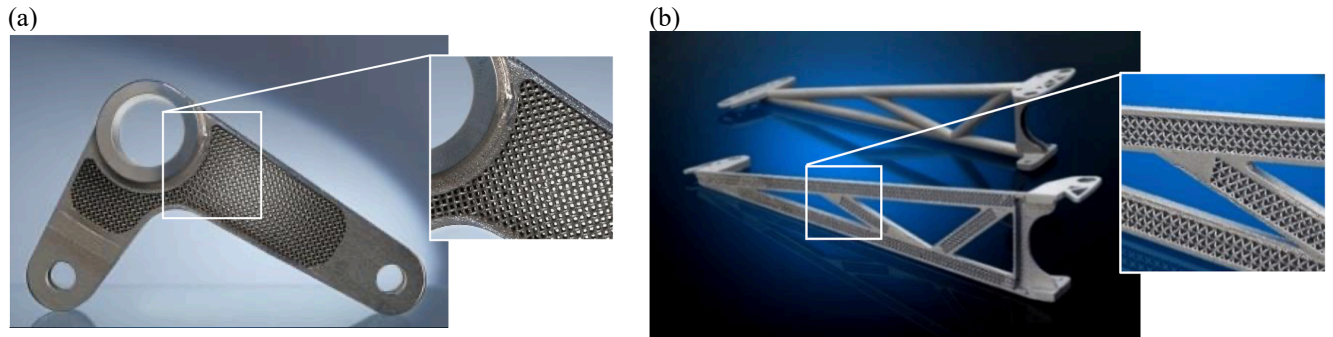


Figure 1 Examples of lightweight geometry while maintaining a high-functional with Lattice Structures: (a) Helicopter part of 316 stainless steel, (b) Control arm in the suspension system [9]

Traditional mechanical manufacturing is a type of subtractive manufacturing, which is a process that involves the removal of material from a larger block or piece of material to create a desired shape or product. The process involves using tools such as drills, lathes, mills, and routers to remove excess material until the desired shape is achieved. The process is shown in Figure 2. However, on the other hand, additive manufacturing technology is a process that involves building up material in layers to create a desired shape or product. This process involves using a computer-aided design (CAD) model, which controls the movements of a printer or other machine that deposits or solidifies material in a specific pattern [10], as shown in Figure 3. Because of the new processing technology of AM, complex structures such as LS that cannot be manufactured by traditional processing can also be easily manufactured.

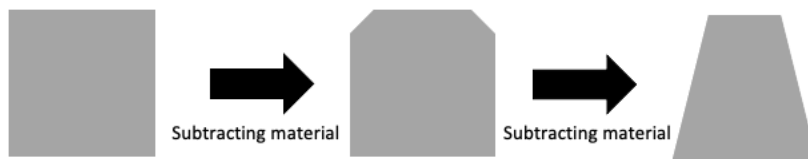


Figure 2 Manufacturing process of Subtractive Manufacturing

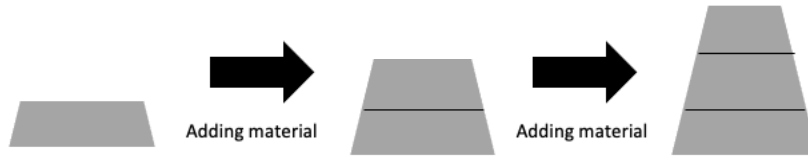


Figure 3 Manufacturing process of Additive Manufacturing

1.2 Research Motivation

Although LS has significant advantages, such as being lightweight and providing remarkable mechanical performance, additive manufacturing technology can also break through the bottleneck of manufacturing LS. However, because of the complexity of designing and producing these structures, products with LS fabricated by AM are still not widely used in most products and mass production and have prevented their widespread adoption in various industries. The printing process can result in issues such as layer-to-layer bonding and cracking, which can affect the final properties of the object [5], [6]. Furthermore, different geometries and materials with varying LS will exhibit vastly different mechanical behaviors. The challenge lies in optimizing the LS for maximum strength while keeping the weight low, presenting a demanding and time-consuming design process. Additionally, the high cost of AM equipment and the lack of standardization in the industry still pose significant challenges to widespread adoption and integration into mainstream manufacturing processes. [11]. This, in turn, affects the development and design of LS products, making it more challenging to apply to common products.

Research into the fundamental properties of LS and the development of standardization protocols are crucial for the advancement and broader adoption of LS in various industries. Currently, LS presents several challenges for accurately predicting their mechanical properties and behaviors. One of the main difficulties is their complex geometries, which can be challenging to model using conventional simulation techniques. Additionally, the behavior of LS can be highly nonlinear, making it difficult to predict their response to different loading conditions. The mechanical properties of LS are also highly dependent on the constituent materials and the manufacturing process used, which can result in significant variations in properties. Another challenge is that LS is often designed with specific performance criteria, such as stiffness, strength, or energy absorption, making it difficult to compare different designs or generalize results. Manufacturing processes for LS can be highly variable, leading to differences in geometry, porosity, and other fundamental properties that can affect the behavior of the final product. Testing methods for LS

are still in development, and existing methods may not fully capture the complex behavior of these materials under different loading conditions. In addition, LS is often used in applications where they experience large deformations or extreme loading conditions, which can further complicate their behavior and make it difficult to predict their performance. These issues make it difficult to integrate LS into mainstream manufacturing processes. By understanding the mechanical properties of LS made from different materials and with different geometries, it may be possible to optimize their design for maximum strength while keeping the weight low. This would make the design process less time-consuming and demanding and would make it easier to apply LS to common products. Developing standardized test methods and design guidelines for LS would help to ensure their quality and reliability and would make it easier for manufacturers to adopt this technology. Therefore, research into the basic properties of LS and the development of standardization protocols is necessary for the successful integration of LS into mainstream manufacturing processes, ultimately leading to improved product performance and cost-effectiveness.

1.2.1 Literature Review

LS has received significant attention in various engineering fields due to its exceptional mechanical properties, lightweight, and high strength-to-weight ratios. There are many studies on LS research and its potential applications. Cross Cubic LS is one of the LS that has been widely studied. Abusabir et al. (2022) conducted a study to examine how the use of architected structural members (ASMs) affects the viscoelastic behavior of cross-cubic liquid structures (LS). Their findings demonstrated that incorporating ASMs resulted in enhanced viscoelastic properties of the LS. The improved viscoelastic properties make it more suitable for applications requiring stability under dynamic loads[12]. Chen et al. (2023) studied the cross-shaped built-in LS and found that it improved the mechanical properties of CFST short columns after fire exposure. This makes it a promising solution for fire-resistant construction [13]. Ye et al. (2022) examined the effectiveness of square cross-sectional truss-based mesoscale lattice architectures for blast shock wave attenuation and found that the truss-based lattice architecture reduced the blast shock wave intensity, making it a potential solution for protection against blast loading in structures[14]. Moreover, Huang et al. (2017) studied the effect of a cross-sectional shape of struts on the mechanical properties of aluminum-based pyramidal LS and found that the mechanical properties

were significantly influenced by the cross-sectional shape of the struts, highlighting the importance of considering strut shape in the design of LS[15].

Another commonly studied LS is the Body-Centered Cubic (BCC) structure. These structures are particularly attractive in engineering applications because of their high strength and stiffness, as well as their ability to deform under compression without cracking while being lightweight and porous. Liu et al. found that the BCC LS had high mechanical performance, especially in terms of tensile and compressive strength, due to the node reinforcement provided by the struts [16]. Poyraz et al. conducted numerical investigations of the physical and elastic properties of 316L cubic LS fabricated by SLM and benchmarked the results against existing theories. The design optimization of BCC LS has also been addressed in recent studies[17]. Park et al. conducted a study to optimize the LS under compression and found that the unit cell type and arrangement played a crucial role in determining the mechanical performance of the LS[18].

Octahedron structures are another type of LS that has been widely studied in materials science, which is a unit cell of a three-dimensional LS consisting of eight equilateral triangular faces. One of the significant advantages of octahedral LS is its high strength-to-weight ratio. This feature is attributed to the efficient use of material and the structural hierarchy that provides significant mechanical stability. For instance, several studies have investigated the mechanical properties of octahedral LS [19]. The results showed the mechanical properties of the octahedral LS with varied parameters. Additionally, octahedral LS has a high degree of design flexibility, which makes it possible to tailor their mechanical properties based on specific requirements. K. M. Park et al. studied the effect of different unit cell types and cell arrangements on the compressive properties of octahedral LS[18]. The results showed that the unit cell type and cell arrangement significantly affect the compressive properties of the structure, providing a unique opportunity for optimizing the mechanical properties of octahedral LS. Another area of application for octahedral LS is biomedical engineering. Octahedral LS has the potential to be used as scaffolds for bone tissue engineering. The porous structure of the Octahedron provides an ideal environment for cell growth, and the mechanical properties of the structure can be octahedral unit cells[20]. Table 1 presents the methodologies for predicting the mechanical properties of LS.

Table 1 Methodologies of Predicting the mechanical properties

Methodology	Mechanical Properties
Finite element analysis [12] [13] [17] [19]	Compression strength, Yield stress, Energy absorption capacity, Young's modulus, Poisson's ratio, Fracture strain
Analytical relationships [20]	Young's modulus, Yield stress, Poisson's ratio, Fracture strain
Numerical investigations [17]	Young's modulus, Yield stress, Poisson's ratio

1.3 Contributions of this Work

This report aims to further understand and develop the LS, including:

1. Experimental data: The report presents empirical evidence regarding the load and extension of diverse LS designs made of various materials and sizes. The experimental data is juxtaposed with simulation results to facilitate the evaluation of the mechanical properties of these structures and provide valuable insight.
2. Programming mechanical behavior: The obtained data is utilized to program the mechanical behavior of LS, which can help increase their usage in specific industries and with appropriate LS and can facilitate their widespread adoption and utilization across various applications.
3. Advancing standardization: The report emphasizes the importance of research into the basic properties of LS and the development of standardization protocols, which can help ensure their quality and reliability and make it easier for manufacturers to adopt this technology. This contribution can ultimately lead to improved product performance and cost-effectiveness.

This study aims to contribute to the development and adoption of LS by means of various initiatives, including the acquisition of experimental data, programming of mechanical behavior, promotion of wider acceptance, and advancement of standardization. It emphasizes the necessity of exploring the fundamental properties of LS and establishing standardization protocols that can facilitate their widespread integration into mainstream manufacturing processes. The research also highlights the significance of comprehending the mechanical properties of LS, which are

dependent on the materials and geometries used and optimizing their design to achieve maximum strength while minimizing weight. Moreover, the study elucidates the challenges and opportunities that LS presents in different industries and underscores the importance of understanding their potential applications and limitations in order to leverage their full potential.

1.4 Organization of this Report

The structure of the report is designed to provide a comprehensive understanding of the research conducted. The report is organized as follows: Chapter 2 provides a detailed description of the experimental setup and procedure, including a discussion of the design of LS, the selection of materials, the printing method, and the process of the compression test. Moving on to Chapter 3, the results of the simulation and compression test are presented, offering valuable insights into the mechanical behavior and performance of the LS with different unit cell designs, materials, and truss diameters. Chapter 4 is dedicated to the discussion of the results and their potential application, providing a deeper understanding of the implications of the research. Finally, Chapter 5 concludes the report by providing an overview of the potential for future development and identifying areas for further research.

2 Experimental Methods

2.1 Lattice Structure Designing

Lattice structures (LS) are an exceptional type of cellular materials that demonstrate a remarkable level of organization, featuring a repetitive arrangement of unit cells. The mechanical behavior and performance of these structures are intrinsically linked to the design of the unit cell, which serves as the smallest repeating building block of an LS. In order to achieve maximum efficiency in the mechanical properties of LS, it is critical to meticulously evaluate the unit cell design, taking into account material selection and truss diameter. Given that LS composed of different materials and sizes possess varying mechanical behavior and performance, identifying and utilizing the most appropriate LS for specific applications is imperative.

The present study aims to delve into and introduce three essential unit cell designs, namely Cross Cubic, Body-Centered Cubic (BCC), and Octahedron. Moreover, the investigation of the mechanical behavior of diverse lattice structures featuring various materials and truss diameters is another focal point of this research. Additionally, this report puts forward four composite unit cell

designs that are generated by combining two or more basic unit cells, namely Cross Cubic + BCC, Cross Cubic + Octahedron, BCC + Octahedron, and Cross Cubic + BCC + Octahedron. These composite designs offer increased structural complexity and potentially enhanced mechanical performance. Each unit cell design is contained within a 10mm cubic unit cell featuring a truss diameter of either 1mm or 2mm, as depicted in Figure 4-6.

By employing this design approach, the study aims to provide a thorough analysis of how varying truss diameters affect the mechanical properties of LS. The unit cell and LS designs are created using Fusion 360, a widely adopted Computer-Aided Design (CAD) software that offers a versatile and intuitive set of design tools. This approach enables a comprehensive exploration of the design space and facilitates the creation of complex LS geometries with ease.

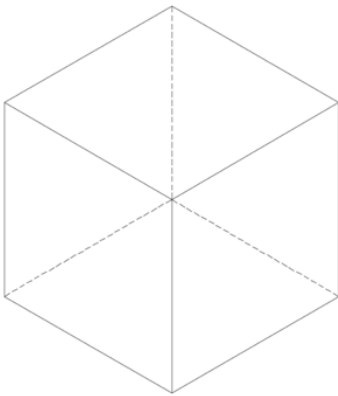


Figure 4 10mm cubic unit cell

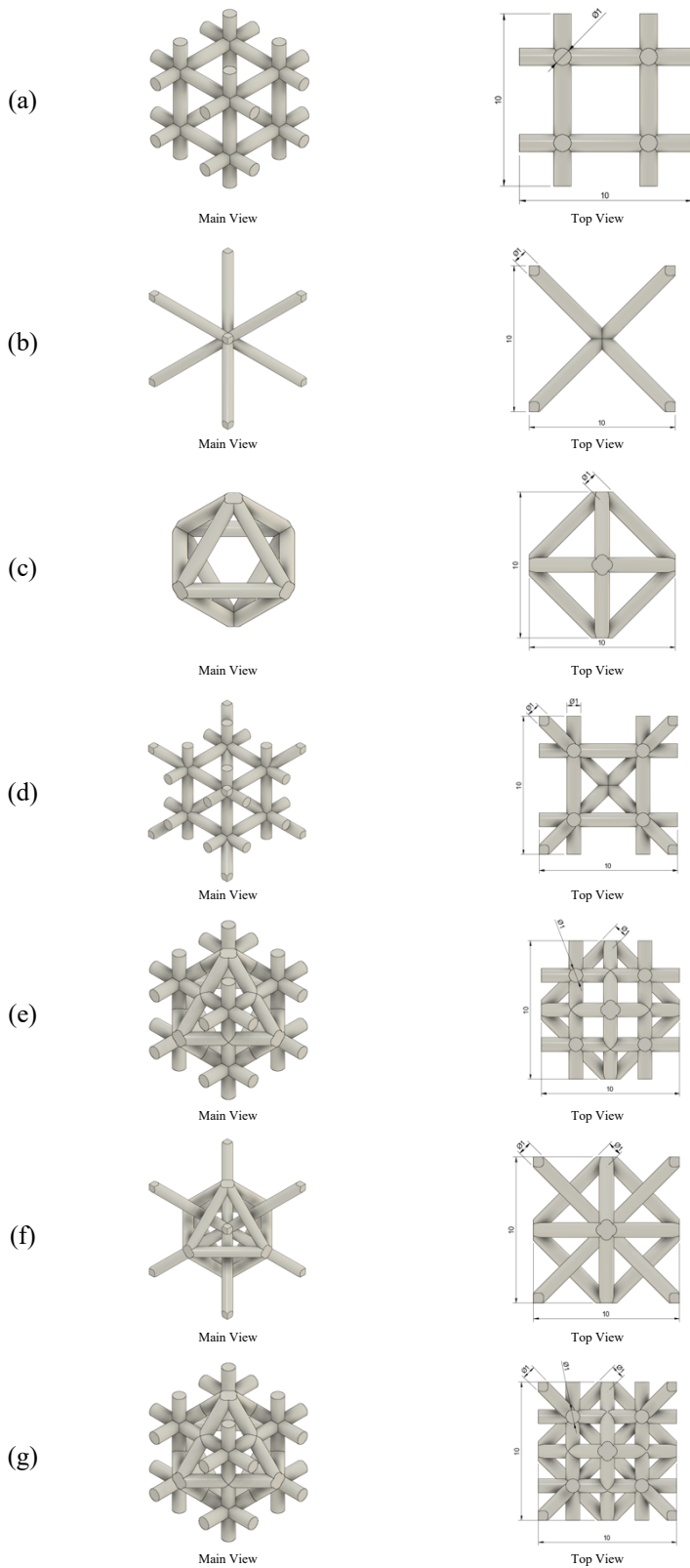


Figure 5: 1mm truss CAD model: (a) Cross Cubic, (b) BCC, (c) Octahedron, (d) Cross Cubic + BCC, (e) Cross Cubic + Octahedron, (f) BCC + Octahedron, (g) Cross Cubic + BCC + Octahedron (unit: mm)

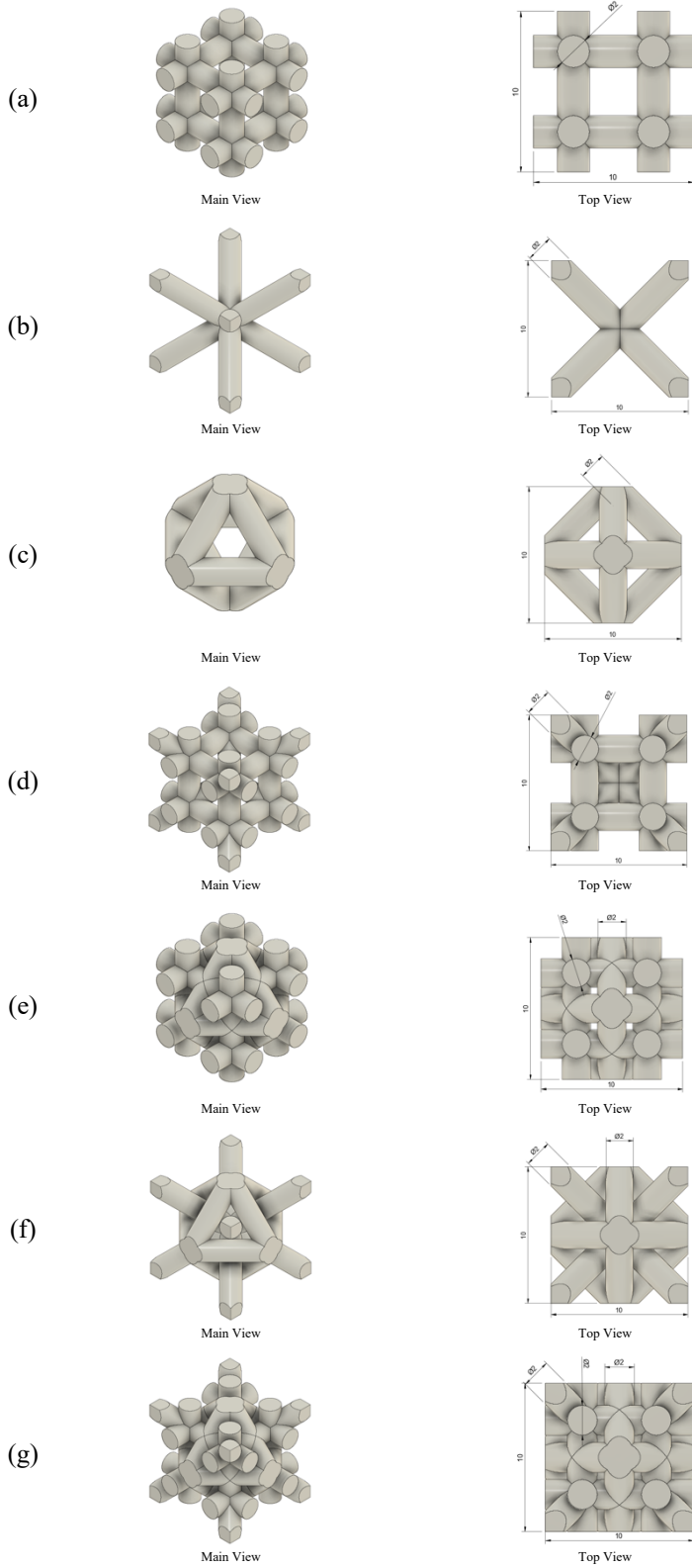


Figure 6: 2mm truss CAD model: (a) Cross Cubic, (b) BCC, (c) Octahedron, (d) Cross Cubic + BCC, (e) Cross Cubic + Octahedron, (f) BCC + Octahedron, (g) Cross Cubic + BCC + Octahedron (unit: mm)

LS are unique types of materials that are comprised of regularly-arranged, repeated unit cells. These structures exhibit a high degree of organization and symmetry, with the unit cell serving as the fundamental building block that governs the material's properties. Figure 7 provides a visual representation of this concept.

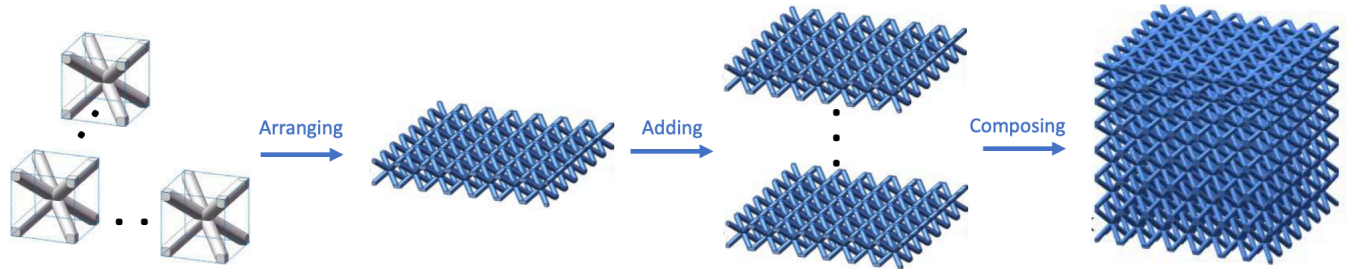


Figure 7 Lattice Structure formed by unit cells (take BCC as an example)

By changing the geometry of the unit cell, it is possible to alter the mechanical properties of the LS, such as its strength, stiffness, and density. This report mainly combines the aforementioned seven different unit cells into a 2x2x2 LS to test its mechanical properties and behaviors, as shown in Figure 8-9.

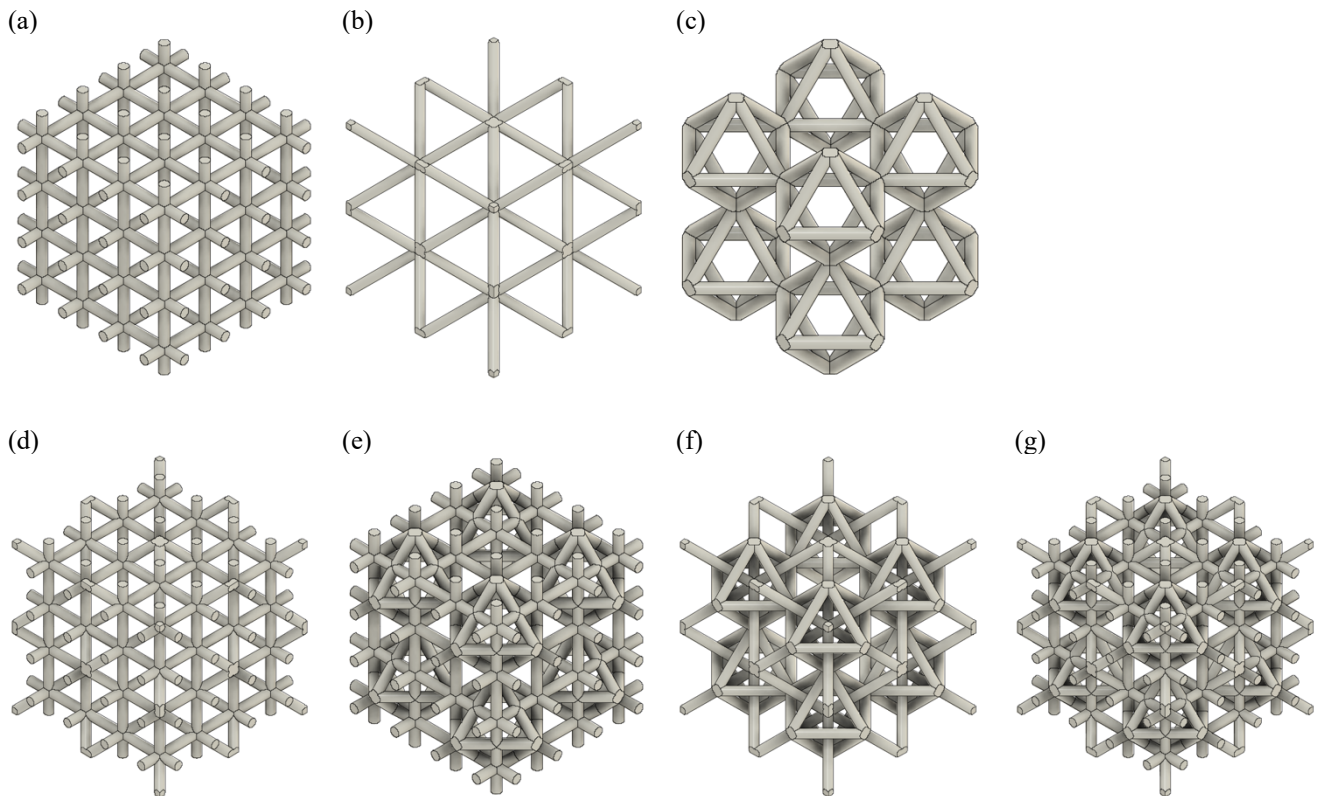


Figure 8 2*2*2 Lattice Structure with 1 mm truss CAD model: (a) Cross Cubic, (b) BCC, (c) Octahedron, (d) Cross Cubic + BCC, (e) Cross Cubic + Octahedron, (f) BCC + Octahedron, (g) Cross Cubic + BCC + Octahedron

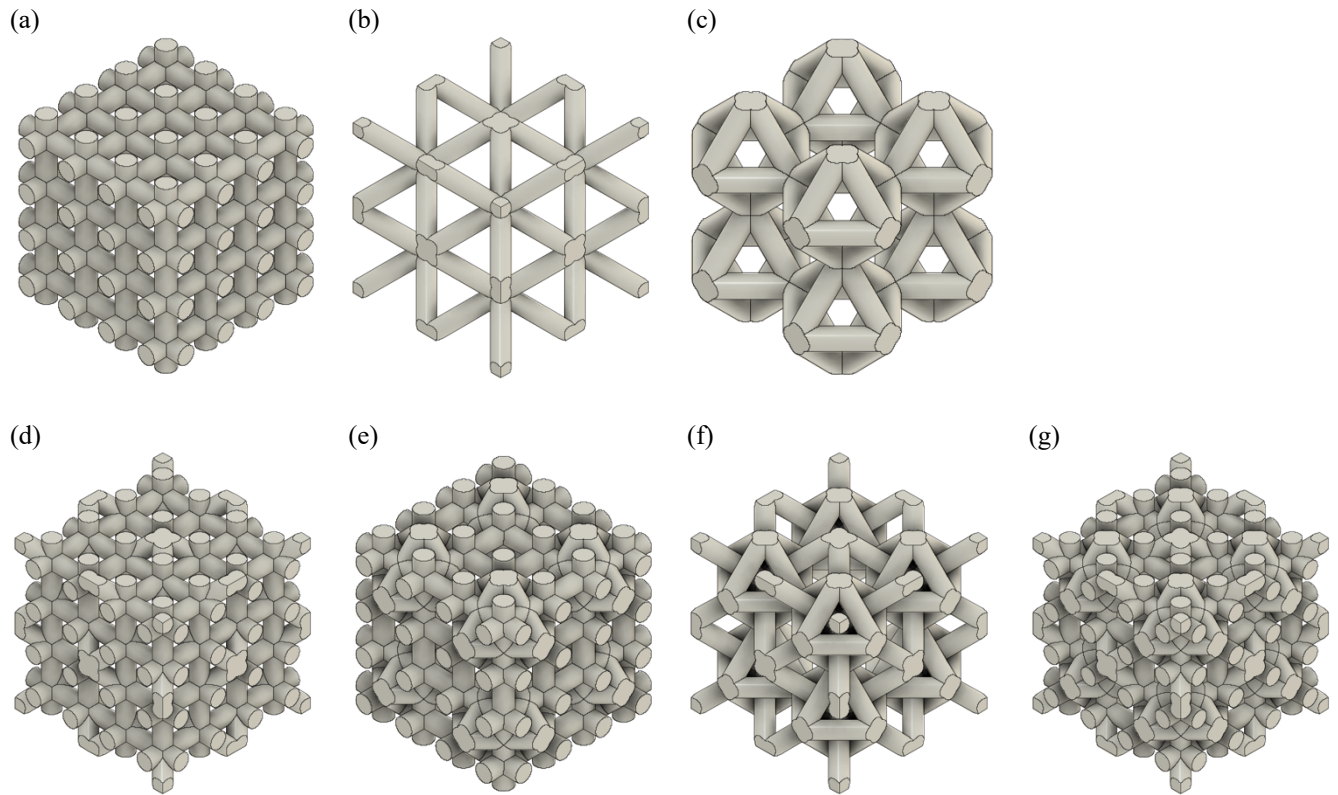


Figure 9 2*2*2 Lattice Structure with 2 mm truss CAD model: (a) Cross Cubic, (b) BCC, (c) Octahedron, (d) Cross Cubic + BCC, (e) Cross Cubic + Octahedron, (f) BCC + Octahedron, (g) Cross Cubic + BCC + Octahedron

2.2 Fabricating and Materials

2.2.1 3D Printer

Additive Manufacturing (AM) techniques have been widely used in various industries, and two of the commonly used methods are Fused Deposition Modeling (FDM) and Stereolithography (SLA). FDM is a process in which a thermoplastic material is extruded through a nozzle and deposited layer-by-layer to form the final product. On the other hand, SLA involves selectively solidifying a liquid photopolymer resin using a laser to create the final product[2], as shown in Figure 10. While both methods have their advantages and limitations, they are suitable for different applications. FDM is often used to create functional parts due to its ability to use strong, engineering-grade thermoplastics. In contrast, SLA is preferred for creating prototypes or intricate designs because of its high precision and smooth surface finish. For the fabrication of test specimens in this report, the Dremel 3D45, an FDM 3D printer, and the Formlabs Form 3+, an SLA 3D printer, are utilized, as Figure 11 shown.

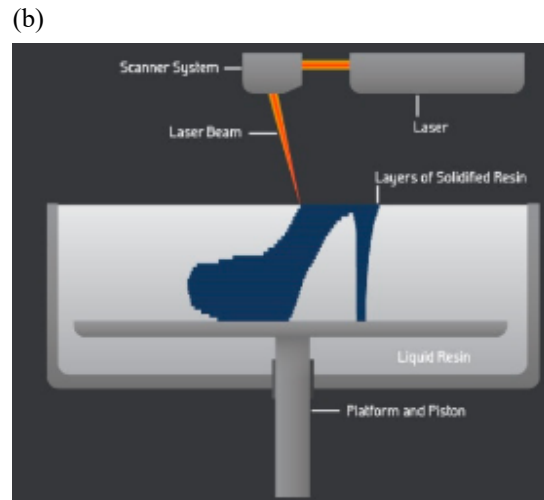
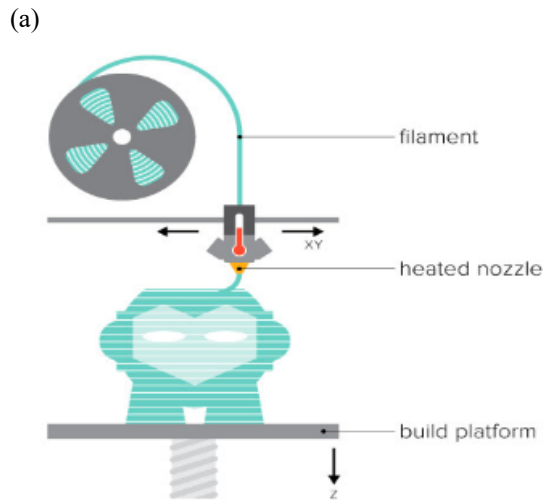


Figure 10 Additive Manufacturing (a) FDM, (b) SLA [2]

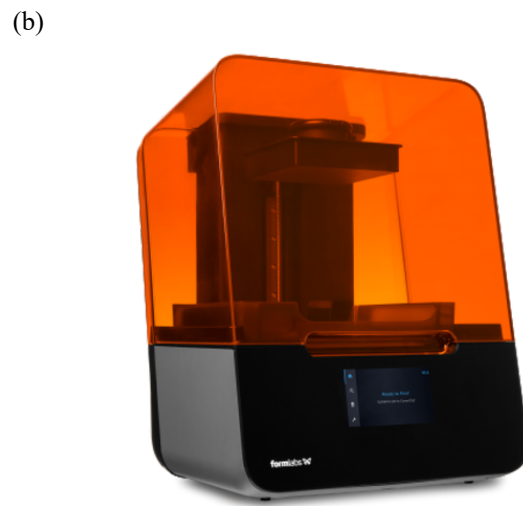
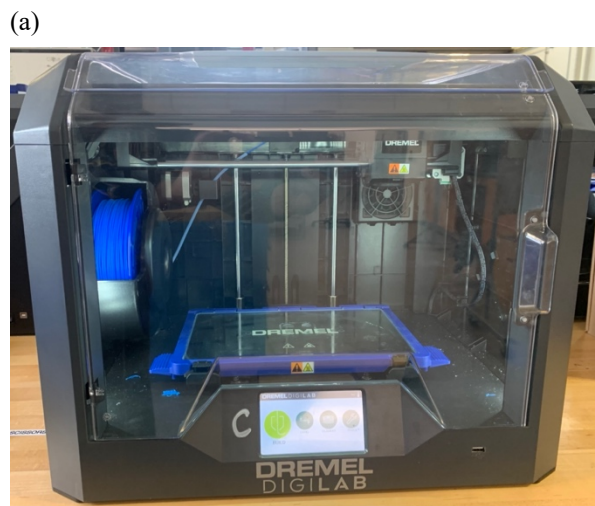


Figure 11 3D printer (a) Dremel 3D45, (b) Formlabs Form 3+

2.2.2 Materials of 3D Printing

Different 3D printing methods require specific materials. Fused Deposition Modeling (FDM) commonly employs Poly Lactic Acid (PLA) and Thermoplastic Polyurethane (TPU) due to their unique properties [21]–[23]. PLA is a renewable, biodegradable, and environmentally friendly polymer utilized in various fields, including biomedical and packaging industries. On the other hand, TPU is a thermoplastic elastomer known for its remarkable toughness, flexibility, and durability, making it suitable for applications such as sports equipment, footwear, and medical devices. PLA and TPU have become prevalent feedstock materials in 3D printing technology. This technology provides high accuracy and precision in producing complex geometries, prototypes,

and functional parts. Researchers have extensively studied various aspects of PLA and TPU, such as their processing techniques [21], color effects [24], crystallinity improvement[24], mechanical properties [22], [25], and composite materials [26]. 3D printing has also made it possible to create novel PLA and TPU-based materials with unique structures and properties, such as composites reinforced with carbon nanofibers [27], self-sensing honeycomb structures [28], and strain-sensing materials [29]. The combination of PLA and TPU in 3D printing has also been explored to produce composites with improved mechanical properties and surface characteristics [30]. In this report, the brand of PLA and TPU are Dremel PLA Blue Filament and Overture. In addition, because of the limitation of fabrication, the specimens of LS are only printed with a truss of 2mm. The printing coefficients are shown in Table 2.

Table 2 Printing parameters of FDM printer

Material	PLA	TPU
Layer Height	0.2 mm	0.2 mm
Printing Temperature	200 °C	220 °C
Print Speed	20 mm/s	20 mm/s
Infill Speed	20 mm/s	20 mm/s
Travel Speed	50 mm/s	50 mm/s

Photoreactive liquid polymer and thermoset resin is a type of resin that is used in Stereolithography (SLA) manufacturing. Photoreactive liquid polymer resins have emerged as a promising material in 3D printing technology due to their ability to solidify upon exposure to UV light. These resins offer a range of advantages over traditional feedstock materials, such as the ability to produce intricate and complex geometries with high precision and accuracy. There are various aspects of photoreactive liquid polymer resins, including the preparation of high solid loading and low viscosity ceramic slurries[31], the development of acid-cleavable PEG-methacrylate networks for biomaterial applications[32], and the impact of using short carbon and glass fibers on both the curing kinetics and precision of photopolymers was investigated. [33]. The potential applications of photoreactive liquid polymer resins are vast and varied, from carabiner remodeling to ceramics[34], [35], and even to multilayer structural composites[36]. As 3D printing technology continues to evolve, photoreactive liquid polymer resins are expected to play an increasingly

important role in the production of functional parts and prototypes with unique structures and properties. Formlab Grey resin and Elastic 50A resin are used for testing in this report. The printing parameters and model volume are presented in Tables 3 and 4.

Table 3 Printing parameters of SLA printer

Material	Grey Resin	Elastic 50A
Layer Height	0.1 mm	0.1 mm
Print setting	Default	Default

Table 4 Model Volume

Lattice Structure	CROSS CUBE		BCC		OCTAHEDRON		CROSS CUBE + BCC		CROSS CUBE + OCTAHEDRON		BCC + OCTAHEDRON		CROSS CUBE + BCC + OCTAHEDRON	
	1mm	2mm	1mm	2mm	1mm	2mm	1mm	2mm	1mm	2mm	1mm	2mm	1mm	2mm
Truss diameter														
Volume (mm ³)	663.5	2291.9	396.1	1427.7	471.3	1638.0	983.4	3110.2	1070.8	3417.9	867.5	3065.7	1390.0	4236.3

2.3 Simulation

Fusion 360 is a powerful 3D CAD and CAM software that offers engineers and designers the ability to perform static stress simulations on their 3D models. This feature is especially useful for engineering design as it allows for the analysis of a structure's behavior under various loads and constraints. Static stress simulation, also known as static analysis, is a simulation method that determines the stress and deformation of a structure under a given load or set of loads. Fusion 360's static stress simulation utilizes a finite element analysis (FEA) algorithm to break down a structure into smaller elements, which are then analyzed for their deformation and stress under applied loads. The simulation results provide a comprehensive view of the structure's behavior and can be used to identify potential failure points, optimize the design for strength and weight, and improve overall performance [37].

In this study, the researchers utilized Fusion 360's static stress simulation for compression simulation, which required specific mechanical properties and strength properties of materials to accurately simulate the behavior of the structures. The required properties for simulation included Young's modulus, Poisson's ratio, shear modulus, density, yield strength, and tensile strength. It is

important to note that the values of these properties may vary depending on various factors, such as the printing method, reinforcement, post-processing treatment, as well as different brand models. From the datasheet of the material brand, some parameters are obtained, such as Flexural Modulus and 100% Modulus. However, not all required parameters can be obtained by the datasheet. To obtain simulation results, Flexural Modulus and 100% Modulus seemed to equal Young's Modulus, and the other mechanical property parameters which cannot be obtained from the datasheet were summarized and presented based on the data provided in the existing literature to obtain more accurate simulation results. The mechanical properties and strength properties of each material are presented in Table 5.

Table 5 Mechanical and Strength properties of materials

<i>Printing Method</i>	Fused Deposition Modeling (FDM)		Stereolithography (SLA)	
Materials	Poly Lactic Acid (PLA)	Thermoplastic Polyurethane (TPU)	Grey Resin	Elastic 50A Resin
Young's modulus	3200 MPa [38]	9.3 MPa [39]	2.8 GPa [40]	1.59MPa [40]
Poisson's ratio	0.36 [22]	0.39 [41]	0.34 [41]	0.34 [41]
shear modulus	1.3 GPa [22]	0.862 GPa [41]	2.5 GPa [42]	2.5 GPa [42]
density	1.24 g/cm ³ [38]	1.19 - 1.24 g/cm ³ [39]	1.08 g/cm ³ [43]	1.08 g/cm ³ [43]
yield strength	70 MPa [22]	21-36 MPa [41]	65 MPa [40]	3.23 MPa [40]
tensile strength	68 MPa [38]	29.1 MPa [39]	65 MPa [40]	3.23 MPa [40]

2.4 Compression Test

The compression experiments were executed utilizing an INSTRON 5867 machine designed for compression and tensile testing, as shown in Figure 12. The machine has a maximum axial load capacity of 30 kN, and its operation is governed by a controller and a PC that is equipped with

software to provide complete control of the system. Load or displacement control can be achieved during the testing process to meet the desired objective. The Bluehill application, specifically designed for static tests, is used to program the testing procedure. During the test, the specimen is subjected to a constant compression displacement rate of 0.15 mm/sec. The load cell is used to continuously monitor the compression force while the position of the load piston is recorded. All tests are conducted until either the specimen fails or the compression extension reaches 15 mm.



Figure 12 INSTRON 5867 compression/tensile machine

3 Result

3.1 Simulation Result

In a compression test, the goal is to determine the behavior of a material under compressive loads. The test typically involves applying a compressive force to a material until it deforms or fails. To simulate this test, aluminum plates are added onto the top and bottom surfaces of the test model to simulate the test fixtures of the gauge of the compression test machine, as shown in Fig 13. This setting is to simulate compression test machines that can apply a compressive force to the upper plate and measure the deformation of the material under test. The lower plate is fixed in place to prevent any movement during the test.

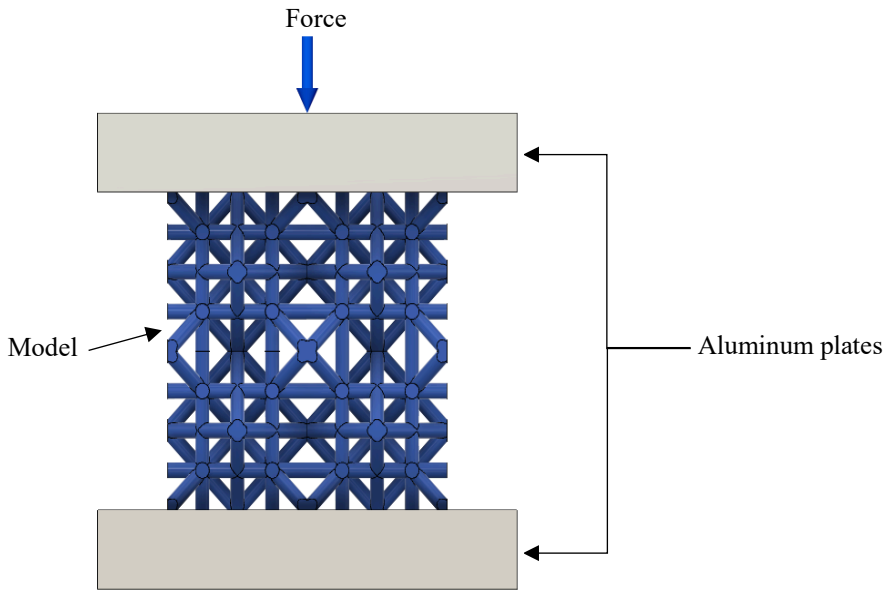


Figure 13 Simulation Model

The mechanical behavior of seven LS models, which included Cross Cube, BCC, Octahedron, Cross Cube + BCC, Cross Cube + Octahedron, BCC + Octahedron, and Cross Cube + BCC + Octahedron, with four materials, PLA, TPU, Grey Resin, and Elastic 50A Resin, are evaluated respectively. The compression simulations of each LS model with the four different materials were conducted, and the results are presented in Fig 14-15.

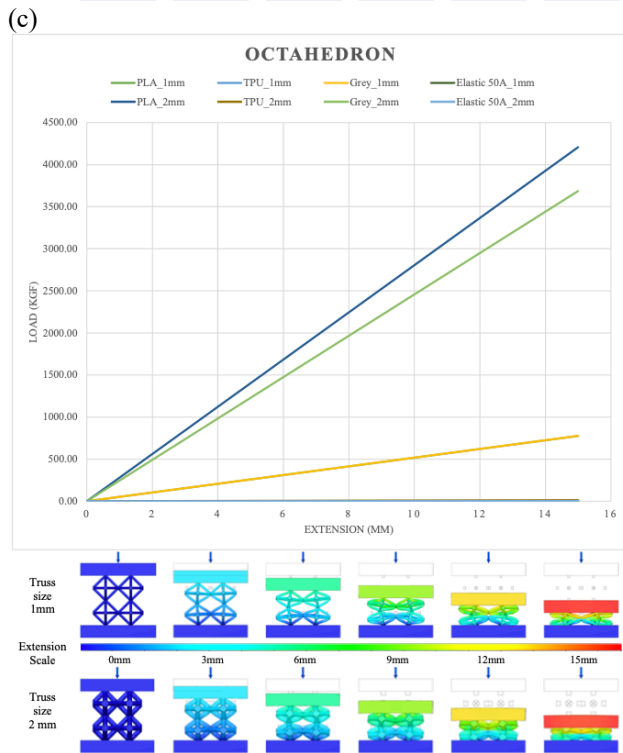
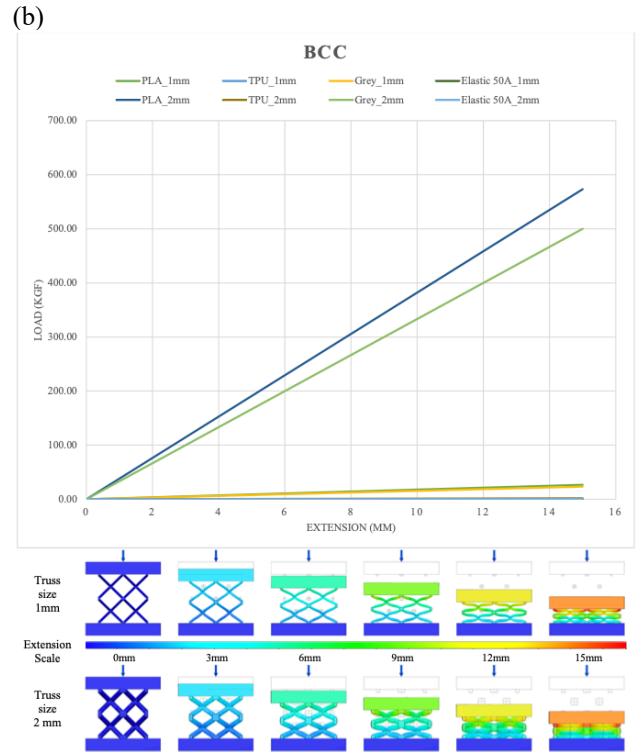
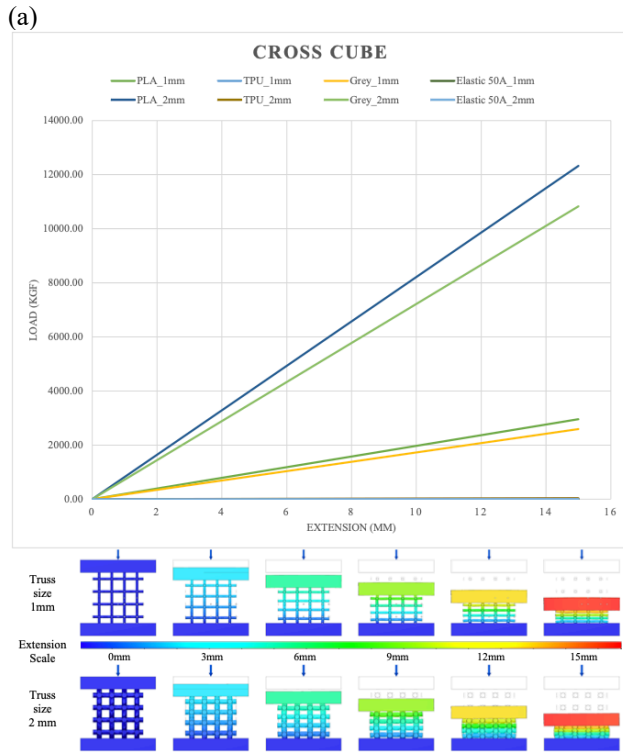


Figure 14 Pure Lattice Structure: (a) Cross Cubic, (b) BCC, (c) Octahedron

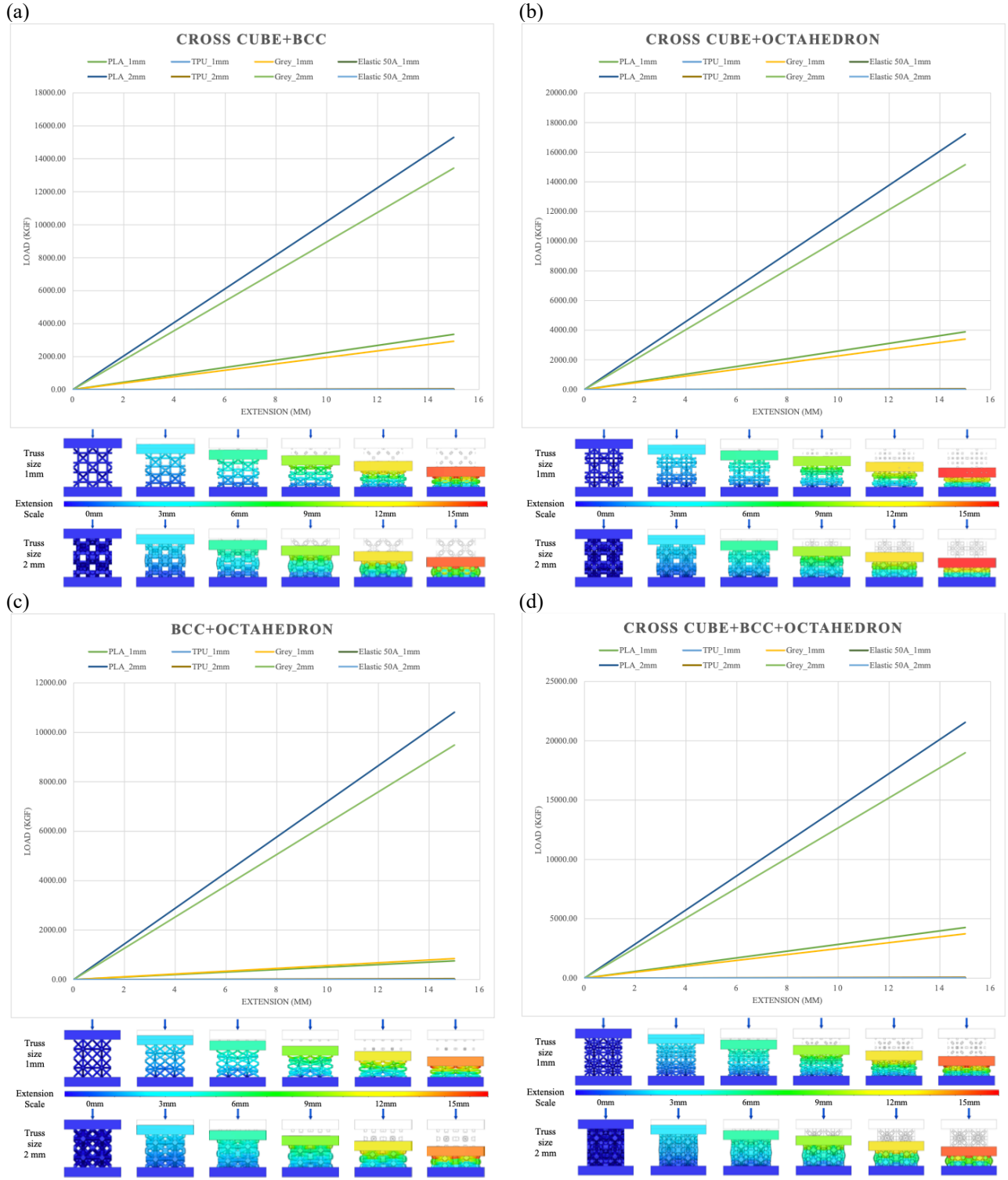


Figure 15 Composed Lattice Structure: (a) Cross Cubic + BCC, (b) Cross Cubic + Octahedron, (c) BCC + Octahedron, (d) Cross Cubic + BCC + Octahedron

The linear results obtained from static stress simulation in finite element analysis (FEA) are based on the assumption that the analyzed uniform and perfect material specimen behaves linearly under loading, following Hooke's law. Within the elastic limit of a material, the principle of Hooke's law asserts that the magnitude of stress experienced by a material is directly proportional to the amount of strain it undergoes, resulting in a linear stress-strain relationship.[45] This simplification is sufficient for many engineering applications as long as the loads are small enough not to cause plastic deformation or yield of the material. The slope of the linear stress-strain curve in the elastic region of a material represents Young's modulus, which is a fundamental material property that can be used to predict the material's behavior under different loading conditions. However, if the applied loads are significant enough to cause plastic deformation or yield, the linear assumption is no longer applicable, and the plastic limit must be determined experimentally for more accurate analysis.

Despite static stress analysis being unable to obtain the plastic limit, it can still analyze the strength relationship between different materials and structures. The slope of the linear results from static stress simulation represents the stiffness or modulus of elasticity of the material being analyzed, which is a measure of how much the material will deform under a given load. It is an important parameter that can be used to design and optimize engineering structures for maximum strength and reliability.

Table 6 displays the Load-Extension values derived from a static stress simulation. While static stress analysis assumes that the material being examined is homogeneous and isotropic, meaning it has the same properties in all directions, materials in the real world can be anisotropic and possess defects or imperfections that can impact their behavior under load. Nevertheless, these values remain useful for evaluating how different materials and structures will behave under various loading conditions. The linear results obtained from static stress analysis can aid engineers and designers in optimizing the design of structures by projecting their performance under different loads. Moreover, based on the Load-Extension values required for the final product, engineers and designers can further screen and select the appropriate materials and structures. From the Load-Extension values given for each LS and material, it can be analyzed the relationship among materials, pure LS, composed LS, and truss diameter as follow:

1. Materials:

PLA has the highest Load-Extension value, and the lowest Load-Extension value is Elastic 50A Resin, Grey Resin is stiffer than TPU, and both of them are in the middle of PLA and TPU. It shows that PLA is the stiffest material among the four, with the highest Load-Extension value. In contrast, TPU is the most flexible material, as it has the lowest Load-Extension value. Grey Resin has slightly more flexibility than PLA, while TPU is stiffer than Elastic 50A Resin. These findings can be useful when selecting the appropriate material for a 3D-printed object based on the desired stiffness and flexibility requirements.

2. Pure Lattice Structure:

Among the three pure LS, the Cross Cube LS has the highest Load-Extension values, followed by the Octahedron LS, and the BCC LS has the lowest Load-Extension values. In other words, the Cross Cube LS seems to provide the most robust and rigid option, followed by the Octahedron LS, and the BCC LS is the lightest option of the three. Hence, when selecting an LS for a 3D-printed object, it is crucial to consider the specific requirements of the application carefully.

3. Composed Lattice Structure:

Table 4 shows that Composed LS has a smaller or equal volume than the actual combined volume of two or three Pure LS, resulting in volume reduction as presented in Table 7. Furthermore, the Load-Extension values of Composed LS differ, as seen in Table 8.

Composed LS comprising a combination of two Pure LS, the bit different Load-Extension changing behaviors. Cross Cube + BCC has a 12%-19% higher Load-Extension value compared to pure Cross Cube and pure BCC composition, while its volume is 7%-18% lower. This implies that adding a Cross Cube or BCC structure improves the overall strength and rigidity of the Composed LS while reducing the ratio of volume. In contrast, although the Load-Extension value of Cross Cube + Octahedron is higher than the composition of pure Cross Cube and pure Octahedron, its volume reduction is only 5%-13%, and Load-Extension increase is only 3%-7%. The BCC + Octahedron LS exhibits unique behavior. For a truss diameter of 1mm, it is weaker than the combination of pure BCC and pure Octahedron structures. This may be due to its combination of two weaker structures, where BCC has a high level of structural integrity, and the Octahedron has a lower level of structural integrity. When combined, the weaker aspects of the Octahedron

structure are added to the BCC structure, resulting in a less interconnected LS and weaker performance. However, for a 2mm truss diameter, the Load-Extension value of BCC + Octahedron increases by 126%-159% without reducing the volume.

For Composed LS comprising three Pure LS, Cross Cube + BCC + Octahedron has a 7%-28% higher Load-Extension value but 7%-18% lower volume than the pure structures combination. Hence, it is apparent that Cross Cube + BCC is superior to Cross Cube + Octahedron, which is superior to BCC + Octahedron in Composed LS comprising two Pure LS, while Cross Cube + BCC + Octahedron outperforms all compositions of two LS.

4. Truss diameter:

From Table 9, it is clear that increasing the truss diameter of LS from 1mm to 2mm has a significant impact on both volume and load-extension for all truss designs and materials tested. The ratio of increased volume ranges from 304.77% for the Cross Cube + BCC + Octahedron design to 360.44% for the BCC design. The ratio of increased load-extension is even more significant, ranging from 416.66% for the Cross Cube design to a massive 2169.49% for the BCC design when printed using TPU material.

In addition, when looking at the Pure LS, it appears that the BCC design consistently shows the greatest increase in both volume and load-extension across all materials tested. In contrast, the Cross Cube design consistently shows the lowest increase in both volume and load-extension. The Octahedron design falls somewhere in between these two extremes. However, when combining multiple LS, the ratio of increased volume and load-extension of increased truss diameter is generally lower than in Pure LS. This suggests that combining LS may have a positive impact on overall stability and strength but at the cost of a decrease in volume and load-extension. It is also worth noting that different materials show different levels of increase in both volume and load-extension. Therefore, the choice of truss design and material can have a significant impact on both volume and load-extension, and these factors should be carefully considered based on the intended use and requirements of the printed object. Additionally, the combination of multiple LS may be beneficial in some cases but can also result in decreased volume and load-extension. These findings provide valuable insights into the impact of truss design and material choice on the strength and stability of 3D-printed structures.

Table 6 Load-Extension Results of Simulation

Materials		Poly Lactic Acid (PLA)		Thermoplastic Polyurethane (TPU)		Grey Resin		Elastic 50A Resin		
		1mm	2mm	1mm	2mm	1mm	2mm	1mm	2mm	
Load-Extension (Kgf/mm)	Pure Lattice Structure	CROSS CUBE	197.21	821.69	0.58	2.54	171.39	711.74	104.53	439.95
		BCC	1.78	38.05	0.01	0.11	1.52	32.15	0.93	19.54
		OCTAHEDRON	51.71	280.50	0.15	0.84	45.07	242.84	27.40	148.65
	Composed Lattice Structure	CROSS CUBE + BCC	223.11	1018.64	0.66	3.11	194.14	881.06	118.22	544.07
		CROSS CUBE + OCTAHEDRON	259.47	1139.99	0.77	3.62	226.86	1000.90	138.60	623.05
		BCC + OCTAHEDRON	50.45	718.91	0.15	2.48	43.94	615.76	26.70	385.51
		CROSS CUBE + BCC + OCTAHEDRON	284.17	1433.90	0.84	4.47	248.51	1248.60	151.45	779.42

Table 7 Ratio of decreasing volume of Composed Lattice Structure

Composed Lattice Structures	Cross Cube + BCC		Cross Cube + Octahedron		BCC + Octahedron		Cross Cube + BCC + Octahedron	
	1mm	2mm	1mm	2mm	1mm	2mm	1mm	2mm
Truss diameter								
The percentage of decreasing volume	7.19%	16.38%	5.64%	13.03%	0%	0%	9.20%	20.93%

Table 8 Ratio of Load-Extension changing of Composed Lattice Structure

Materials		Poly Lactic Acid (PLA)		Thermoplastic Polyurethane (TPU)		Grey Resin		Elastic 50A Resin		
		1mm	2mm	1mm	2mm	1mm	2mm	1mm	2mm	
The Ratio of Load-Extension Changing	Composed Lattice Structure	CROSS CUBE + BCC	12.24%	18.66%	10.88%	16.95%	12.07%	18.59%	3.45%	16.98%
		CROSS CUBE + OCTAHEDRON	4.24%	4.18%	4.35%	6.67%	1.01%	4.45%	5.12%	7.11%
		BCC + OCTAHEDRON	-5.67%	126.22%	-5.87%	158.58%	6.26%	126.62%	-7.13%	157.01%
		CROSS CUBE + BCC + OCTAHEDRON	13.45%	26.02%	12.40%	27.77%	10.09%	26.48%	6.67%	27.96%

Table 9 Ratio of increased Volume and Load-Extension from truss diameter 1mm to 2mm

Materials		Poly Lactic Acid (PLA)	Thermoplastic Polyurethane (TPU)	Grey Resin	Elastic 50A Resin
The ratio of increased Volume and Load-Extension from Truss diameter 1mm to 2mm	CROSS CUBE	345.43%			
		416.65%	432.71%	417.74%	433.09%
	BCC	360.44%			
		2148.73%	2169.49%	2148.15%	214.77%
	OCTAHEDRON	347.55%			
		542.45%	560.00%	538.81%	542.52%
	CROSS CUBE + BCC	316.27%			
		456.56%	471.21%	453.83%	460.22%
	CROSS CUBE + OCTAHEDRON	319.19%			
		442.53%	467.91%	445.60%	465.99%
	BCC + OCTAHEDRON	353.39%			
		1429.03%	1671.49%	1116.80%	1286.93%
	CROSS CUBE + BCC + OCTAHEDRON	304.77%			
		505.29%	533.97%	508.60%	529.44%

Overall, the simulation results highlight the significant impact that material selection, LS, and dimensions can have on the strength and performance of a product. While static stress simulation may not obtain yield the plastic limit, it still remains a valuable tool for analyzing strength

relationships among different materials, structures, and sizes. Such analyses can inform the preliminary selection of suitable materials, structures, and sizes based on the final product's loading requirements or be used to optimize existing products. Further compression experimental testing can be conducted to gain deeper insights into the mechanical behavior of the material.

3.2 Compression Test Result

Compression testing is a common method used in materials science and engineering to evaluate the mechanical behavior of a specimen under compressive loads. The test involves applying compressive forces to the specimen until it deforms or fails to analyze the materials and structures of the specimen's response to different compressive loads. The mechanical behavior of the specimen during the test can help to understand its performance, such as strength, stiffness, and deformation characteristics, and determine its suitability for various applications and industry standards. Generally, the specimen undergoes stages of elastic deformation, yield, plastic deformation, and fracture during the compression test. During the elastic deformation stage, the load-extension curve is expected to be approximately linear, following Hooke's law until the yield point is reached. The yield point marks the transition from elastic to plastic deformation and is a critical property of the material to withstand the maximum stress before permanent deformation occurs. Subsequently, during the yield stage, as the material is subjected to increasingly higher compressive loads, it begins to exhibit reversible plastic deformation and no longer follows Hooke's law. The load-extension curve starts to bend and plateaus at a certain load, which is the yield strength. After that, as the load continues to increase, the material begins to undergo irreversible plastic deformation, and the load-extension curve enters the plastic deformation stage. During the plastic deformation stage, the material undergoes significant deformation, and the load-extension curve is nonlinear. The material continues to deform until ultimate failure occurs. When the maximum load is reached, the material begins to exhibit local deformation and eventually fractures. The fracture point usually occurs at the thinnest part of the material or a pre-existing crack. Understanding these stages can help us to determine the performance and strength of the material under compressive loads. In addition, FDM printing uses a layer-by-layer stacking method, and the connection between layers has a greater impact, resulting in the orientation of these layers affecting the mechanical performance of the sample during testing, depending on whether they are parallel or perpendicular to the loading surface. To consider this factor, samples

printed using FDM printing will be additionally distinguished between being tested parallel or perpendicular to the applied force. In contrast, SLA printing uses a layer-by-layer curing method, and the connection between layers has less impact, thus reducing the influence of layer orientation. Therefore, the testing process does not distinguish between layer directions. To comprehensively evaluate the mechanical performance of SL, different materials and truss diameters were tested for each specimen, and each specimen was tested three times, with the results as follows.

1. Cross Cube:

Fig. 16 shows the mechanical behavior of PLA samples with different truss diameters and layer orientations. For a truss with a diameter of 1mm, the maximum stress is approximately 70 MPa, and the strain parallel to the loading plate is around 5%. When the layer is perpendicular to the loading plate, the stress is also approximately 50 MPa, with a strain of around 15%. The 1mm truss diameter exhibits elastic behavior similar to the simulated predictions and experiences brief plastic behavior after exceeding the yield point, followed by significant buckling until reaching a steady state. Then, the stress increases until the next highest but not exceeding the previous load, and then buckles again, repeating this cycle until densification occurs. For a truss with a diameter of 2mm, the maximum stress is around 80 MPa, and the strain parallel to the loading plate is around 6%. When the layer is perpendicular to the loading plate, the stress is approximately 110 MPa, with a strain of around 10%. Specifically, the elastic behavior is similar to the simulated predictions, with significant buckling until reaching a steady state after exceeding the yield point and then an increase in stress until reaching the next highest but not exceeding the previous load, and then buckling again, repeating this cycle until densification occurs. It is noteworthy that although the maximum stress load in the vertical layer orientation of the 2mm truss diameter specimen is higher than that in the parallel layer orientation, its buckling amplitude is significantly higher than that in the parallel layer orientation. This indicates that the supporting capacity in the parallel layer orientation is higher than that in the vertical layer orientation beyond the range of plastic deformation.

Samples made of TPU exhibit slightly different mechanical properties in parallel and perpendicular directions to the loading plate. The sample with a 1mm truss diameter shows brief elastic deformation and yields at a stress of 0.9 MPa with 5% strain in the parallel layer orientation, exhibiting clear buckling behavior. For the perpendicular layer

orientation, the highest stress is about 0.6 MPa with 5% strain, and it undergoes smooth buckling. The sample with a 2mm truss diameter undergoes longer but not significant elastic deformation, with stresses of 4.2 MPa and 3.4 MPa produced in the horizontal and vertical layers with 13% and 10% strain, respectively, as shown in Fig. 17. Both samples exhibit long platform behavior before densification.

For Grey Resin, the results in Fig. 18 show that the maximum stresses for truss diameters of 1mm and 2mm are approximately 45 MPa and 80 MPa, respectively, with both strains around 5%. When the load exceeds the maximum load, the 1mm sample fractures without any significant plastic deformation or buckling, while the 2mm sample fractures immediately but undergoes long plastic deformation before failure. This is because the 2mm truss diameter has a larger cross-sectional area, allowing it to withstand greater loads before failure. However, once the load exceeds its maximum carrying capacity, the 2mm sample undergoes long plastic deformation because the material can absorb and distribute stress over a larger area. In contrast, the smaller cross-sectional area of the 1mm sample cannot withstand such high stress before failure, resulting in immediate failure without any significant plastic deformation or buckling.

Based on the mechanical performance data of the Cross Cube LS sample made of Elastic 50A resin material provided in Fig. 19, the sample with a 1mm truss diameter exhibits significant but brief elastic deformation, followed by yielding a maximum stress of approximately 0.3 MPa with a strain of about 7%. For the 2mm truss diameter, the sample undergoes significant but longer elastic deformation, followed by yielding at a stress of approximately 0.5 MPa with a strain of about 16%. Both undergo long plastic deformation near the plateau after yielding, followed by densification. Additionally, the elastic behavior differs from the predicted results. It is worth noting that the 1mm truss diameter sample exhibits a linear shape with serrations, which may be due to irregularities and defects during the manufacturing process. Small variations in the geometric shape of the LS may lead to slight variations in the mechanical properties of the sample. The small size of the 1mm lattice may make it more susceptible to manufacturing defects and inaccuracies, leading to the observed linear serrated shape.

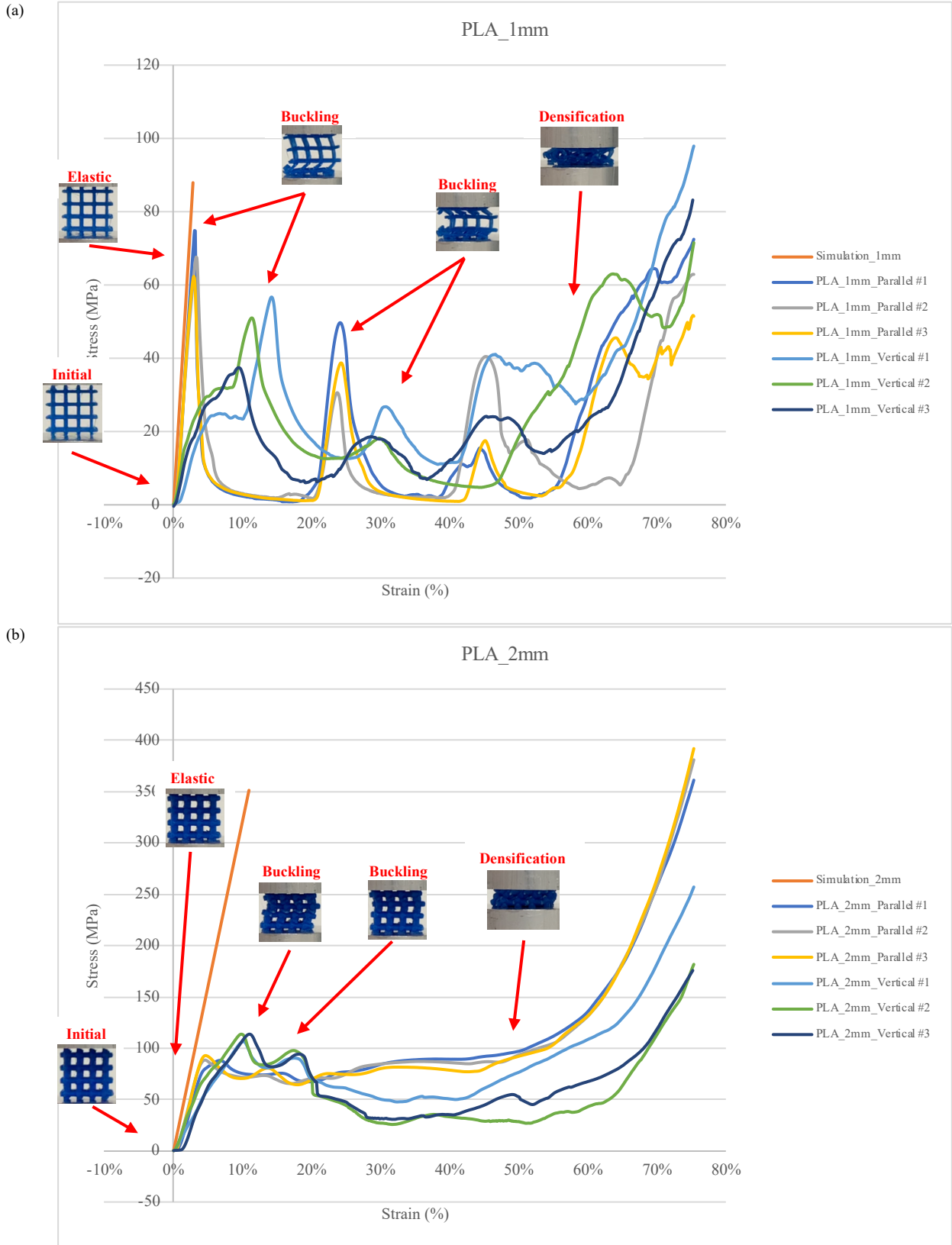


Figure 16 Cross Cube (PLA) - Compression Test and Simulation Results: (a) 1mm truss diameter, (b) 2mm truss diameter

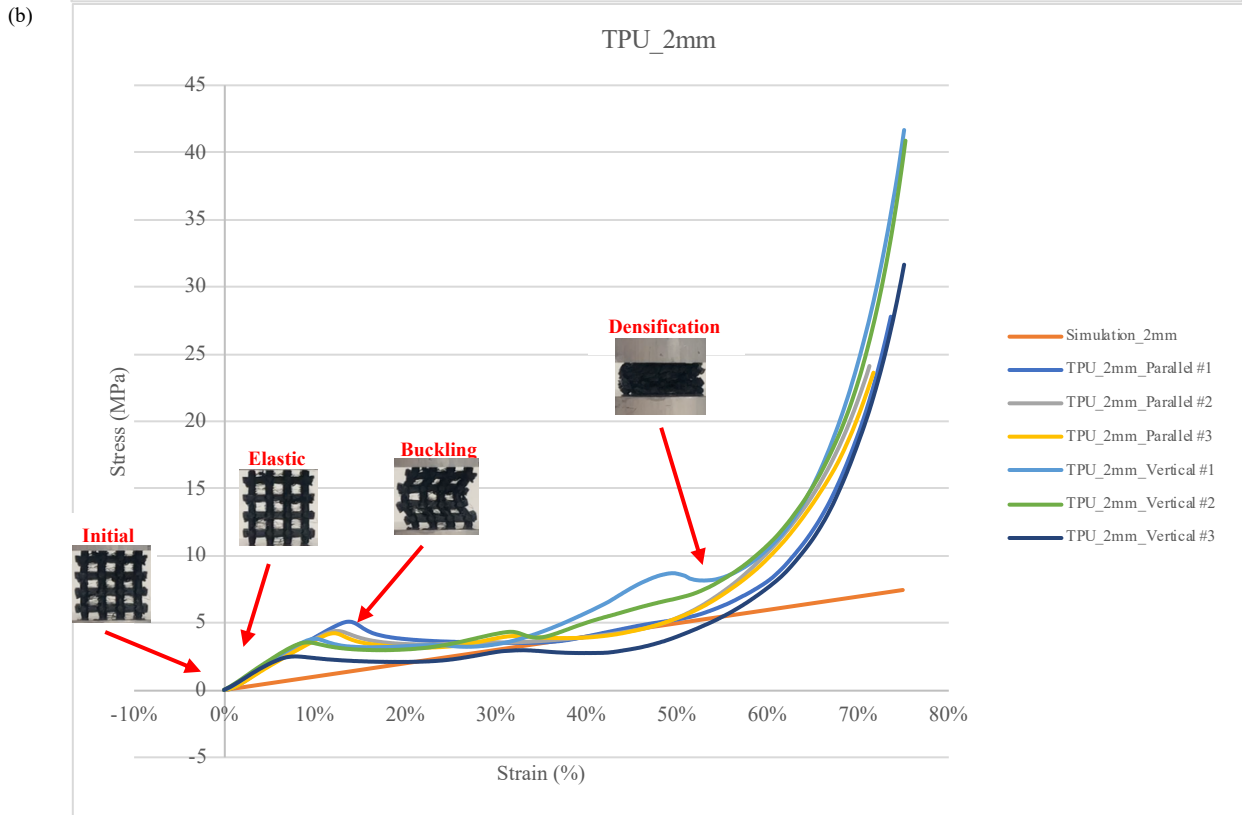
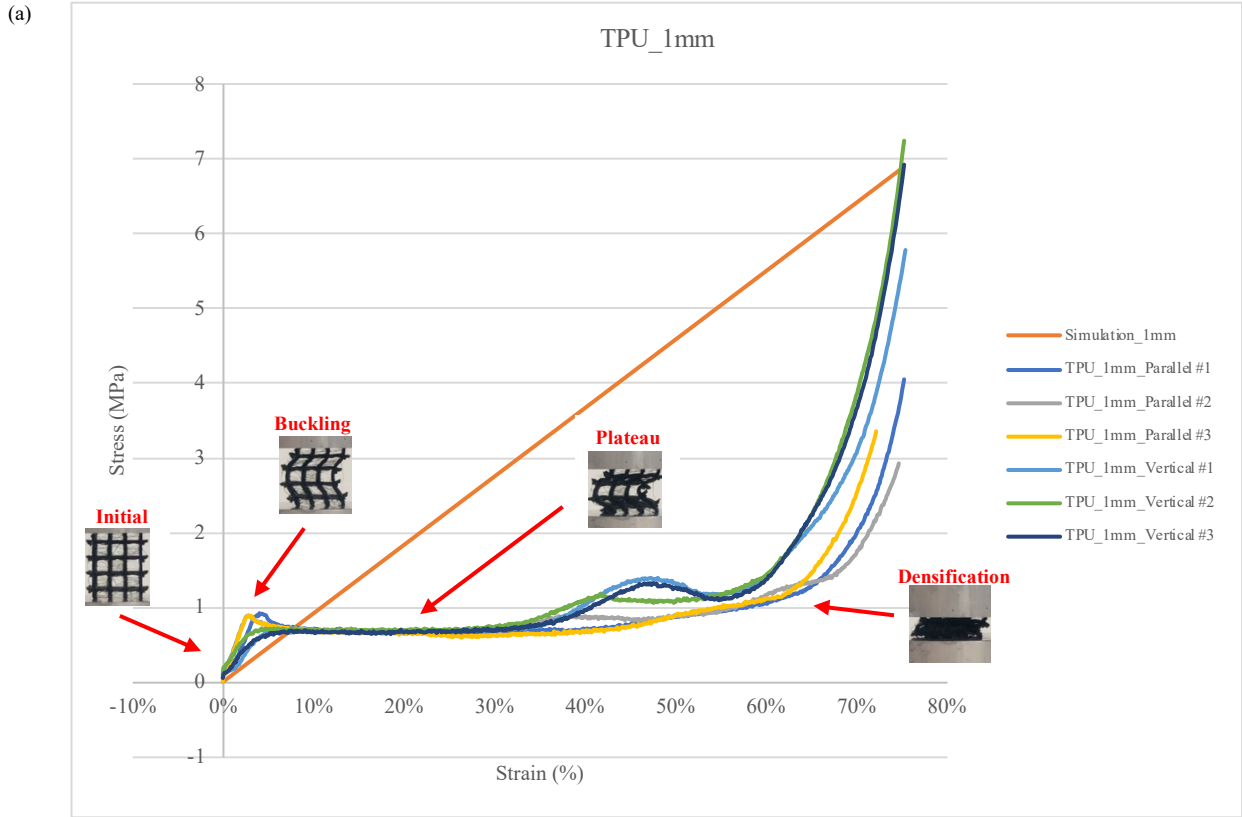


Figure 17 Cross Cube (TPU) - Compression Test and Simulation Results: (a) 1mm truss diameter, (b) 2mm truss diameter

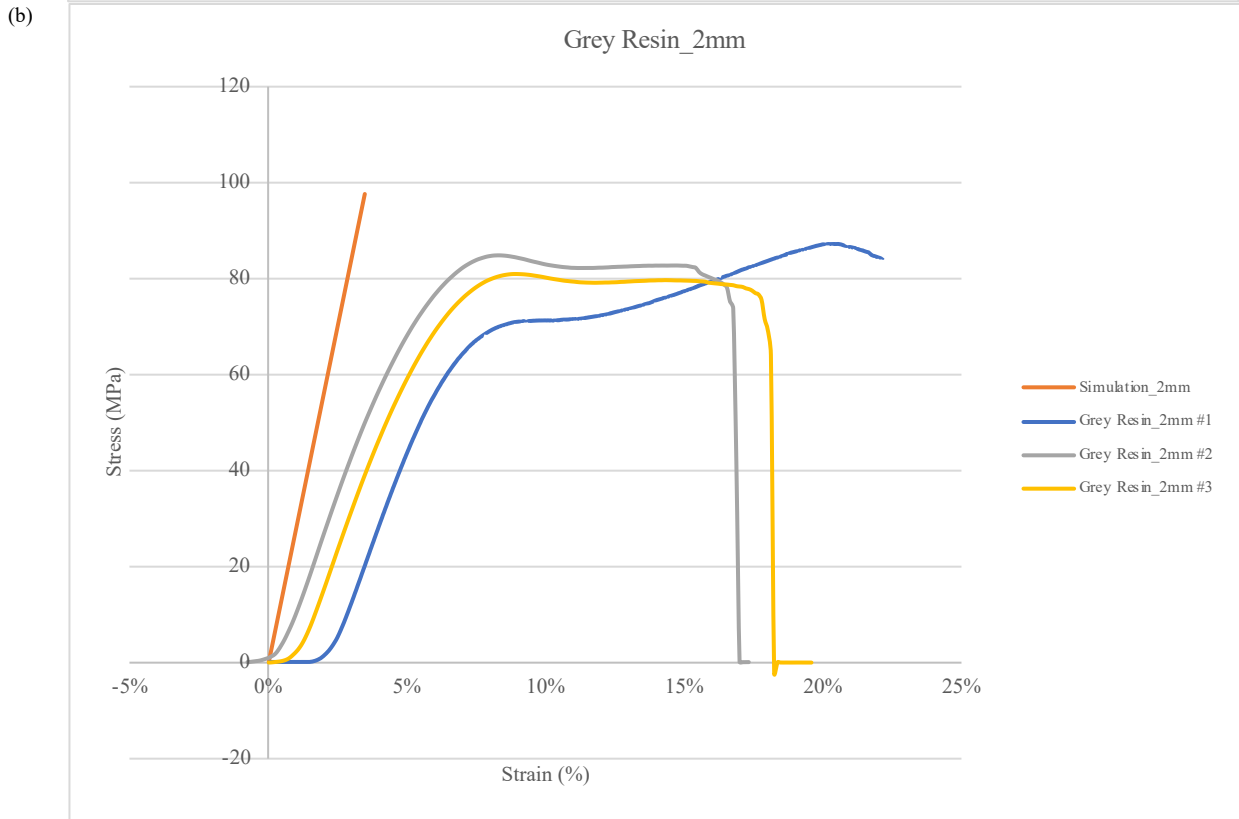
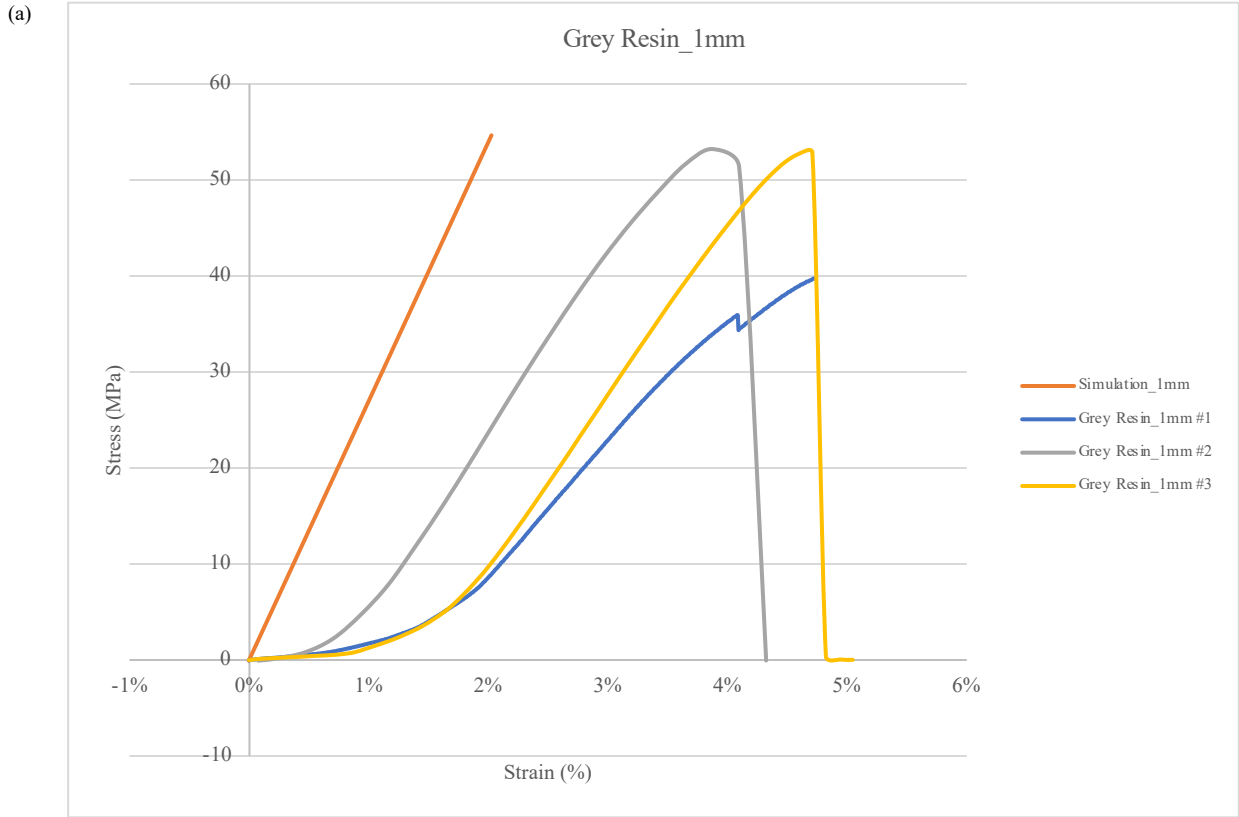


Figure 18 Cross Cube (Grey Resin) - Compression Test and Simulation Results: (a) 1mm truss diameter, (b) 2mm truss diameter



Figure 19 Cross Cube (Elastic 50A Resin) - Compression Test and Simulation Results: (a) 1mm truss diameter, (b) 2mm truss diameter

2. BCC:

The similar mechanical behavior was observed in BCC made of PLA materials with different truss diameters and layer orientations, as shown in Fig. 20. They initially exhibited elastic behavior similar to simulation data, with a 1 mm truss diameter sample reaching a maximum load of 7 MPa at 17% strain regardless of layer orientation, while 2 mm truss diameter samples in parallel and vertical orientation reached maximum stress of 17 MPa and 12 MPa, respectively, with 11% strain. They then began to bend until reaching a brief stable state. The load increased until the next maximum load was reached, which was lower than the previous one, and this cycle repeated until densification occurred. The similar mechanical behavior was observed in the sample made of TPU materials with different truss diameters and layer directions. The samples exhibited elastic behavior matching the simulation results, reaching a maximum of around 60% strain with 0.4 MPa stress for truss diameter, 1 MPa and 2 MPa stress for 2mm truss diameter parallel and vertical one before densification, as shown in Fig. 21. In contrast to the mechanical behavior of the previous two materials, BCC made of Grey resin exhibited rigid behavior. Both 1 mm and 2 mm truss diameter samples initially showed elastic behavior similar to the simulation results. After reaching the yield point, they reached maximum stresses of around 4.3 MPa and 9 MPa and elongated around 17% and 6.5% strain, respectively, before rapidly breaking into small pieces, causing a sudden drop in the load. It is worth noting that while the carrying capacity of the 2 mm truss diameter is ten times that of the 1 mm truss diameter, its elongation capability is only about 50% of the 1 mm truss diameter, elongating only about 1.3 mm. This indicates that increasing the truss diameter makes the specimen stronger when the BCC structure is made of gray resin, as shown in Figure 22. The samples in elastic 50A resin showed linear elastic behavior with approximately 60% and 65 % strain with 0.15 MPa and 0.2 MPa for 1 mm and 2 mm truss diameter, respectively, from compression to densification, as shown in Figure 23. Additionally, significant serrations were observed in the 1 mm sample in TPU and Elastic 50A resin, indicating that this material is very unstable when used in BCC LS. Moreover, the actual linear elastic behavior of load extension was much smaller than the simulation result, indicating that the sample is weaker than expected, or in other words, softer

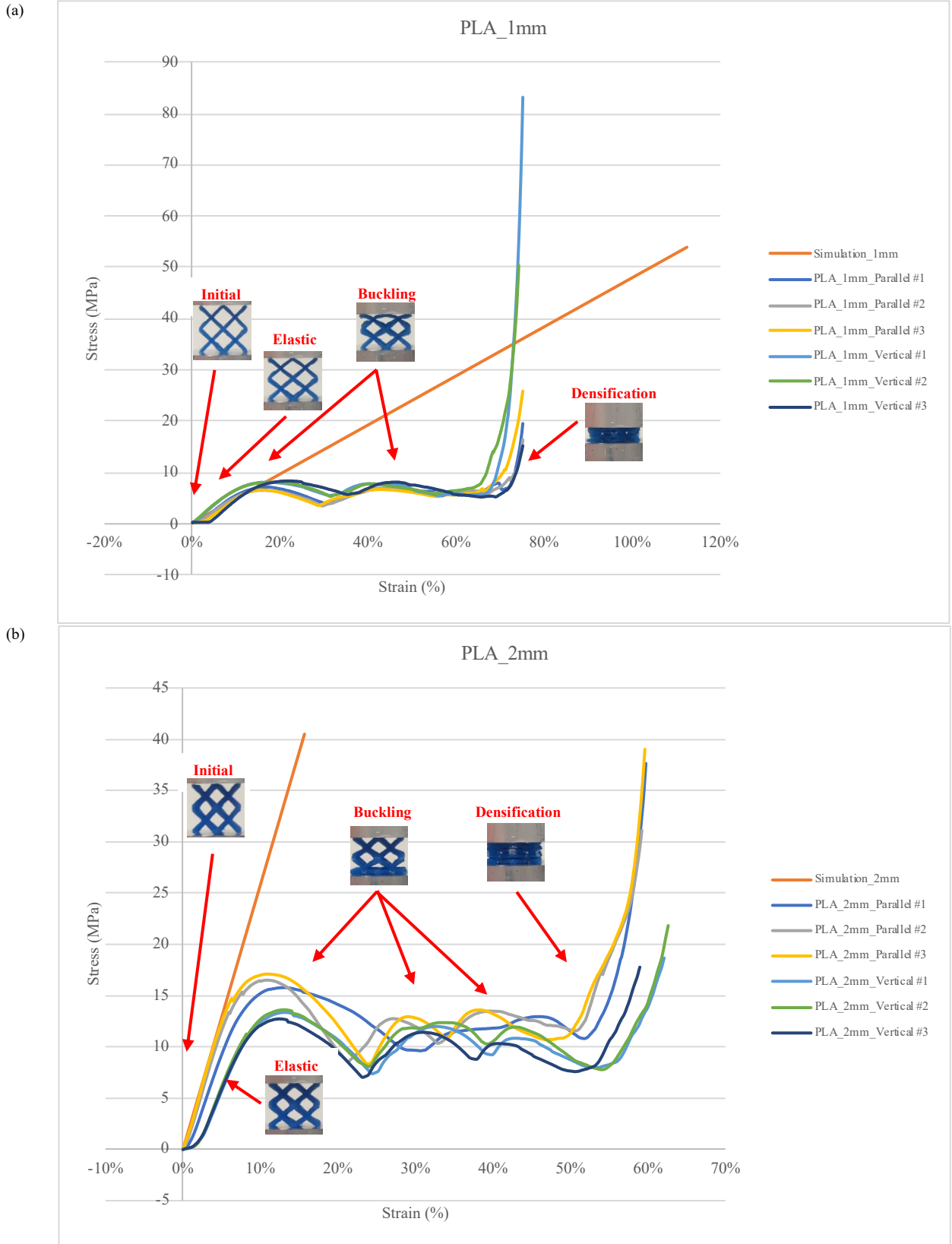


Figure 20 BCC (PLA) - Compression Test and Simulation Result: (a) 1mm truss diameter, (b) 2mm truss diameter

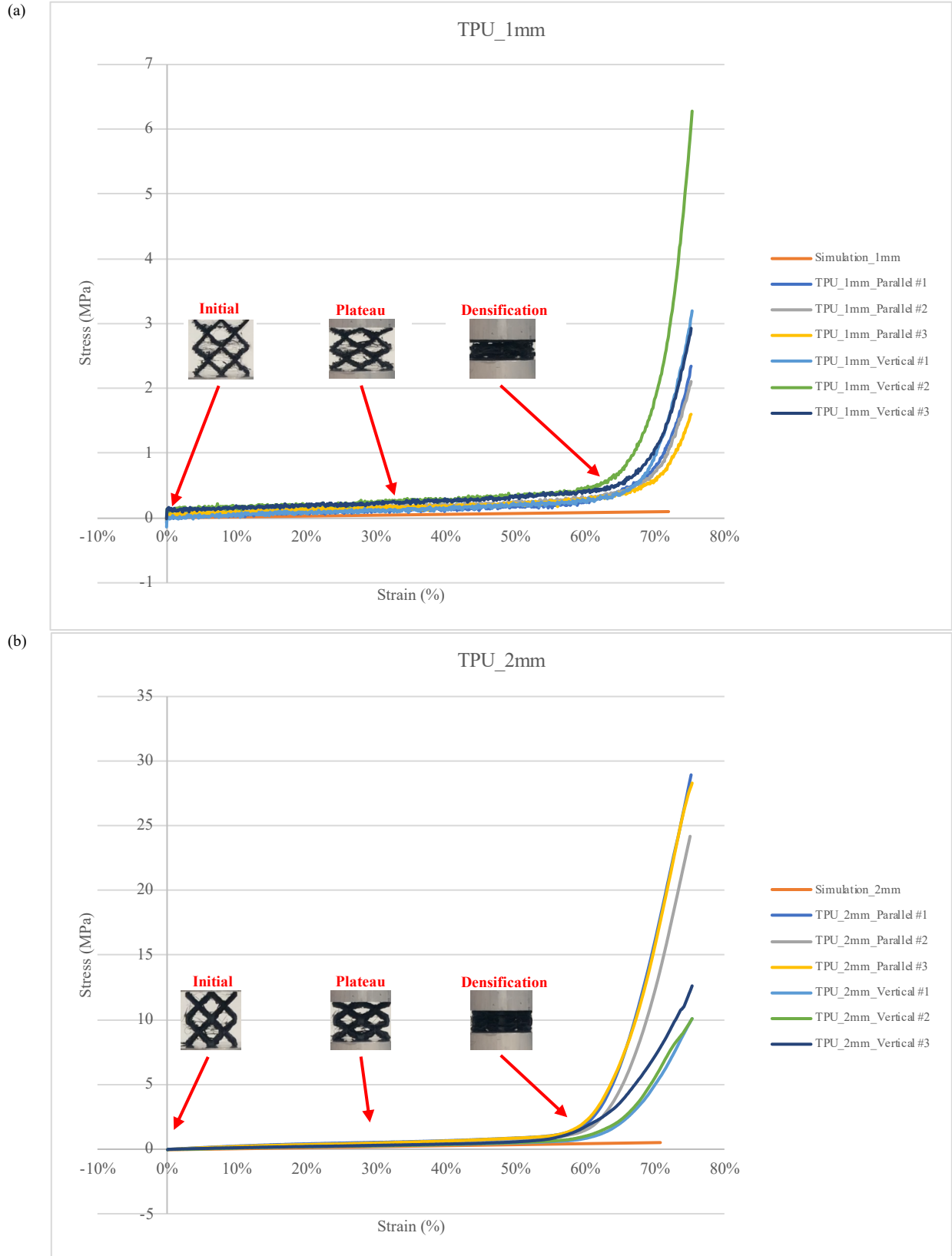


Figure 21 BCC (TPU) - Compression Test and Simulation Result: (a) 1mm truss diameter, (b) 2mm truss diameter

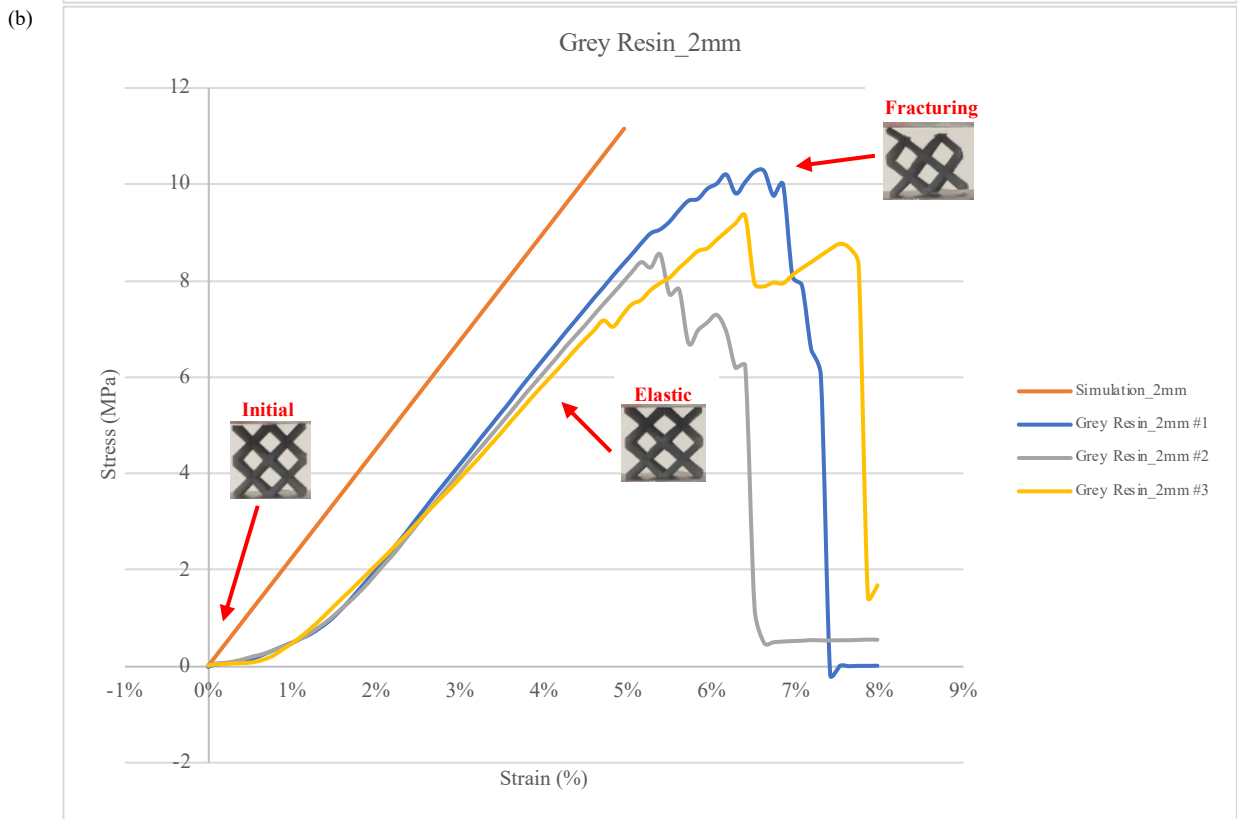


Figure 22 BCC (Grey Resin) - Compression Test and Simulation Result: (a) 1mm truss diameter, (b) 2mm truss diameter

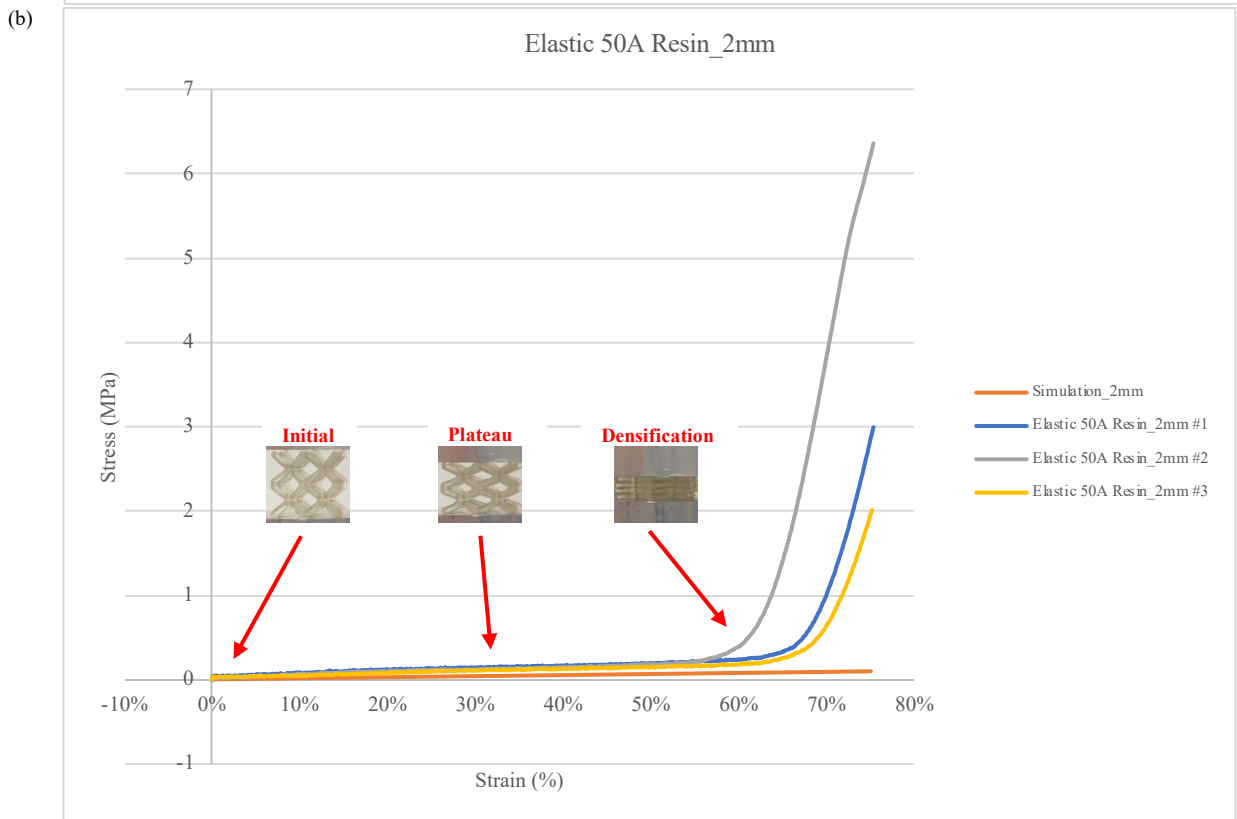
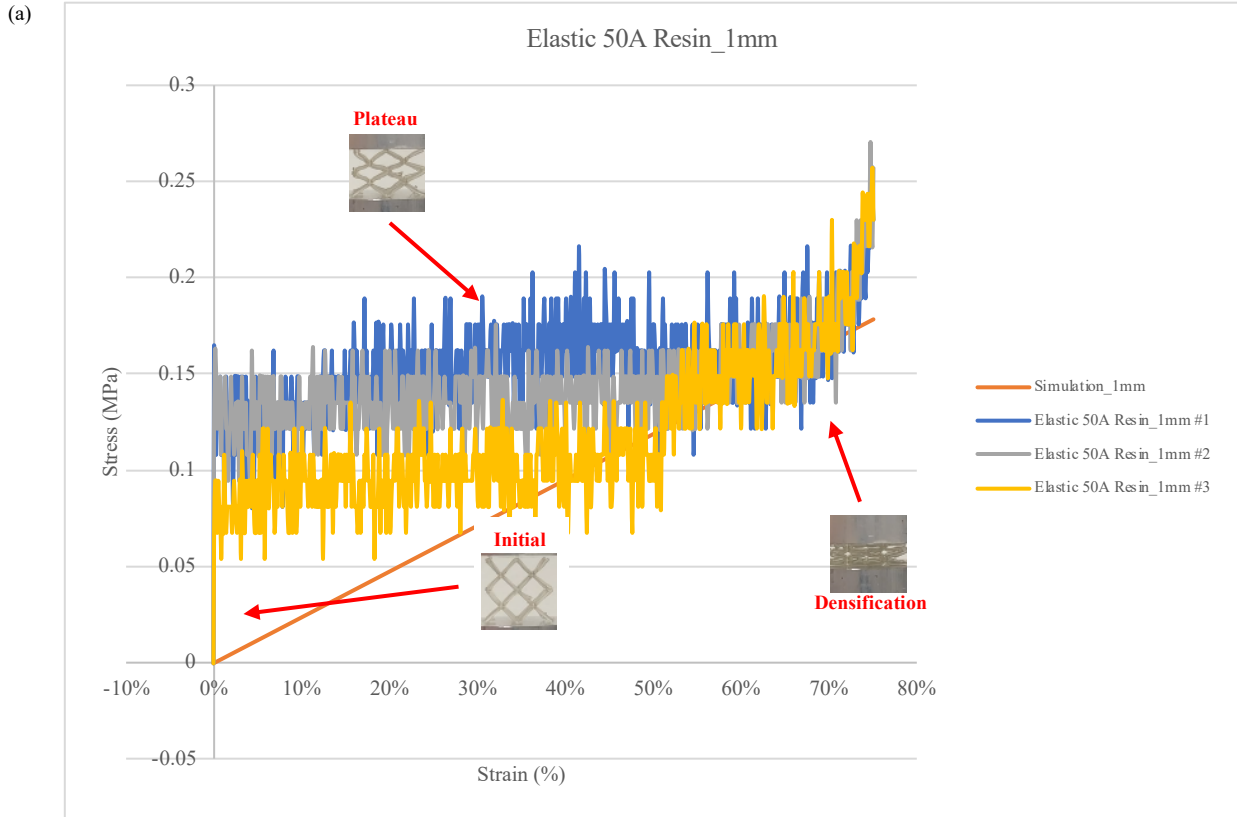


Figure 23 BCC (Elastic 50A Resin) - Compression Test and Simulation Result: (a) 1mm truss diameter, (b) 2mm truss diameter

3. Octahedron:

As shown in Fig. 23, in PLA, a sample with a truss diameter of 1mm exhibits maximum stress of about 80 MPa and 5% strain in the parallel layer direction and about 60 MPa maximum stress and 5% strain in the perpendicular direction. Both show similar mechanical behavior and fracture into small pieces after exceeding the maximum load. The 2mm truss diameter sample is less affected by the layer direction and shows about 100 MPa maximum stress and 7% strain. In the parallel layer direction, bending rapidly until a temporary stable state is reached after exceeding the maximum load. The load increases until reaching the next maximum load, and then the second buckling occurs until densification. In the perpendicular direction, the sample shows faster buckling but then exhibits behavior more similar to a platform until densification occurs. Additionally, the elastic behavior of the 1mm and 2mm samples is similar to the simulation. TPU samples with 1mm and 2mm truss diameters exhibit similar but not identical mechanical behavior, with elastic and plateau behavior before densification occurs. The 1mm truss diameter sample exhibits slightly higher elastic and more pronounced buckle behavior than the simulation, with stress and strain of about 1 MPa and 6%, respectively, while the 2mm truss diameter one exhibits linear elastic behavior and plateau behavior with maximum stress and strain of about 4 MPa and 17%, respectively, as shown in Fig. 24. Samples with 1mm and 2mm truss diameters exhibit rigid behavior in the Grey resin material, as shown in Fig. 25. After experiencing elastic behavior until reaching the maximum load, they immediately fracture into small pieces and lose load-bearing capacity, with stress values of around 65 MPa and 90 MPa, respectively. It is worth noting that although the maximum load of the 2mm truss diameter sample is 1.5 times that of the 1mm truss diameter sample, their strains are both around 6%, indicating that increasing the truss diameter increases the stiffness of the structure. Fig. 26 shows the mechanical behavior of the Elastic 50A resin in this structure, which is similar to TPU. For samples with 1mm diameter, a slight buckle occurred after elastic behavior until reaching the maximum stress of 0.5 MPa with 15% strain until densification occurred. For the 2mm truss diameter, after experiencing elastic behavior until reaching the maximum stress of 0.5 MPa with 20% strain, a plateau was observed until densification occurred. Additionally, due to the unstable mechanical properties of the LS, the 1mm truss diameter sample exhibited a serration behavior.

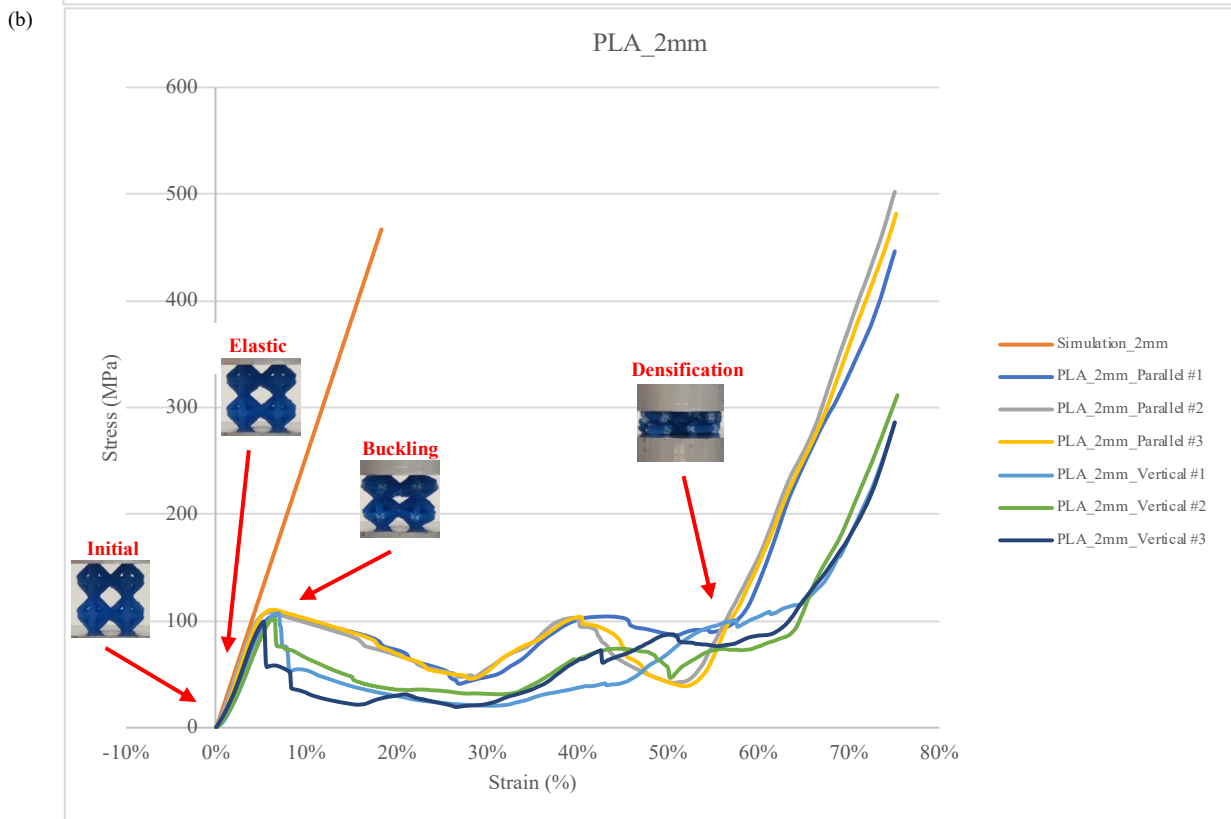
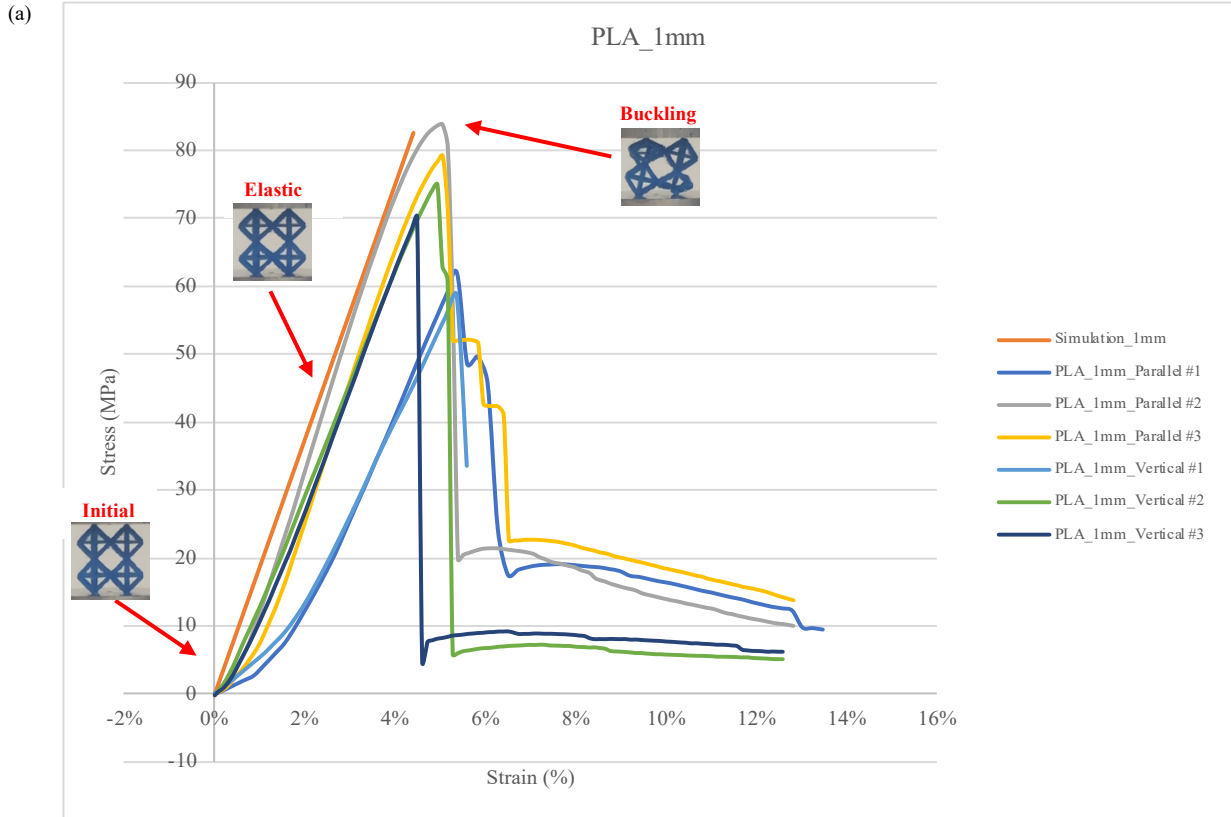


Figure 24 Octahedron (PLA) - Compression Test and Simulation Result: (a) 1mm truss diameter, (b) 2mm truss diameter

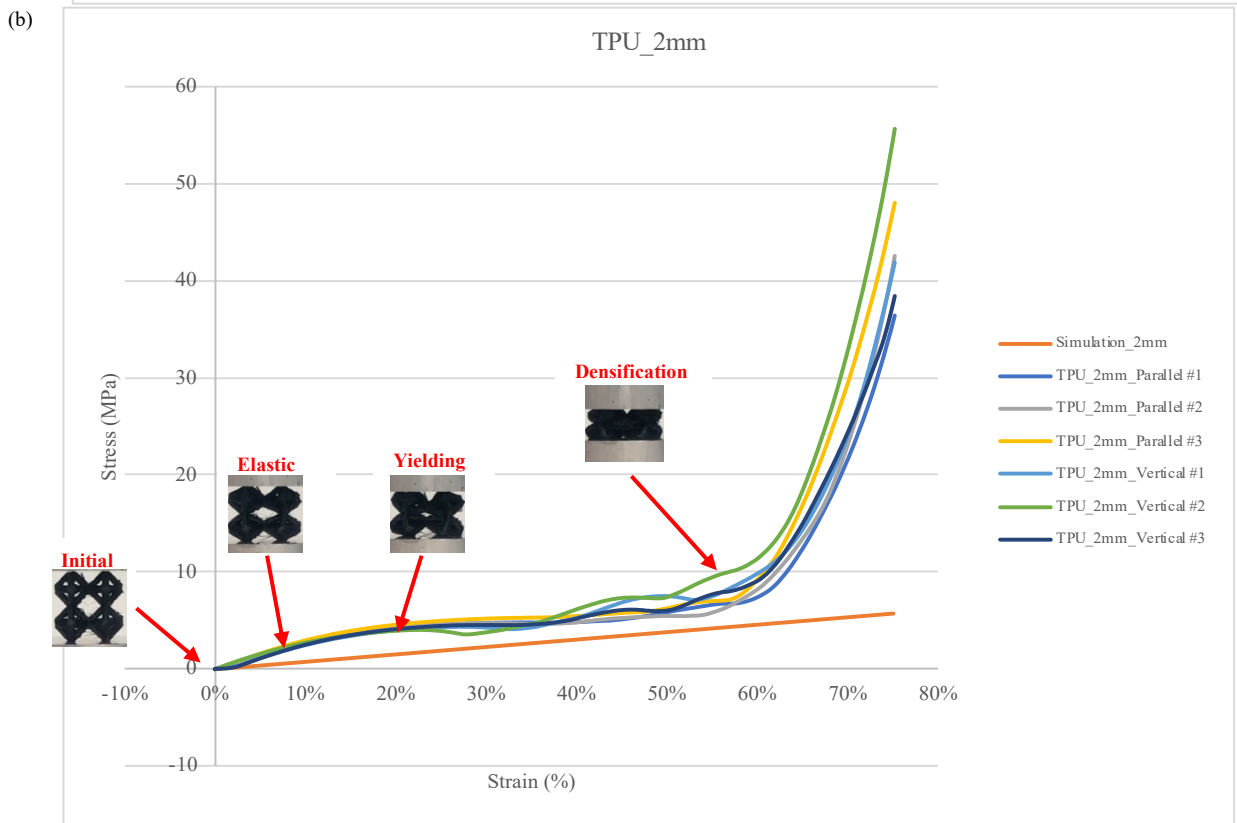
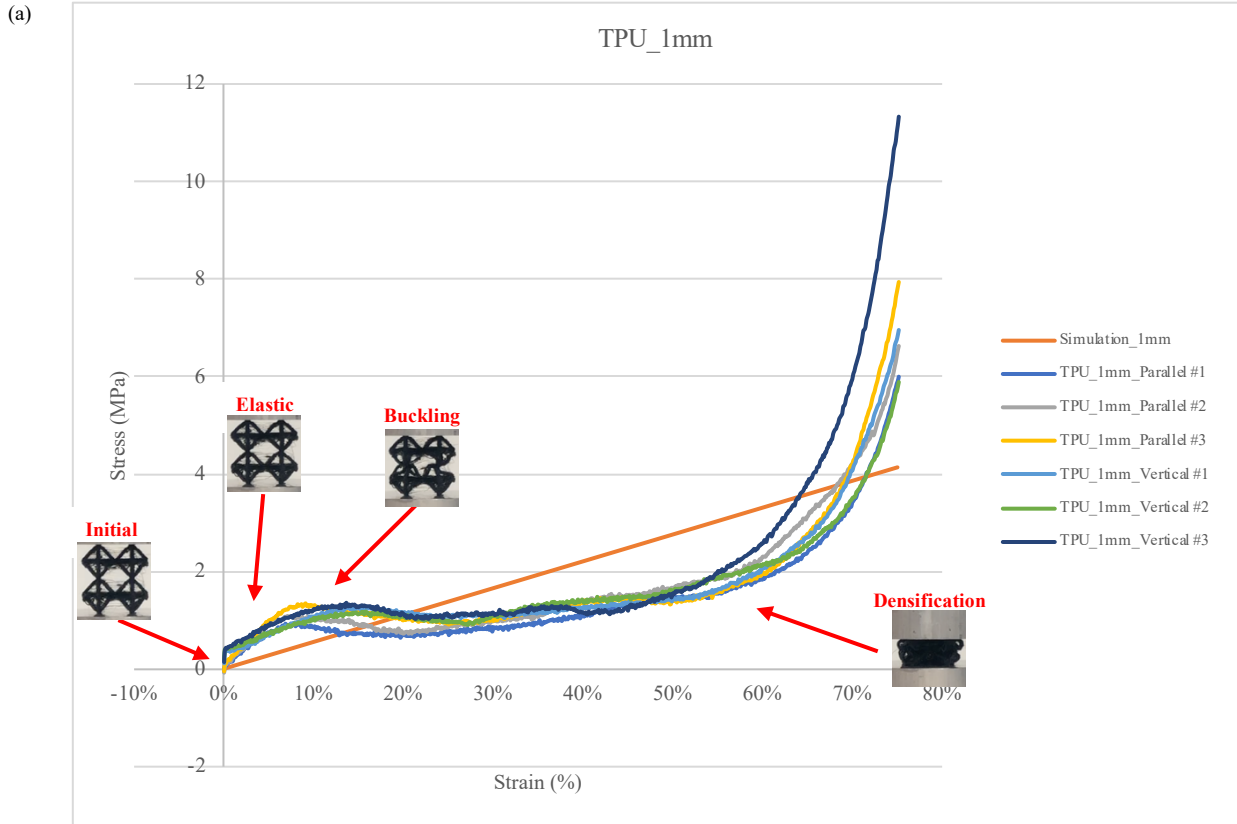


Figure 25 Octahedron (TPU) - Compression Test and Simulation Result: (a) 1mm truss diameter, (b) 2mm truss diameter

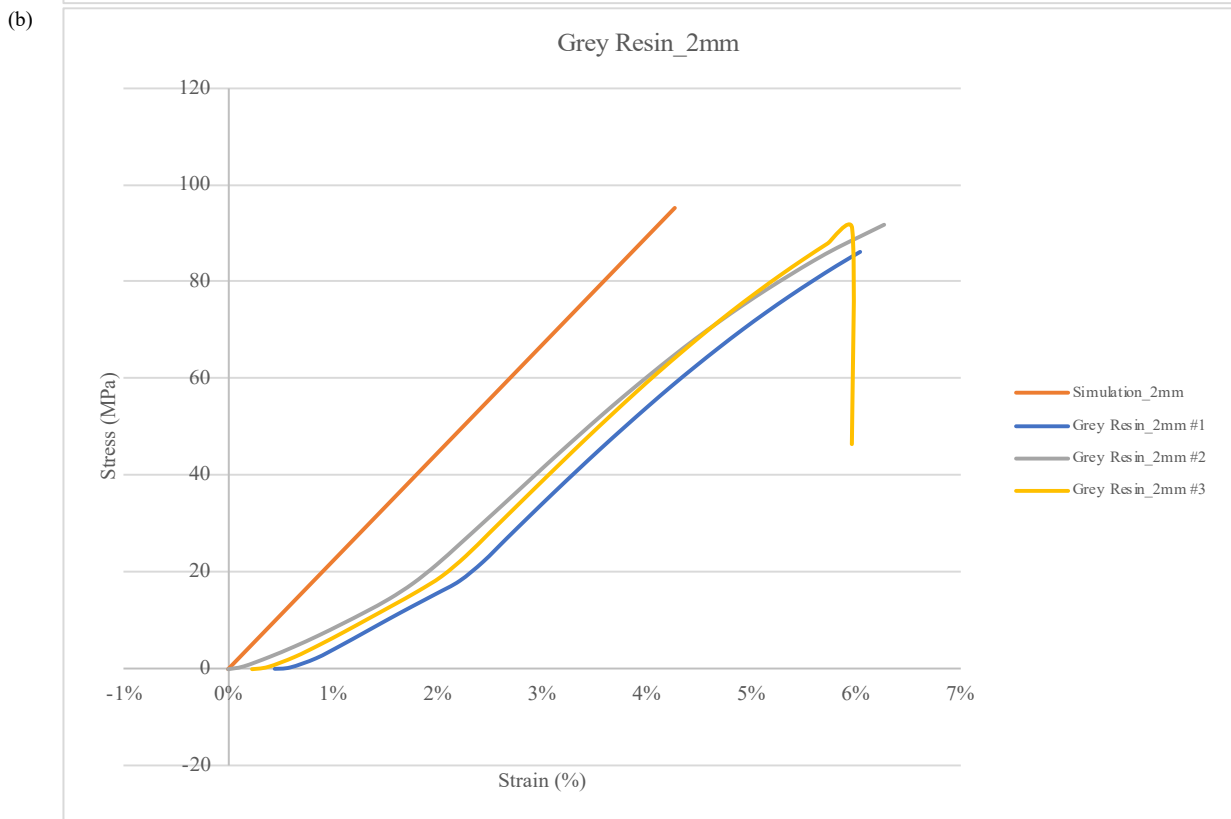
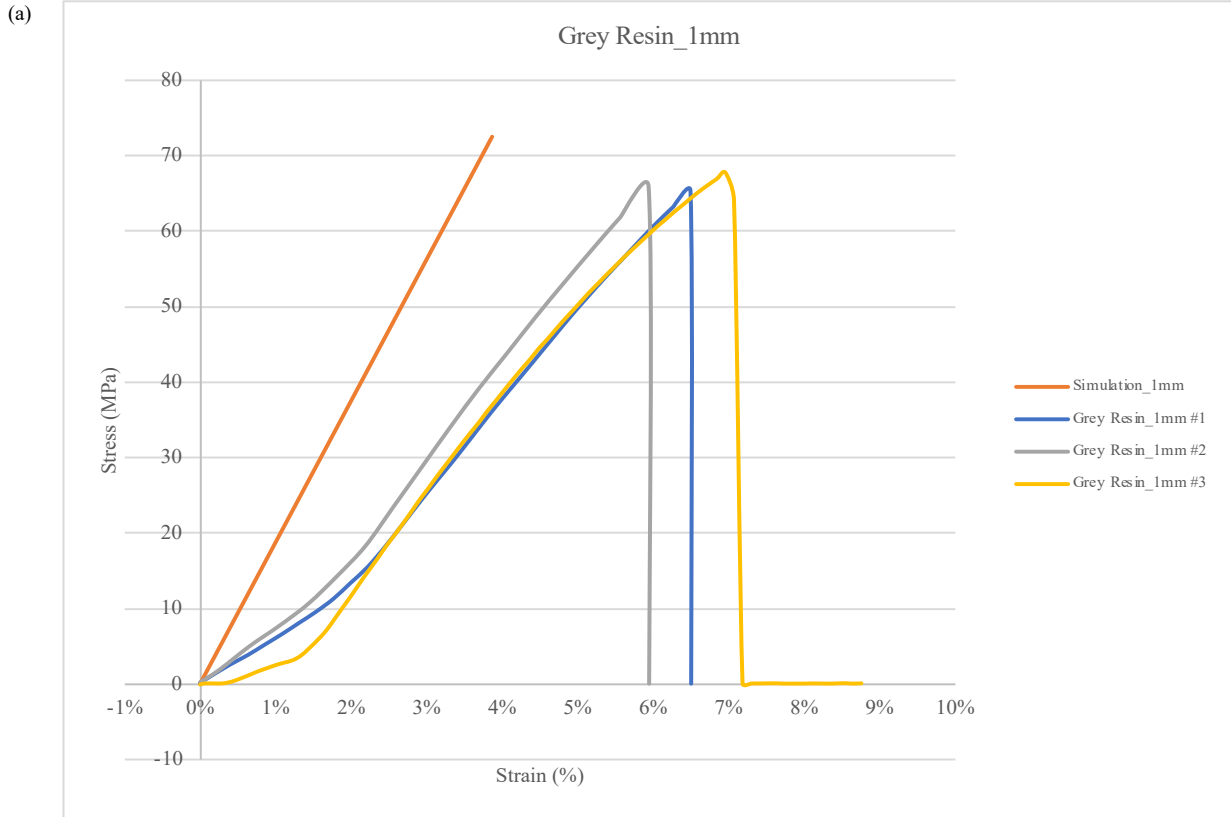


Figure 26 Octahedron (Grey Resin) - Compression Test and Simulation Result: (a) 1mm truss diameter, (b) 2mm truss diameter

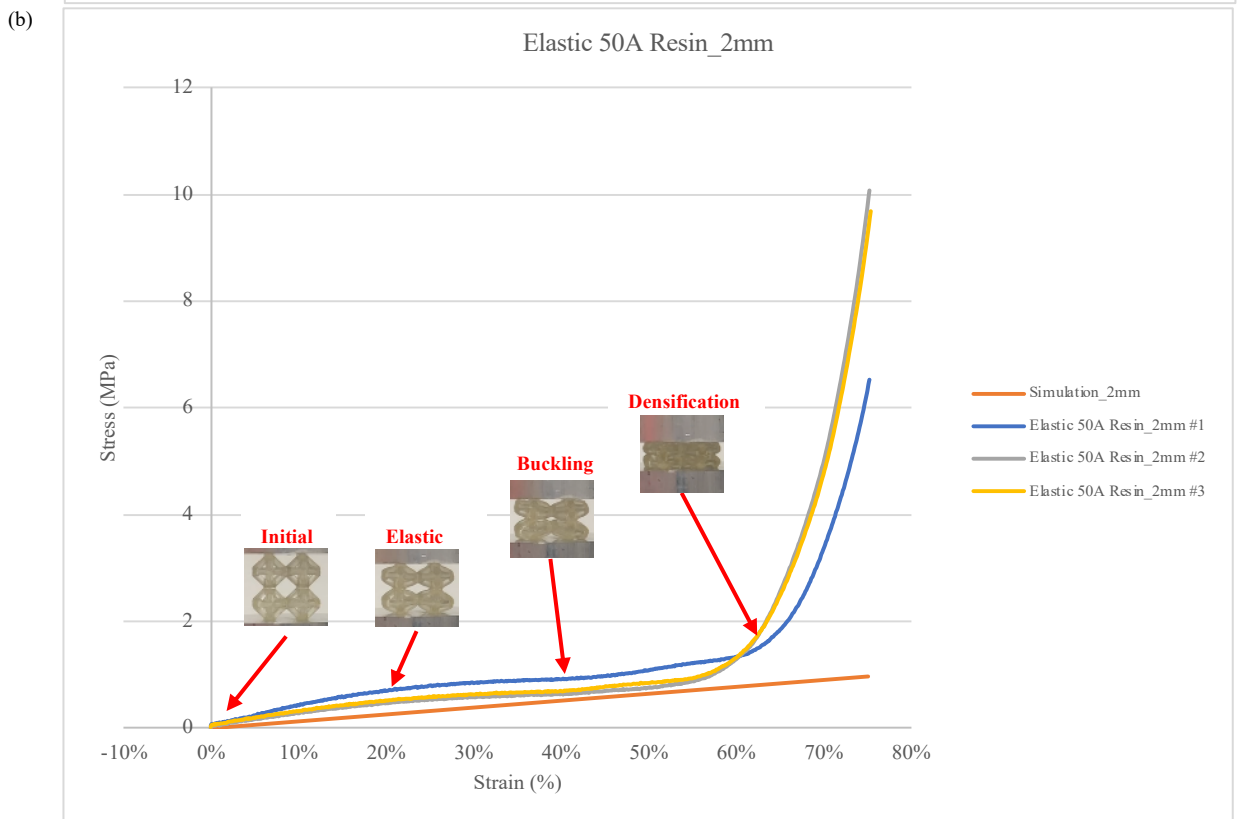
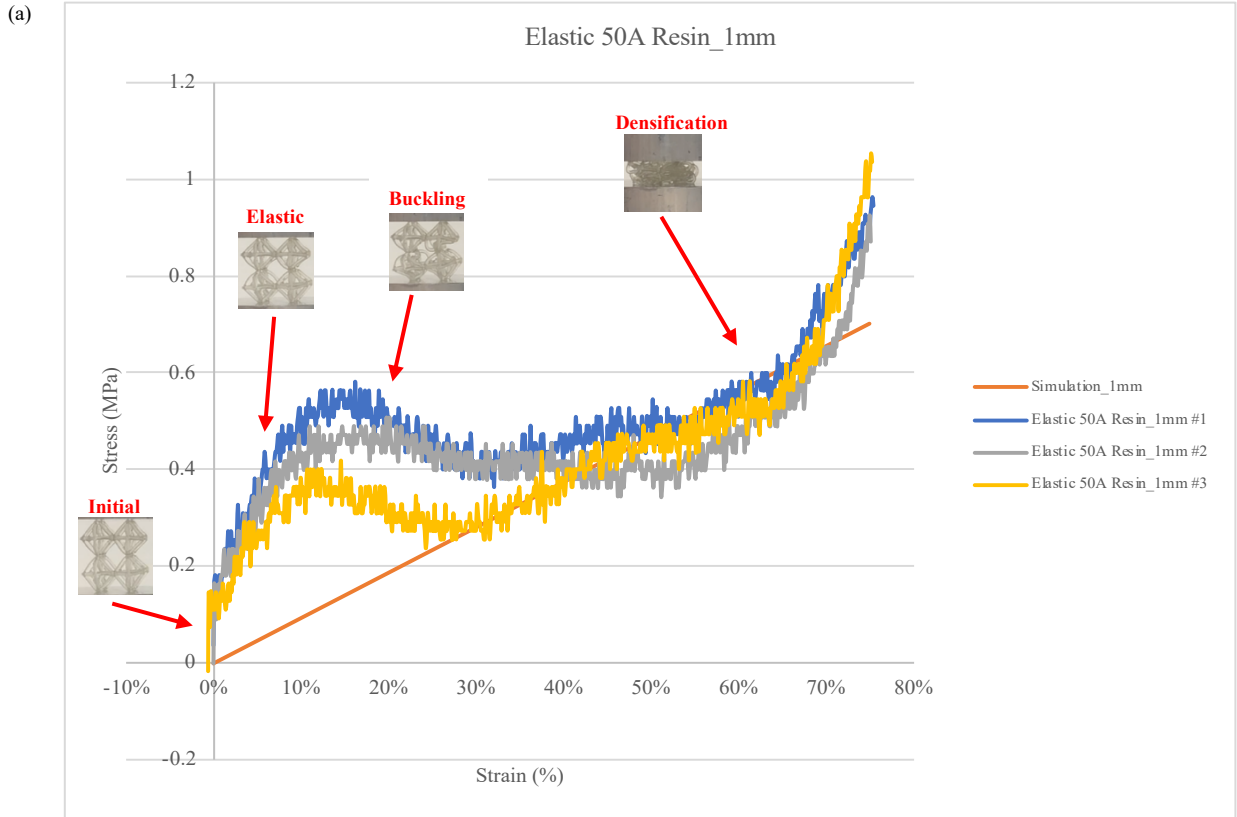


Figure 27 Octahedron (Elastic 50A Resin) - Compression Test and Simulation Result: (a) 1mm truss diameter, (b) 2mm truss diameter

4. Cross Cube + BCC:

For specimens with a 1mm diameter in PLA, the maximum stress and strain are about 80 MPa and 10% for the parallel layer. It initially exhibits an elastic behavior similar to the simulation results and then starts to bend after reaching the maximum stress. When the layer is perpendicular to the loading plate, the maximum stress drops to around 45 MPa, and the strain is about 20%. It shows a brief elastic behavior until it exceeds the maximum load. Then, it exhibits oscillating plateau behavior until densification. For the 2 mm truss diameter parallel layer one, the stress is about 80 MPa with 10% strain. It shows elastic behavior similar to the simulation results until plateau behavior occurs before densifying. When the layer is perpendicular to the plate, the maximum stress slightly decreases to 75 MPa with 7% strain. It initially exhibits elastic behavior similar to the simulation and undergoes brief plastic deformation. Then, buckling behavior occurred until densifying, as shown in Fig. 28. The sample in TPU with a 1mm truss diameter exhibits significant but brief elastic deformation, followed by yielding of samples parallel and perpendicular to the loading plate at about 9% and 15% strain, respectively, with 1.8 MPa. Although the elastic behavior is higher than the simulation results, the overall behavior follows the simulation results. The sample with a 2 mm truss diameter exhibits longer but less elastic deformation, followed by the onset of plastic behavior at a stress of 6 MPa and strain of 25%, with plateau behavior in perpendicular to the loading plate before densification occurs. The overall behavior is similar to the simulation, as shown in Fig. 29. In Grey Resin material, with stress reaching 55 MPa and 65 MPa for 1 mm and 2 mm diameter samples, respectively, after exhibiting elastic behavior similar to the simulation, followed immediately by fracture into small pieces and loss of load-bearing capacity. Although the maximum stress of the 2mm sample is higher than the 1 mm one, its strain is approximately 8%. This indicates that increasing the truss diameter will increase the stiffness, as shown in Fig. 30. The mechanical behavior of Elastic 50A resin is shown in Fig. 31. For the sample with a diameter of 1mm, a buckling occurs after the elastic behavior exceeds the stress, 0.3 MPa with 10% strain, followed by a platform behavior until densification occurs. On the other hand, the truss specimens with a diameter of 2mm exhibit elastic behavior with a strain of nearly 30% until exceeding the yield point and reaching the maximum stress, 0.8 MPa, followed by a platform phenomenon until densifying.

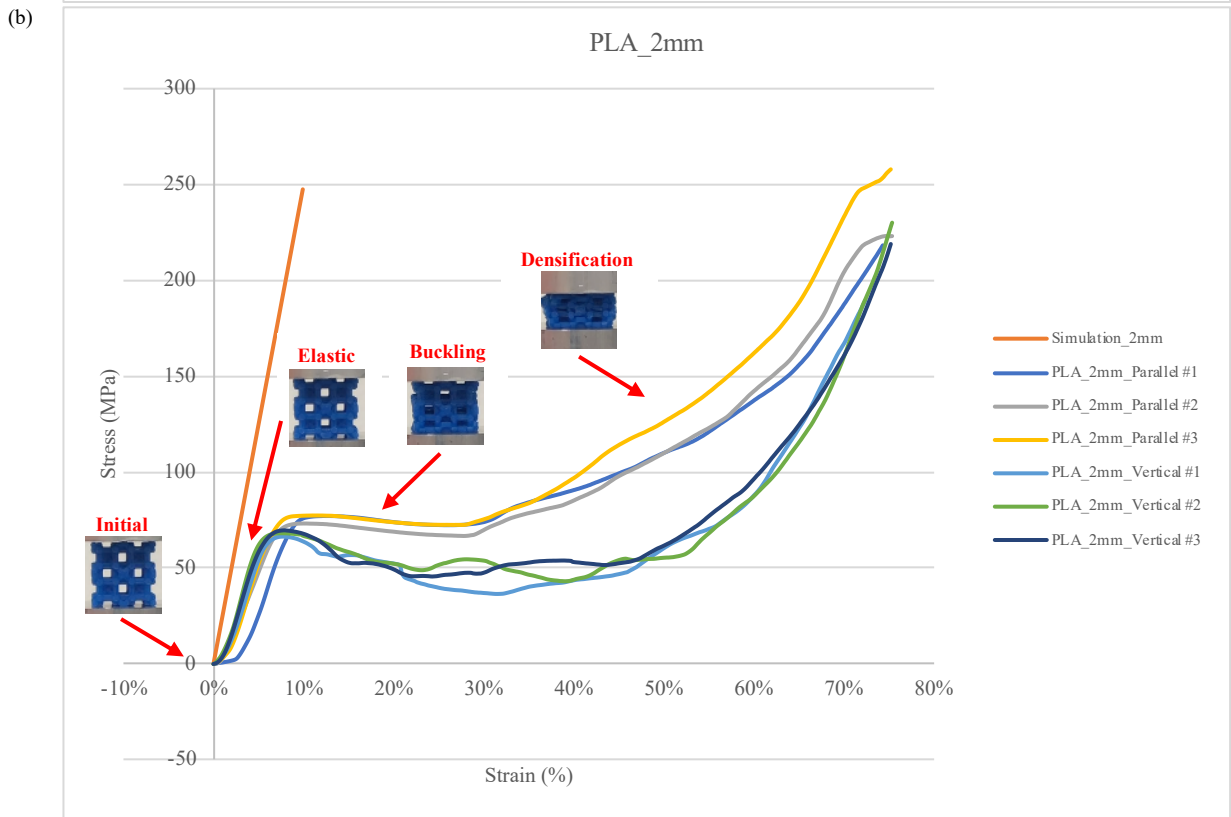
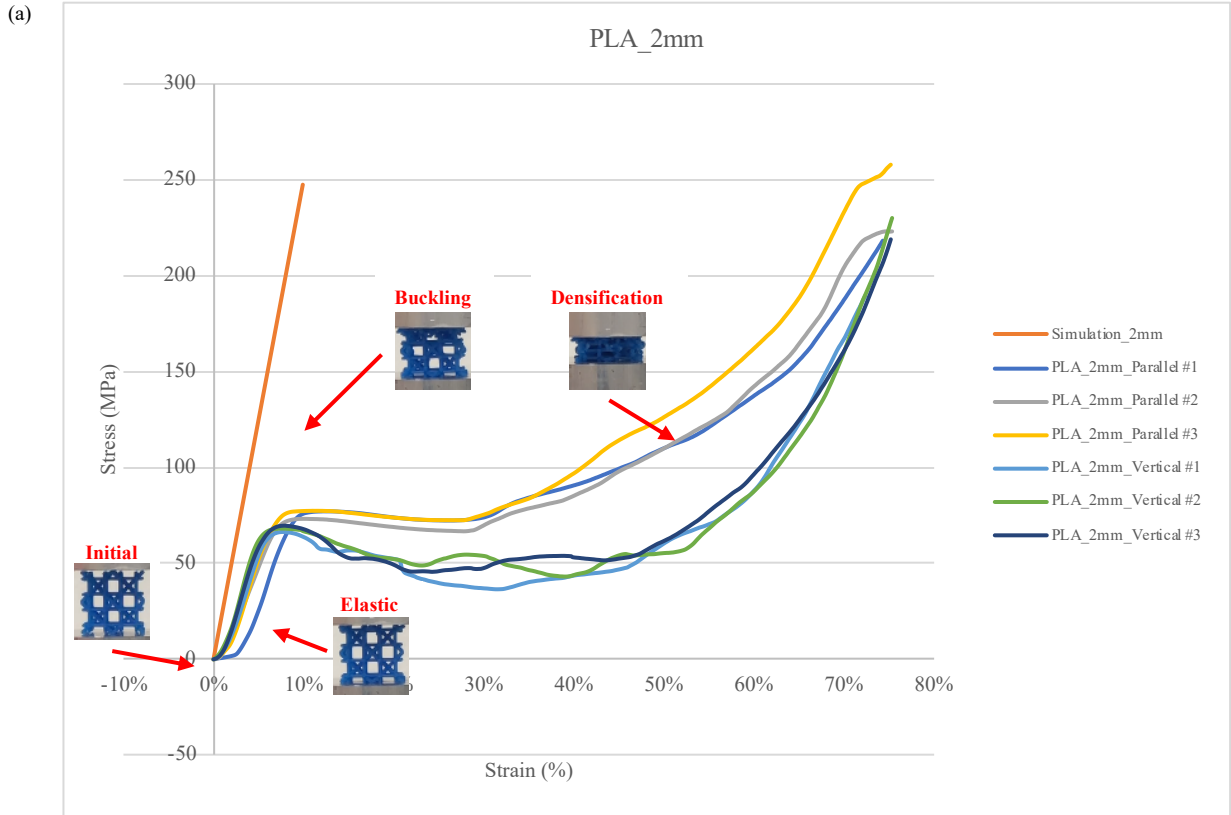


Figure 28 Cross Cube + BCC (PLA) - Compression Test and Simulation Results: (a) 1mm truss diameter, (b) 2mm truss diameter

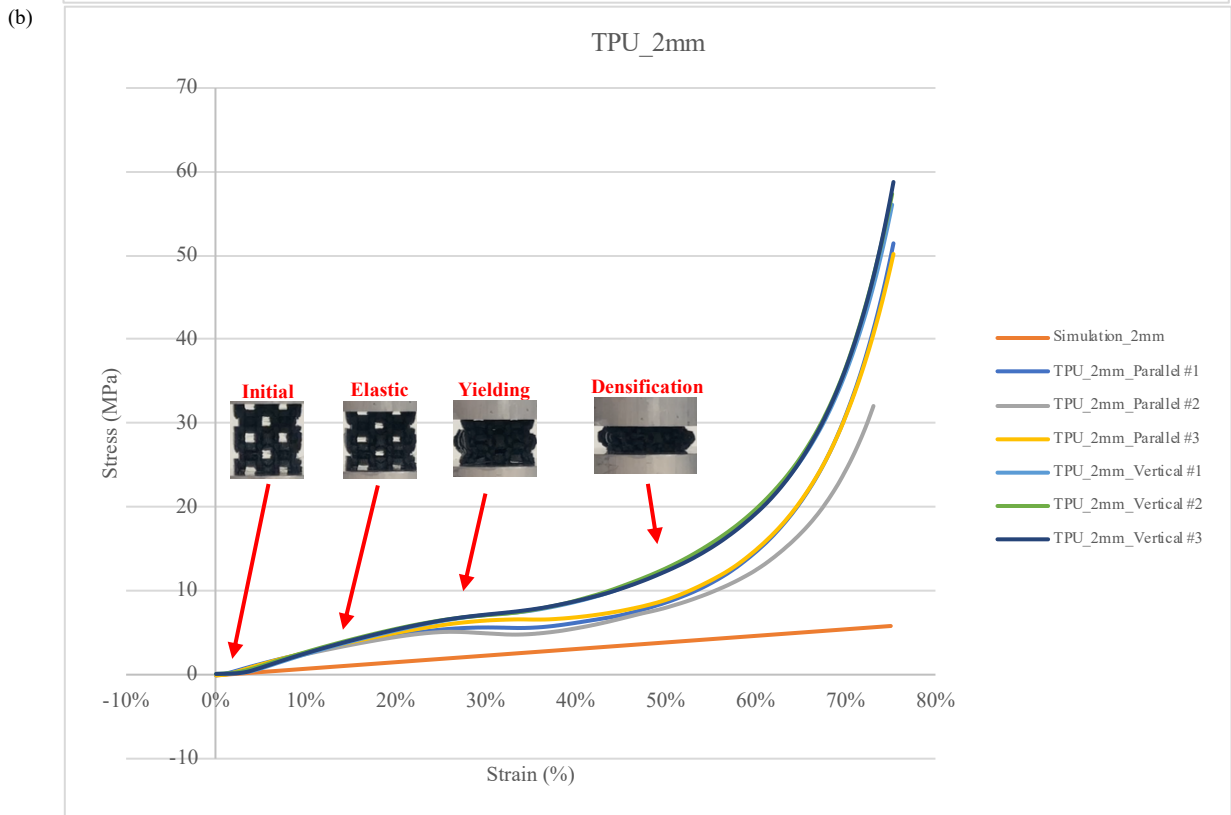
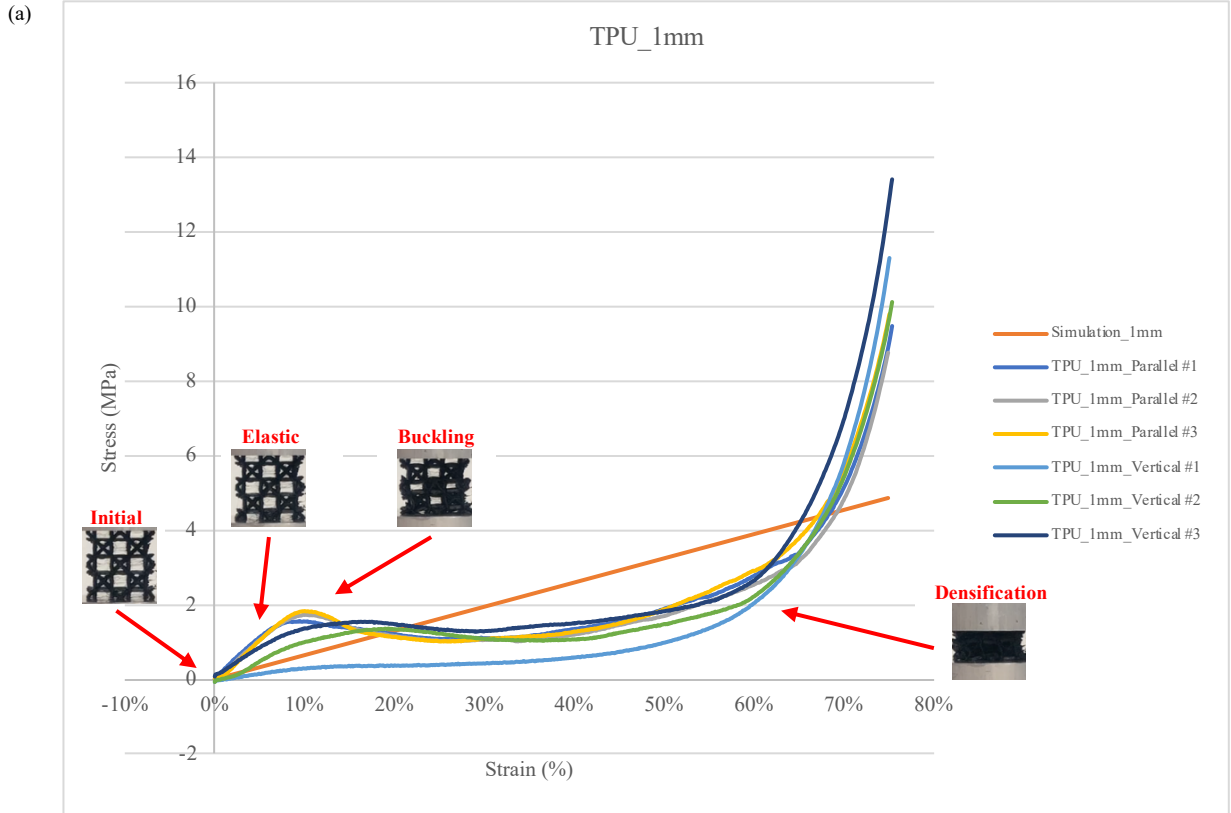


Figure 29 Cross Cube + BCC (TPU) - Compression Test and Simulation Results: (a) 1mm truss diameter, (b) 2mm truss diameter

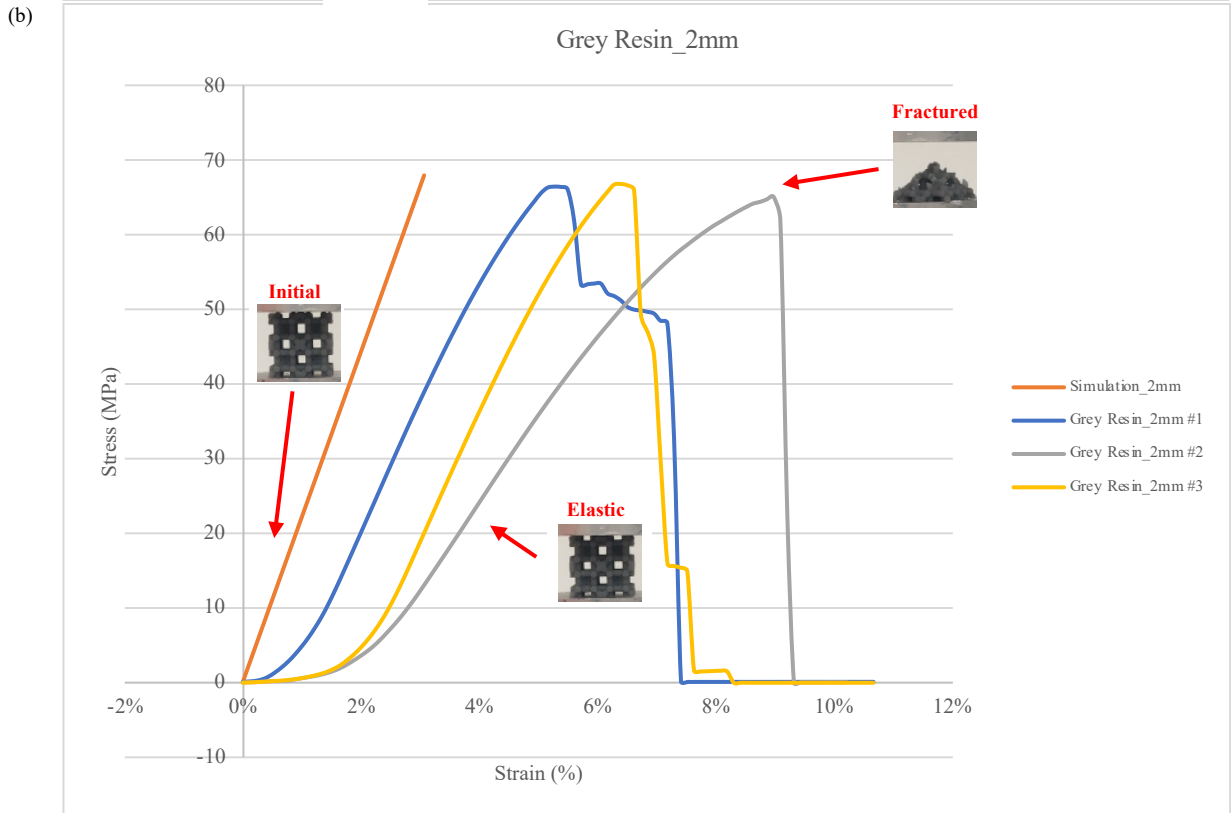
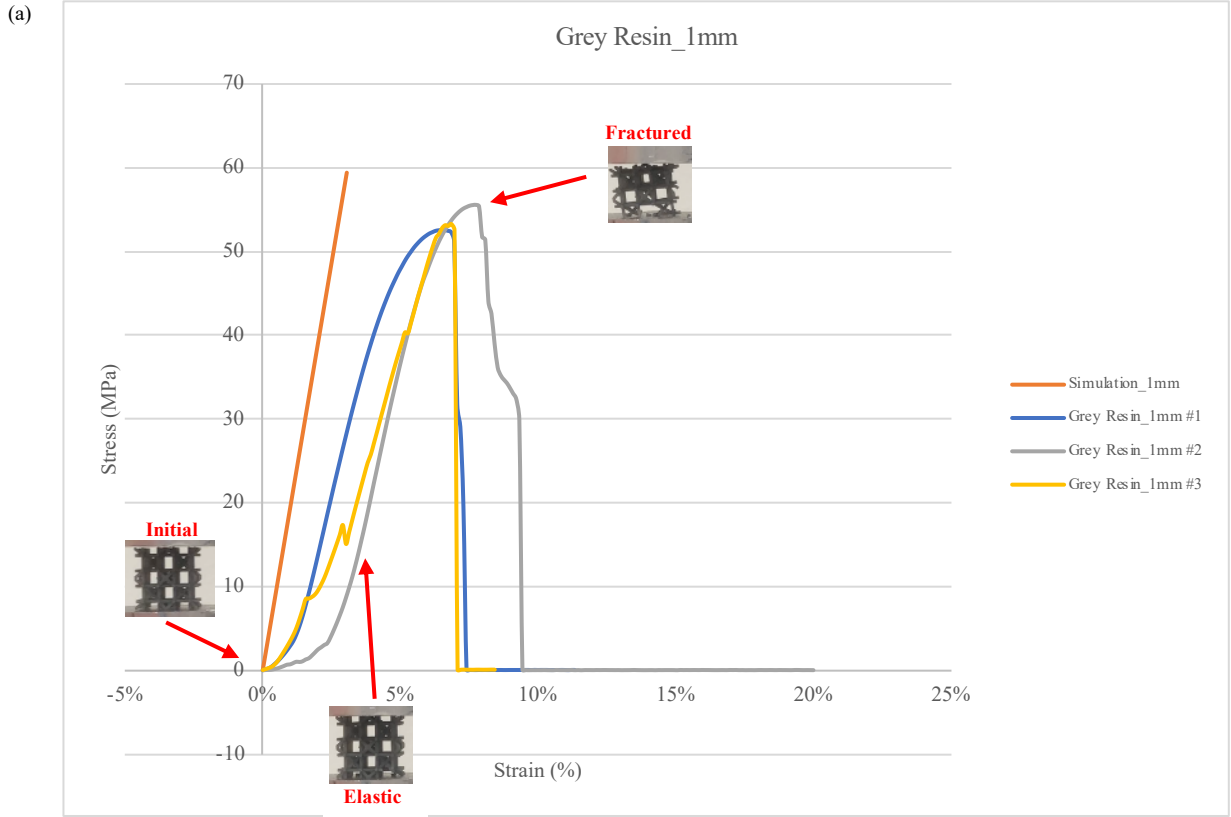


Figure 30 Cross Cube + BCC (Grey Resin) - Compression Test and Simulation Results: (a) 1mm truss diameter, (b) 2mm truss diameter

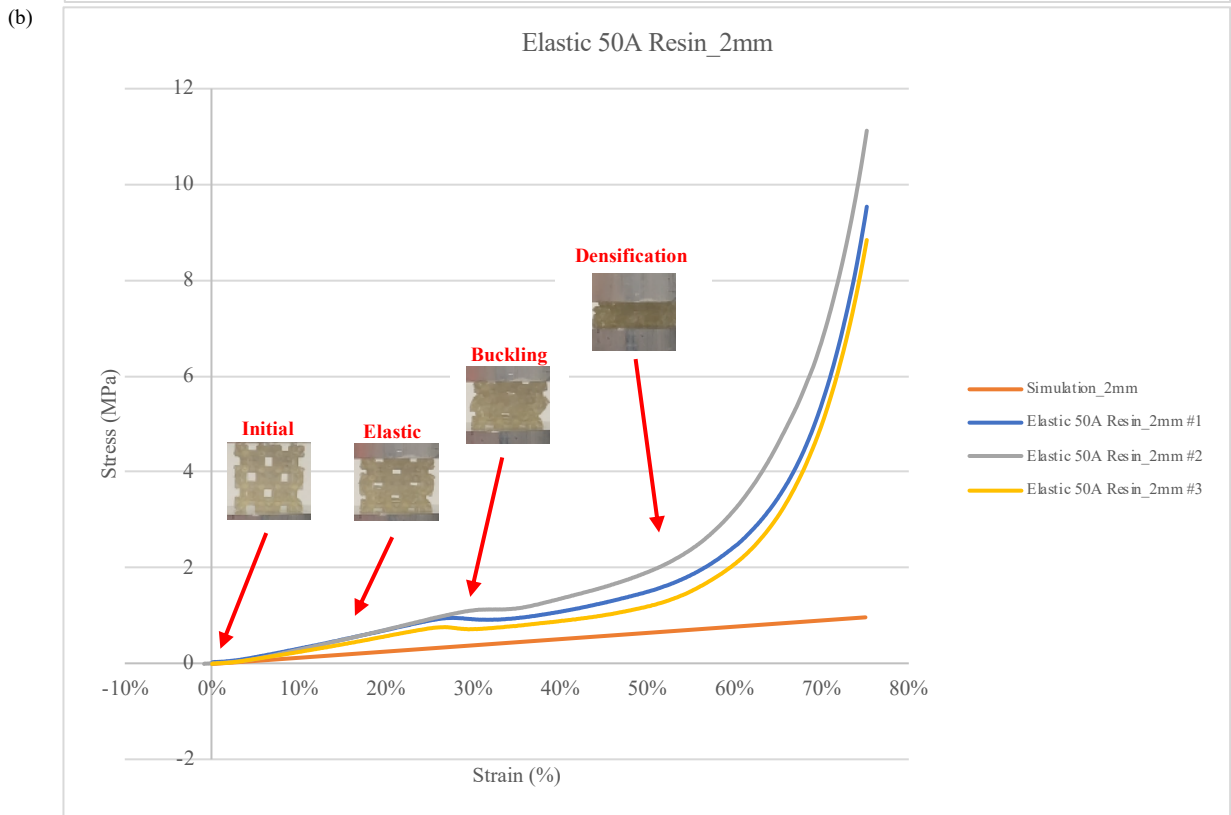
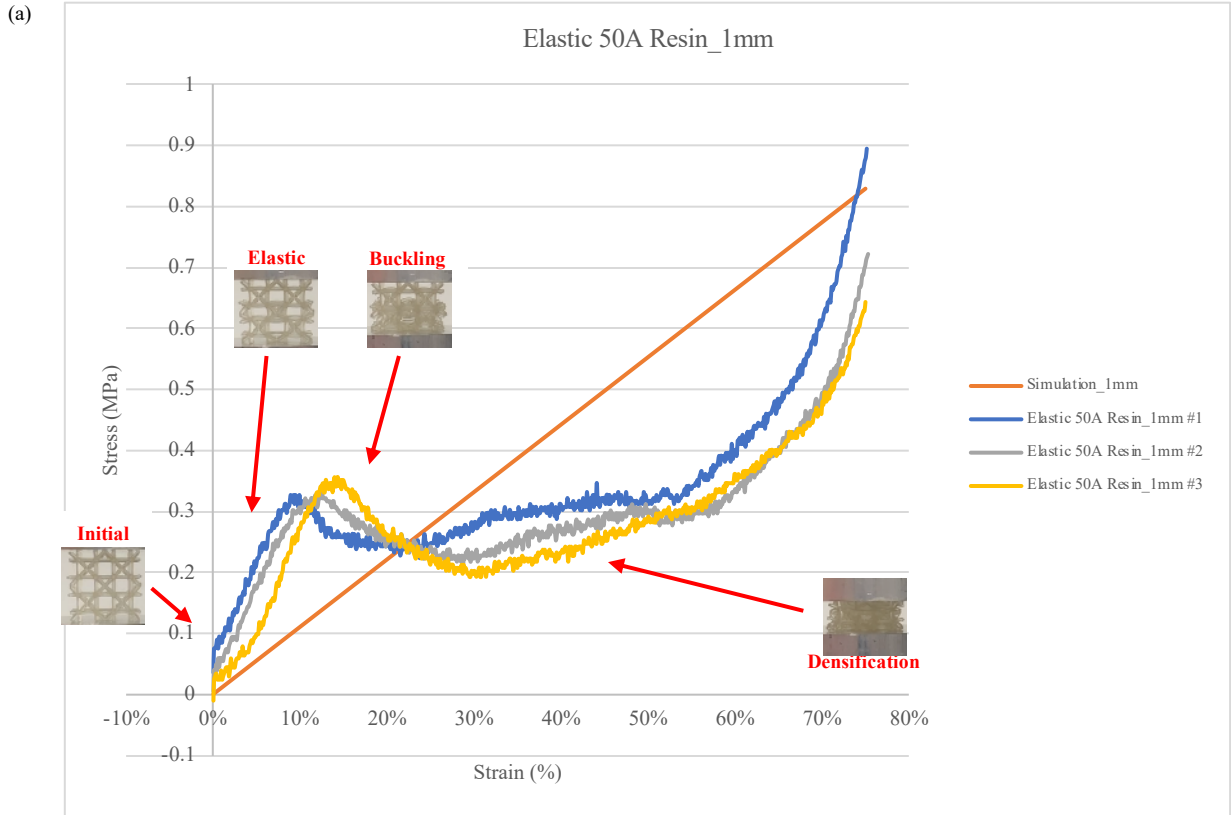


Figure 31 Cross Cube + BCC (Elastic 50A Resin) - Compression Test and Simulation Results: (a) 1mm truss diameter, (b) 2mm truss diameter

5. Cross Cube + Octahedron:

For PLA material, with a 1 mm truss diameter, when the layer is oriented parallel to the loading plate, the maximum stress is 82 MPa with 10% strain. When the layer is oriented perpendicular to the loading plate, the maximum stress is 60 MPa with 10% strain. Both exhibit elastic behavior similar to the simulation result and begin to bend after surpassing the yield point until densification occurs. The 2 mm truss diameter samples are less affected by the direction and show elastic behavior similar to the simulation results. When extended to 10% strain and loaded beyond the yield point to reach maximum stress of 100 MPa, they exhibit plateau behavior until densification occurs, as shown in Fig. 32. The mechanical properties of TPU samples are not significantly affected by the orientation of the layers, shown in Fig. 33. Samples with 1mm truss diameter exhibit significant but short elastic deformation, followed by maximum stress at 2 MPa with 10% and 15% strain for the parallel and vertical sampled respectively. Although the elastic behavior is slightly higher than predicted by the simulation, the overall mechanical behavior follows the simulation results. The samples undergo long periods of plastic deformation before beginning to densify. Samples with a 2 mm truss diameter exhibit longer but less significant elastic deformation, followed by maximum stress at 1.5 MPa with 25% strain. After the plateau behavior, the samples begin to densify. The elastic behavior is slightly higher than the simulated results. Grey Resin material exhibited rigid behavior. After reaching the highest stress following elastic behavior and surpassing the yield point, both 1mm and 2mm samples underwent plastic deformation before reaching the maximum load, approximately 50 MPa and 85 MPa, respectively, with a strain of approximately 6%. Subsequently, the samples fractured, as shown in Fig. 34. 1mm and 2mm truss diameters samples in Elastic 50A Resin show similar mechanical behavior. The 1mm sample undergoes elastic behavior until reaching the yield point and the highest load, then exhibits a plateau until densification occurs at stress around 0.5 MPa with 12% strain. The 2mm sample shows less obvious elastic behavior until exceeding the yield point and reaching the highest stress, approximately 1.3 MPa with 27%, showing a similar plateau phenomenon until densification occurs, as shown in Fig. 35.

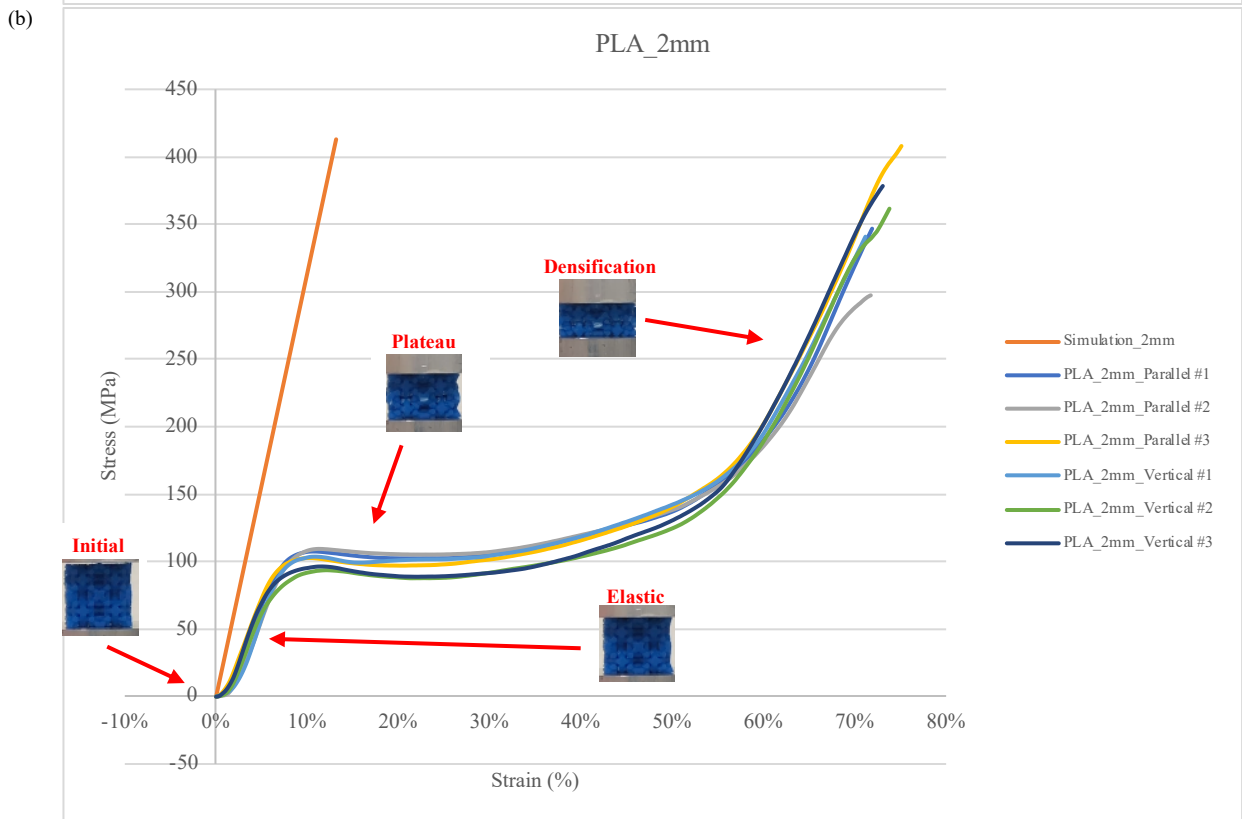
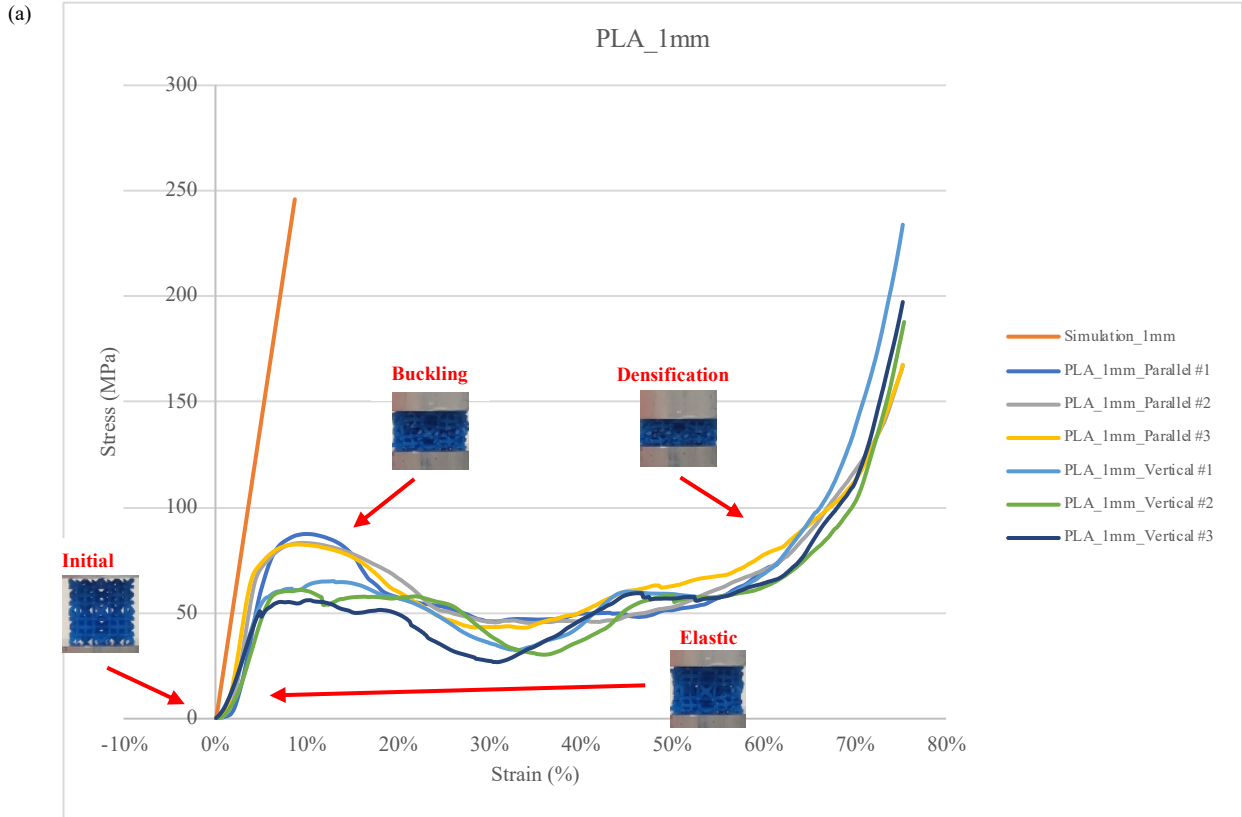


Figure 32 Cross Cube + Octahedron (PLA) - Compression Test and Simulation Results: (a) 1mm truss diameter, (b) 2mm truss diameter

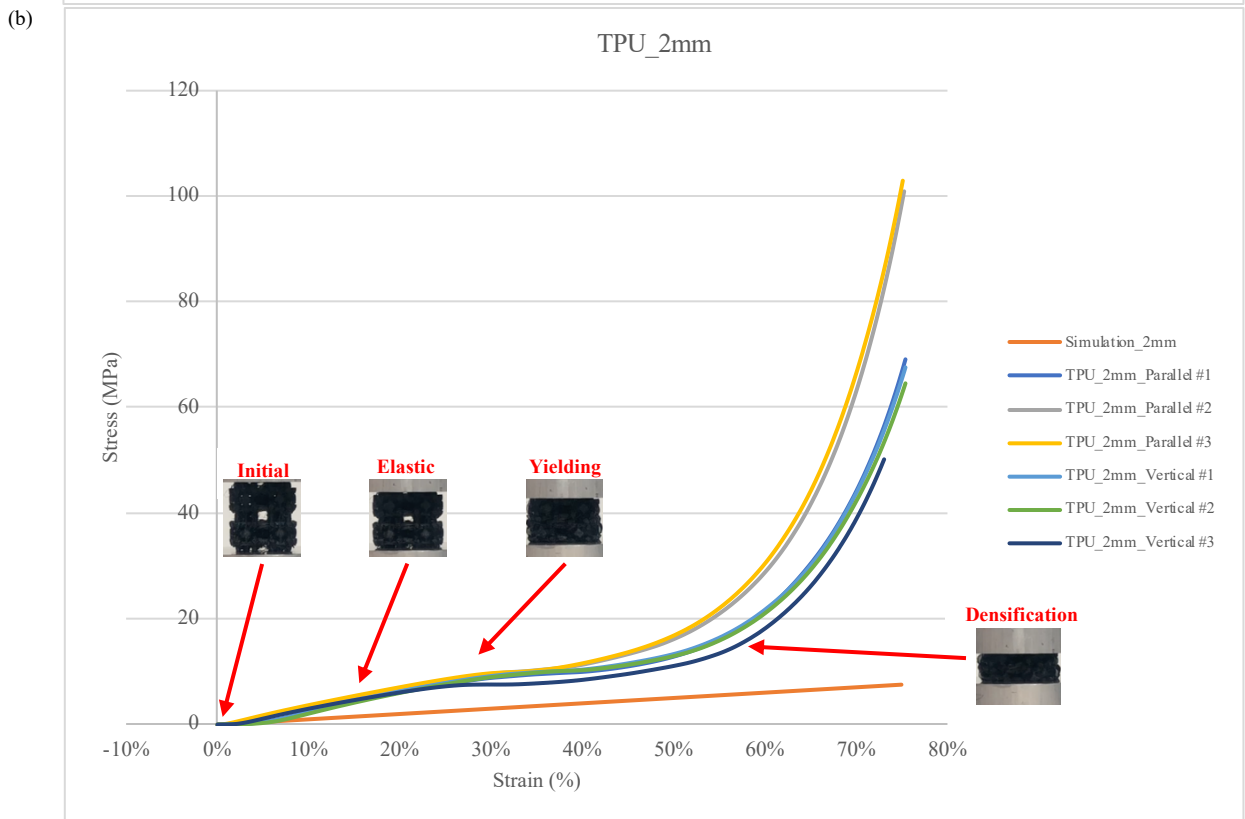
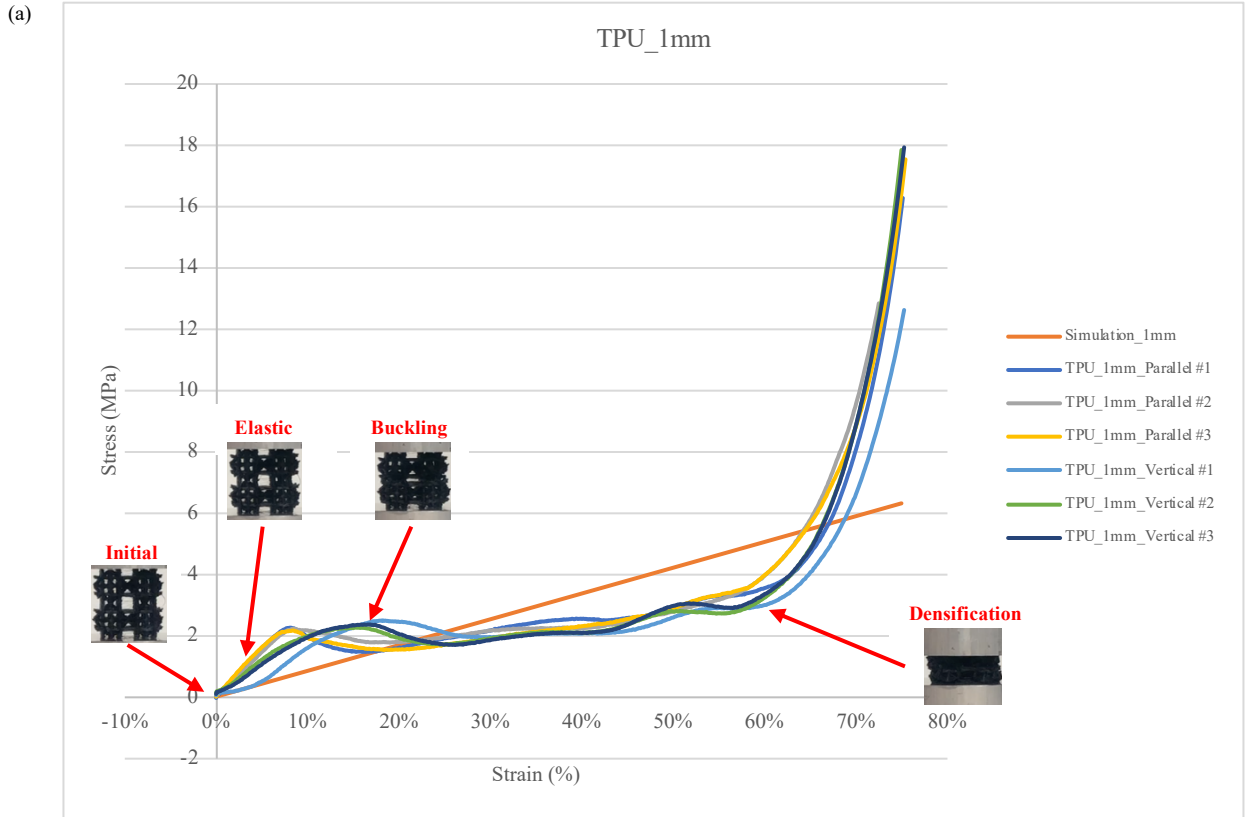


Figure 33 Cross Cube + Octahedron (TPU) - Compression Test and Simulation Results: (a) 1mm truss diameter, (b) 2mm truss diameter

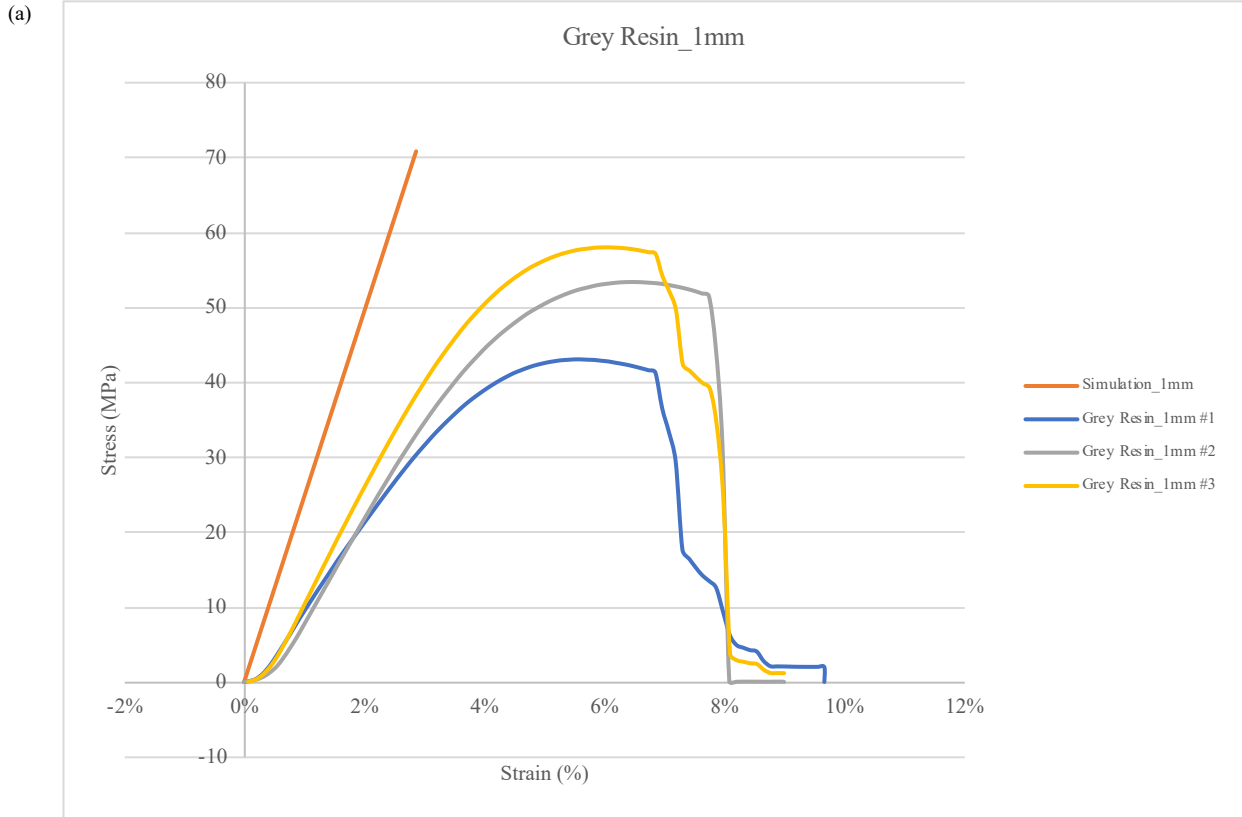


Figure 34 Cross Cube + Octahedron (Grey Resin) - Compression Test and Simulation Results: (a) 1mm truss diameter, (b) 2mm truss diameter

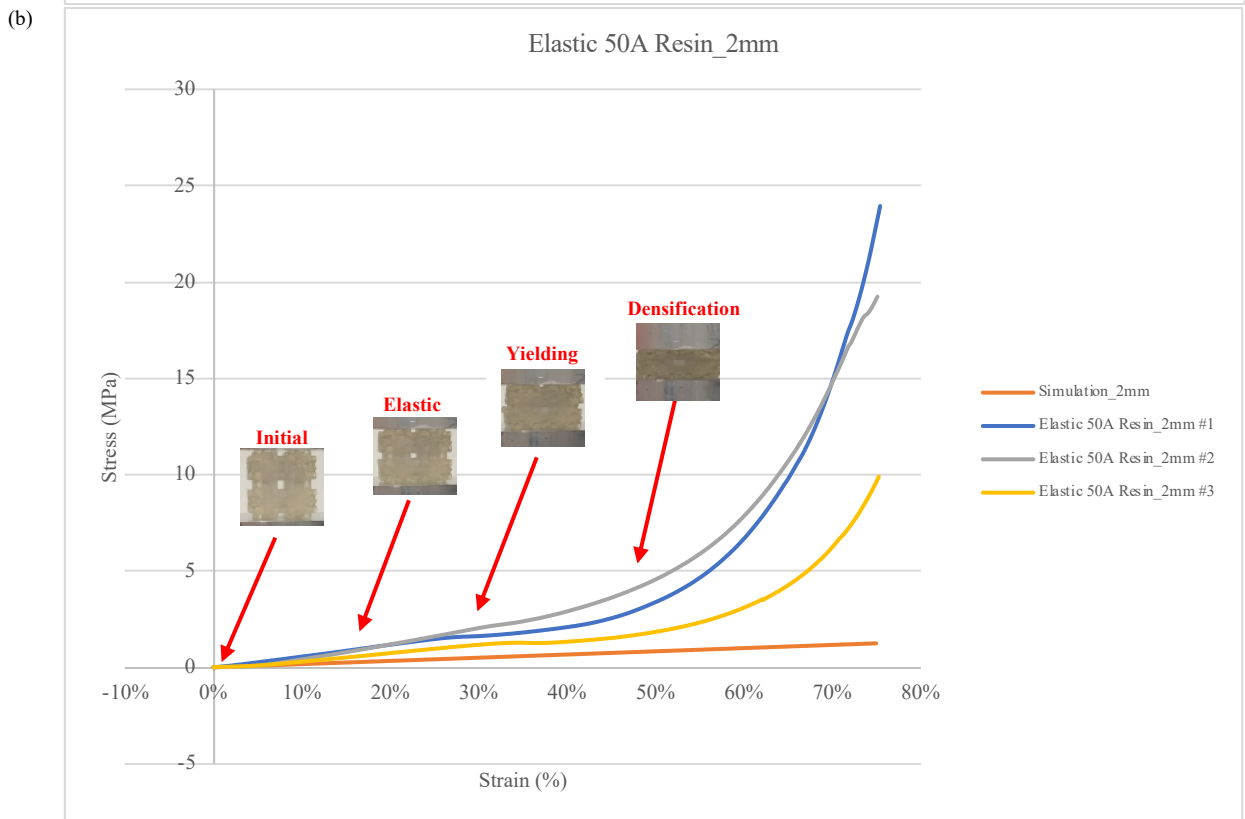
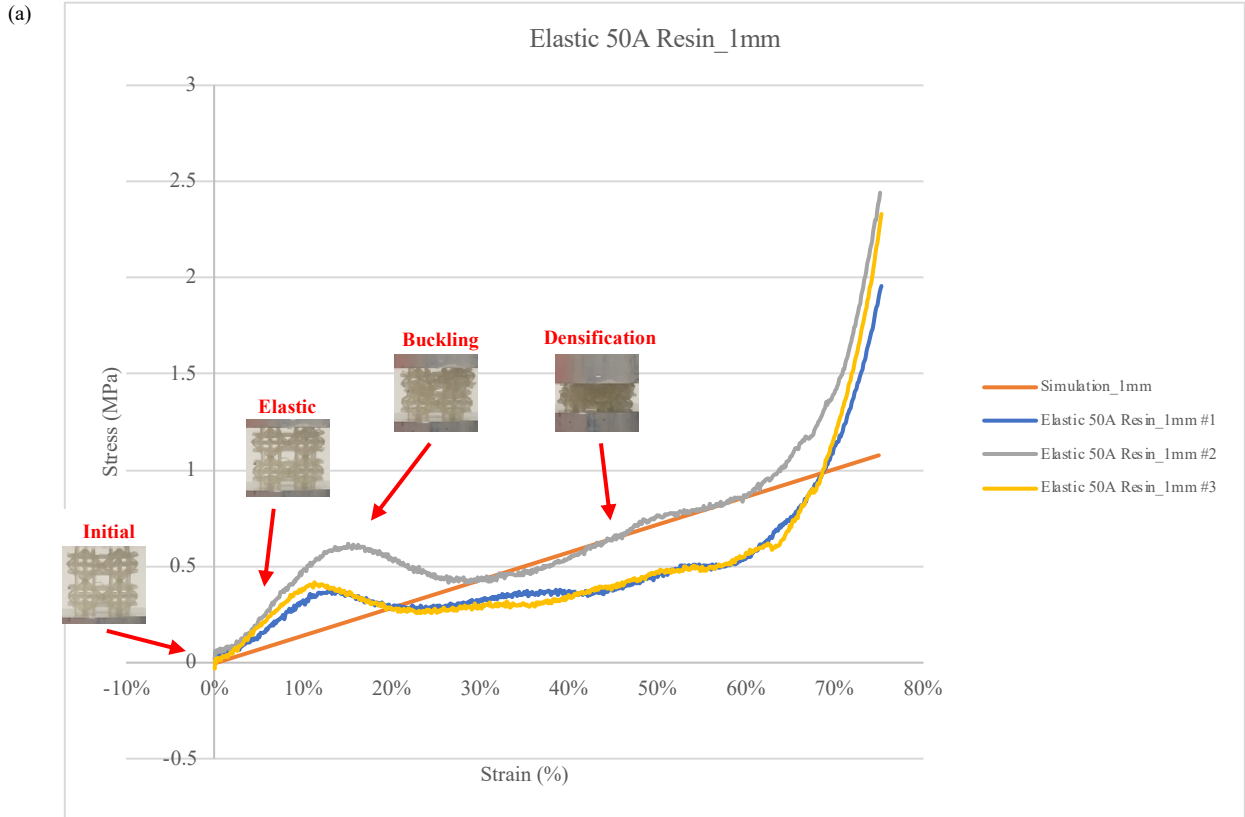


Figure 35 Cross Cube + Octahedron (Elastic 50A Resin) - Compression Test and Simulation Results: (a) 1mm truss diameter, (b) 2mm truss diameter

6. BCC + Octahedron:

In PLA, layer direction has a light impact on mechanical performance. For the 1mm truss diameter sample, elastic behavior is exhibited before reaching the yield point, with rigid behavior shown after reaching a maximum stress of around 35 MPa and a 7% strain. The sample then rapidly bends and reaches a steady state, exhibiting a plateau behavior before densification occurs. For the 2mm truss diameter sample, the maximum stress is around 75 MPa with an 8% strain, exhibiting elastic behavior before reaching high load capacity, followed by plateau behavior and densification. Both exhibit elastic behavior similar to the simulation results, as Fig. 36 shows. The mechanical behavior of TPU material specimens is shown in Fig. 37. The sample with a truss diameter of 1mm exhibits elastic behavior in the initial 13% strain, with a stress around 0.8 MPa, followed by plateau behavior until densification occurs. The sample with a truss diameter of 2mm initially exhibits approximately 30% strain of elastic behavior from 0-6 MPa, until densification occurs. Importantly, the linear results of elastic behavior and plateau phenomenon are consistent with simulation results, and the orientation of the layer has no effect on the mechanical properties. The Grey Resin material specimens with 1mm and 2mm truss diameters exhibit a significant stiffness, with linear behavior similar to simulation results, up to the yield point and reaching maximum stress of approximately 28 MPa and 55 MPa, respectively. After expanding to 8% and 7% strain, respectively, both immediately fracture into small fragments and lose their load capacity. It is worth noting that although the maximum load capacity of the 2mm lattice size samples is nine times that of the 1mm lattice size samples, their tensile strength did not increase, even decreasing. This indicates that increasing the truss diameter will increase the stiffness of this structure, as shown in Fig. 38. The mechanical behavior of structures produced using Elastic 50A is shown in Fig. 39. For the sample with a truss diameter of 1 mm, it exhibits plateau elastic behavior in the initial 10% strain, with stress ranging from 0 to 0.2 MPa followed by a plateau behavior until densification occurs. The sample with truss diameter of 2 mm initially shows elastic behavior of approximately 40% strain and a stress of 0-2 MPa until densification occurs. In addition, the serration phenomenon occurs in the 1mm truss diameter sample.

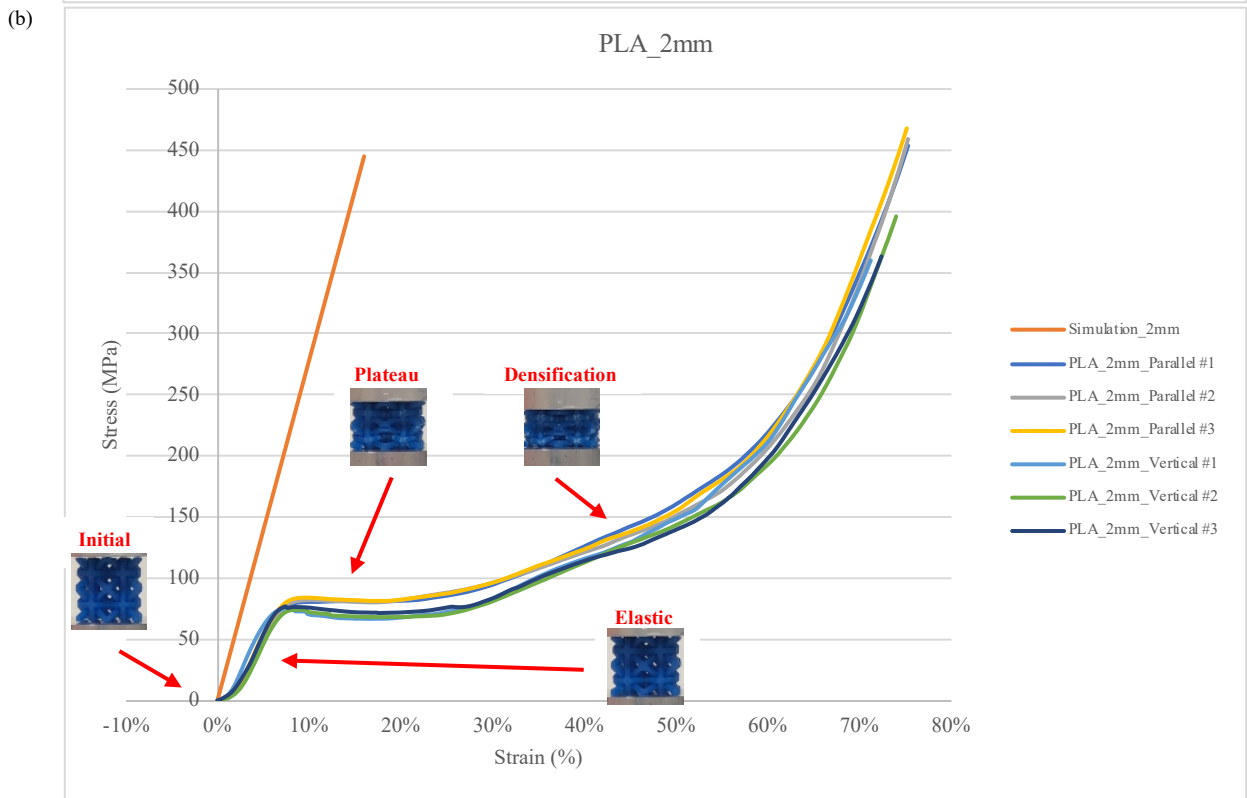
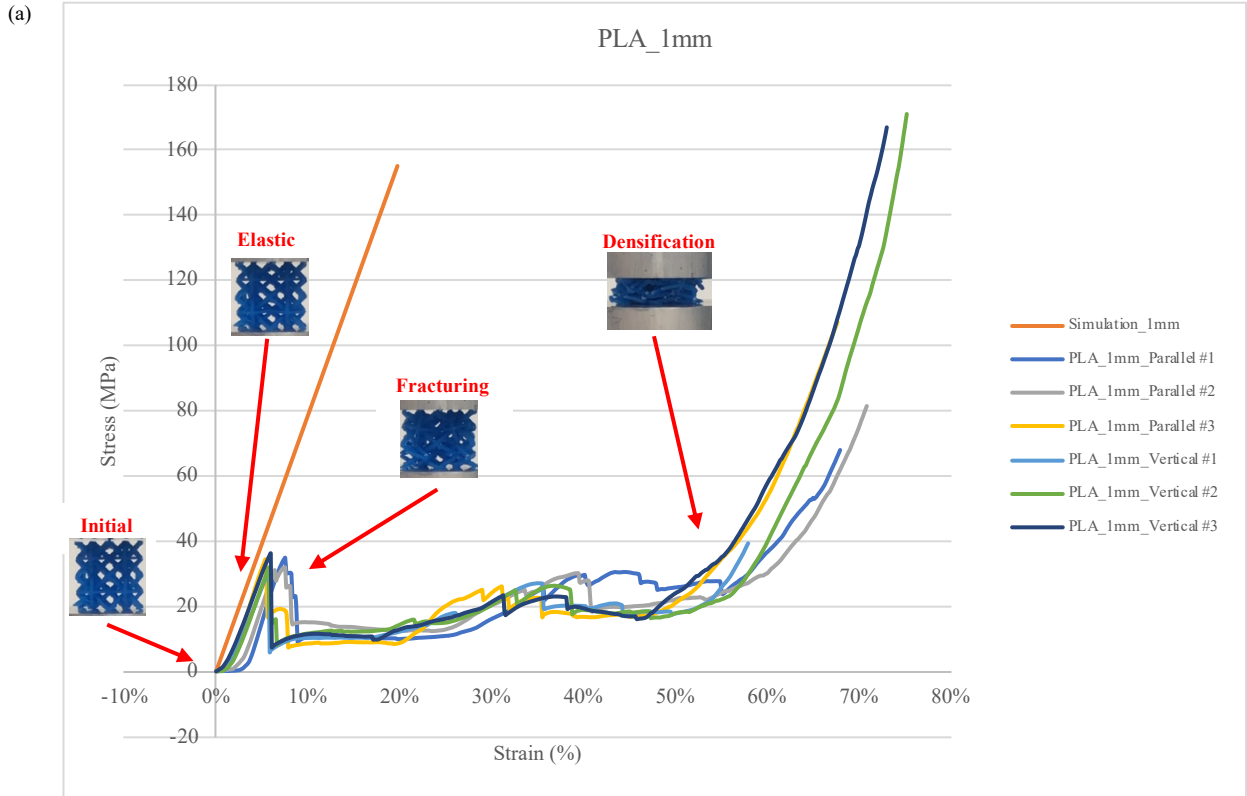


Figure 36 BCC + Octahedron (PLA) - Compression Test and Simulation Results: (a) 1mm truss diameter, (b) 2mm truss diameter

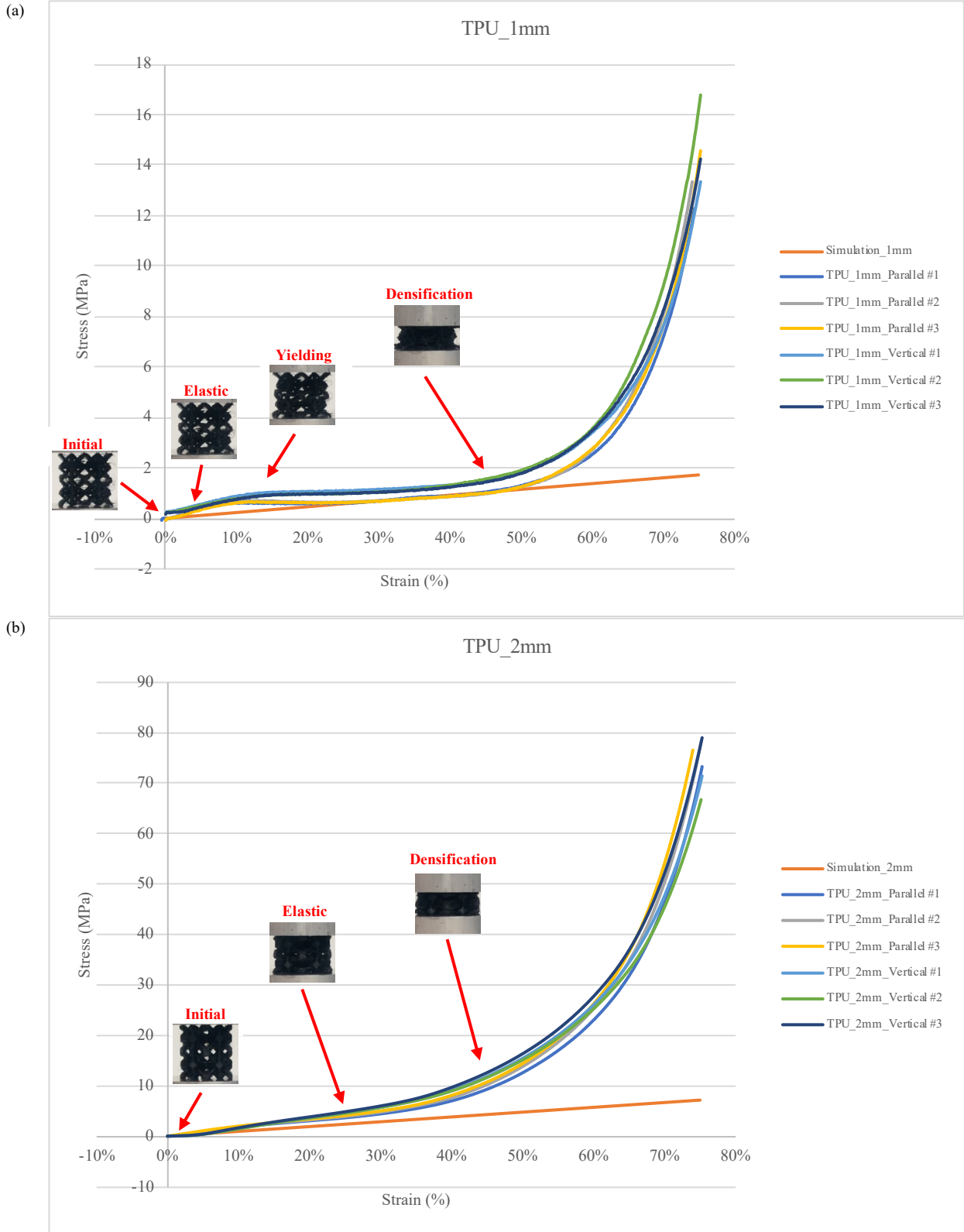


Figure 37 BCC + Octahedron (TPU) - Compression Test and Simulation Results: (a) 1mm truss diameter, (b) 2mm truss diameter

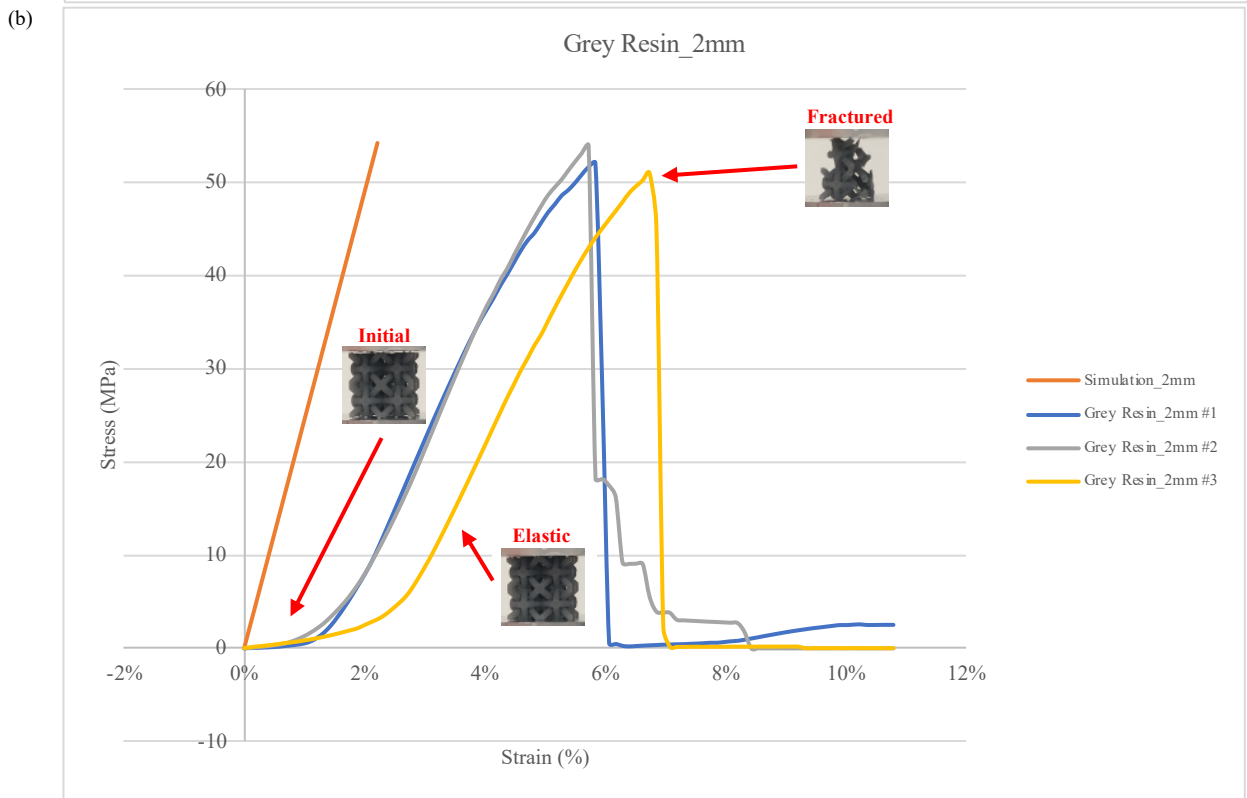
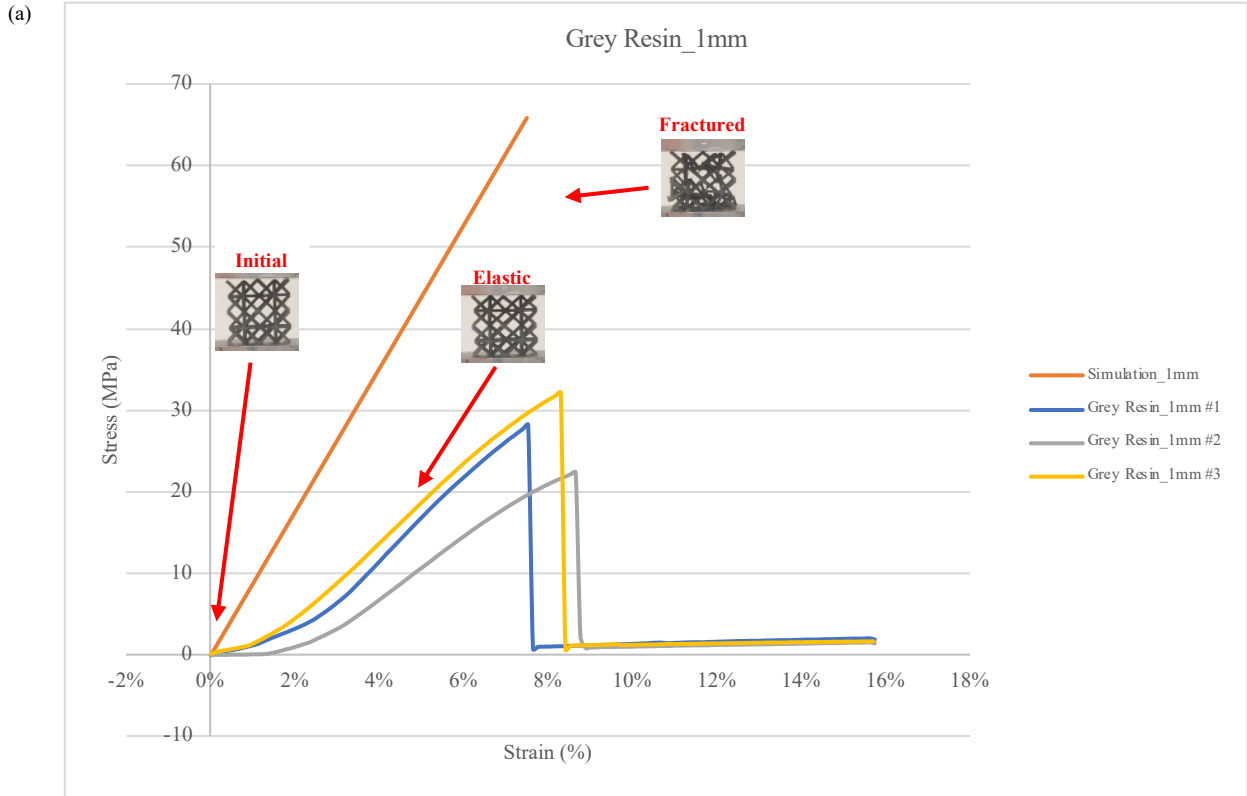


Figure 38 BCC + Octahedron (Grey Resin) - Compression Test and Simulation Results: (a) 1mm truss diameter, (b) 2mm truss diameter

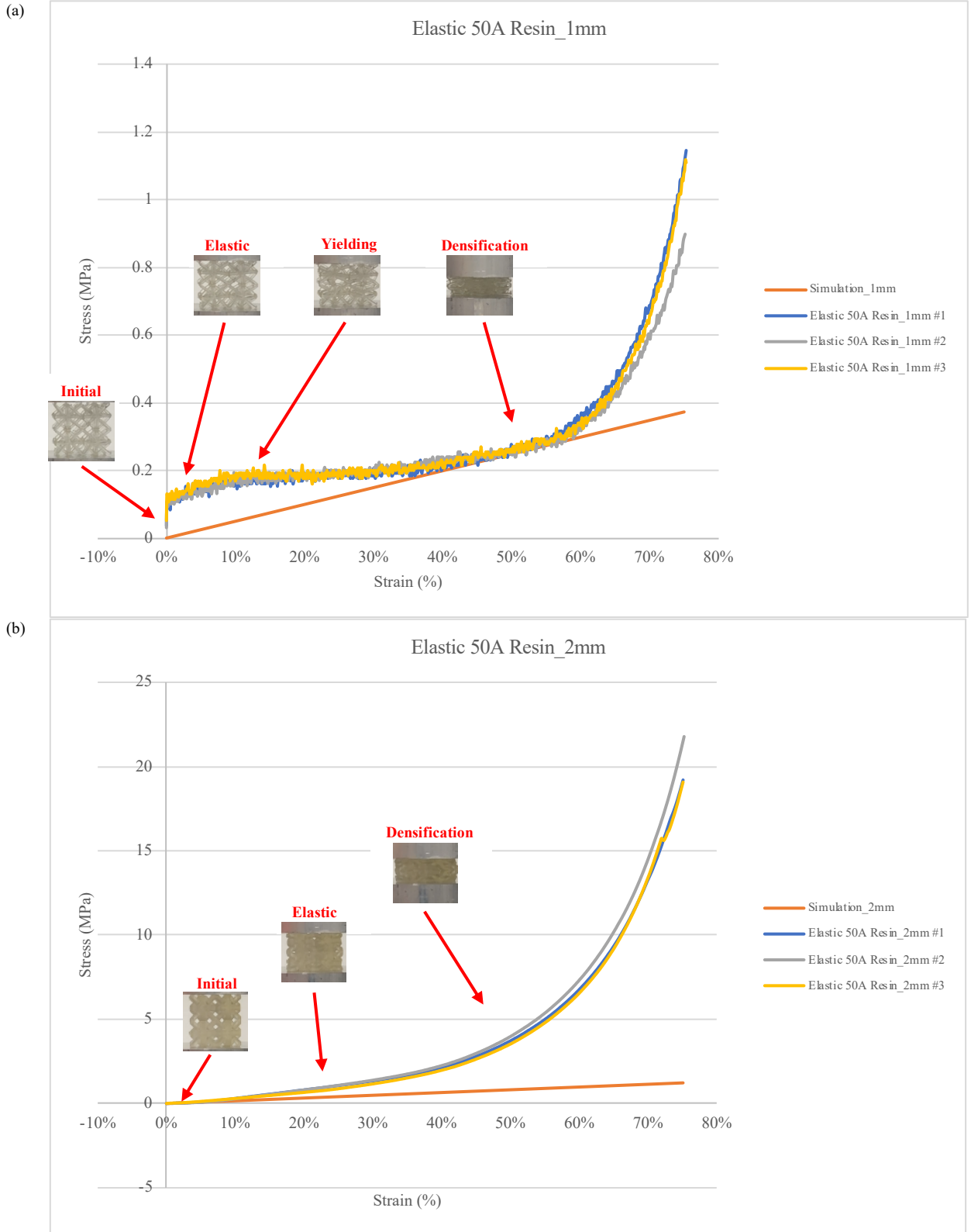


Figure 39 BCC + Octahedron (Elastic 50A Resin) - Compression Test and Simulation Results: (a) 1mm truss diameter, (b) 2mm truss diameter

7. Cross Cube + BCC + Octahedron:

For the PLA with a truss diameter of 1mm samples, both layer direction parallel and perpendicular to the loading plate exhibited elastic behavior similar to the simulation. However, after reaching the yield point, the samples with horizontal and vertical layer show maximum stress of around 78 MPa and 50 MPa with 9% strain, respectively, followed by buckling until densification. With a truss diameter of 2 mm and layer direction parallel or perpendicular to the loading plate, both exhibit elastic behavior similar to simulation and reach maximum stress and strain are same as 1mm ones. The difference in mechanical behavior between 1 mm and 2mm samples is that 2mm one followed by a plateau behavior before densification rather than buckling, as shown in Fig. 40. TPU samples with a truss diameter of 1mm exhibit slightly higher elastic behavior in compression in initial. After a small buckling around 2.5 MPa with 15% and 24% strain of parallel and vertical layer orientation, respectively, the specimen undergoes plastic behavior similar to simulation, exhibiting linear behavior until densifying. For specimens with a lattice size of 2 mm, they initially exhibit elastic behavior of around 40% strain, followed by densification after reaching a linear maximum load of around 12 MPa and 7 MPa of parallel and vertical layer orientation, respectively, as shown in Fig. 41. In Gray Resin material, both 1mm and 2mm truss diameter samples exhibit a rigid behavior, as shown in Fig. 42. The samples show elastic behavior similar to the simulation results before exceeding the yield point, reaching maximum stress, 70 MPa and 75 MPa with a 9% strain, respectively, then immediately fracturing into small pieces and losing their load-bearing capacity. In addition, the 2mm truss diameter sample initially exhibits a flatter linear elastic behavior of around 0.75mm, followed by elastic behavior similar to the simulation results. Finally, Fig. 43 shows the mechanical behavior in the Elastic 50A resin. The 1mm truss diameter sample exhibits an elastic behavior until reaching the maximum stress, around 0.4 MPa, with a 15% strain. After a slight buckling to the equilibrium point, it begins to undergo a dense compaction process that is close to linear until exponential compaction occurs. The 2mm truss diameter specimen exhibits an elastic behavior of approximately 40% strain in the initial stage until it reaches the highest point of linear behavior, which is around 2 MPa. Then, it starts to exhibit exponential compaction until it extends to nearly 70%, and the stress reaches approximately 12 MPa, at which point a significant fracture occurs.

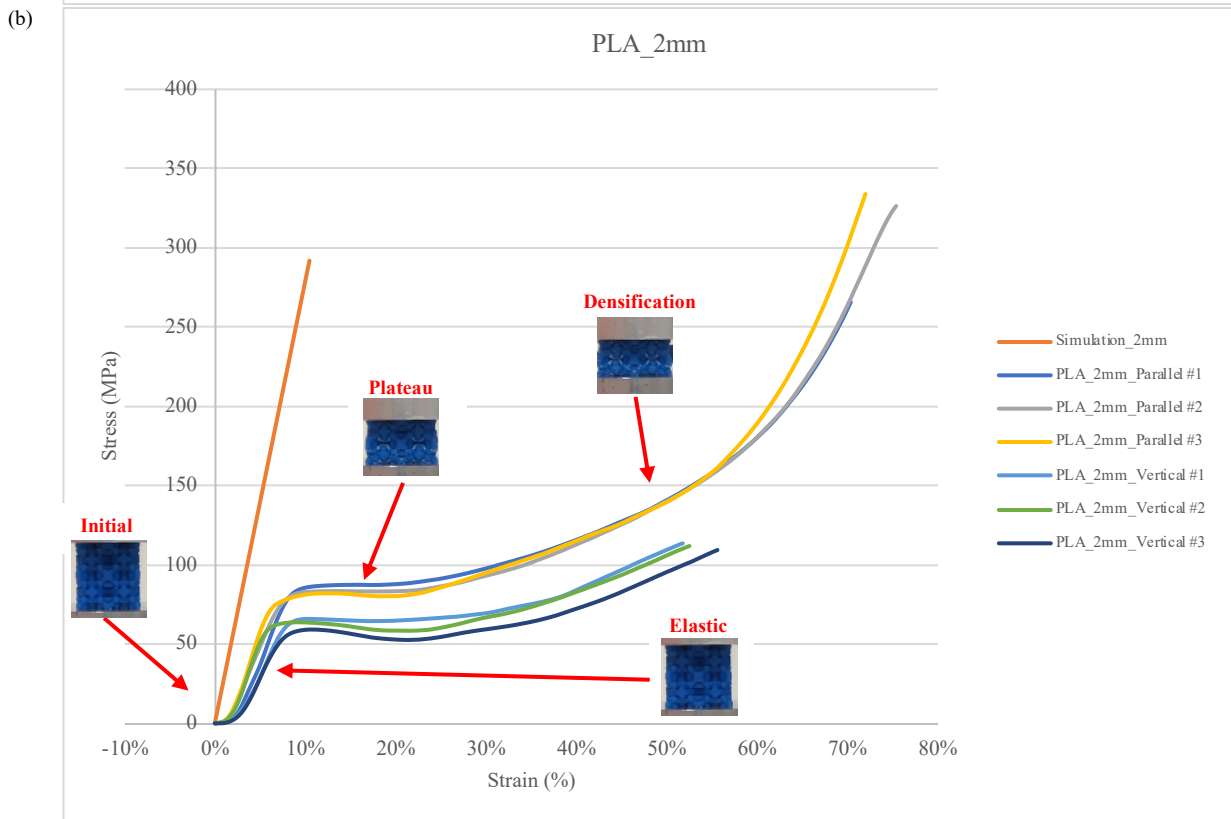
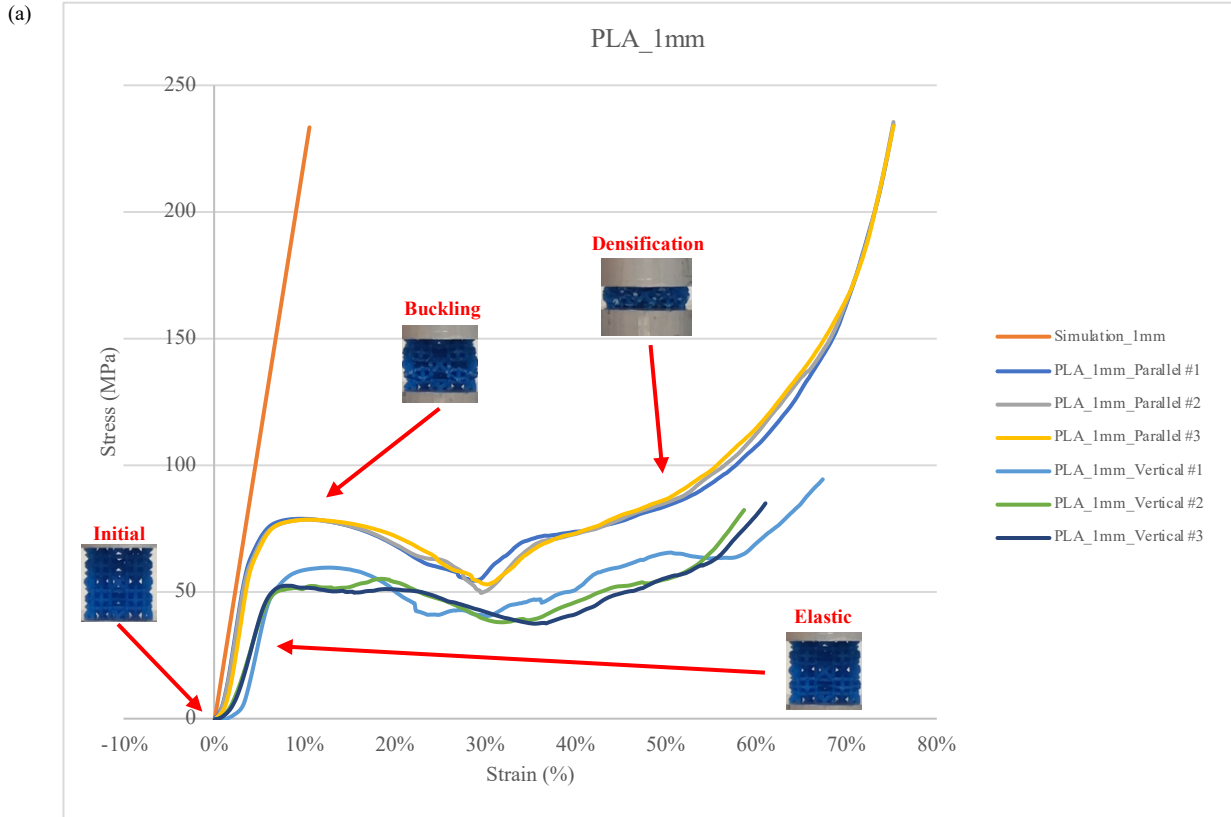


Figure 40 Cross Cube + BCC + Octahedron (PLA) - Compression Test and Simulation Results: (a) 1mm truss diameter, (b) 2mm truss diameter

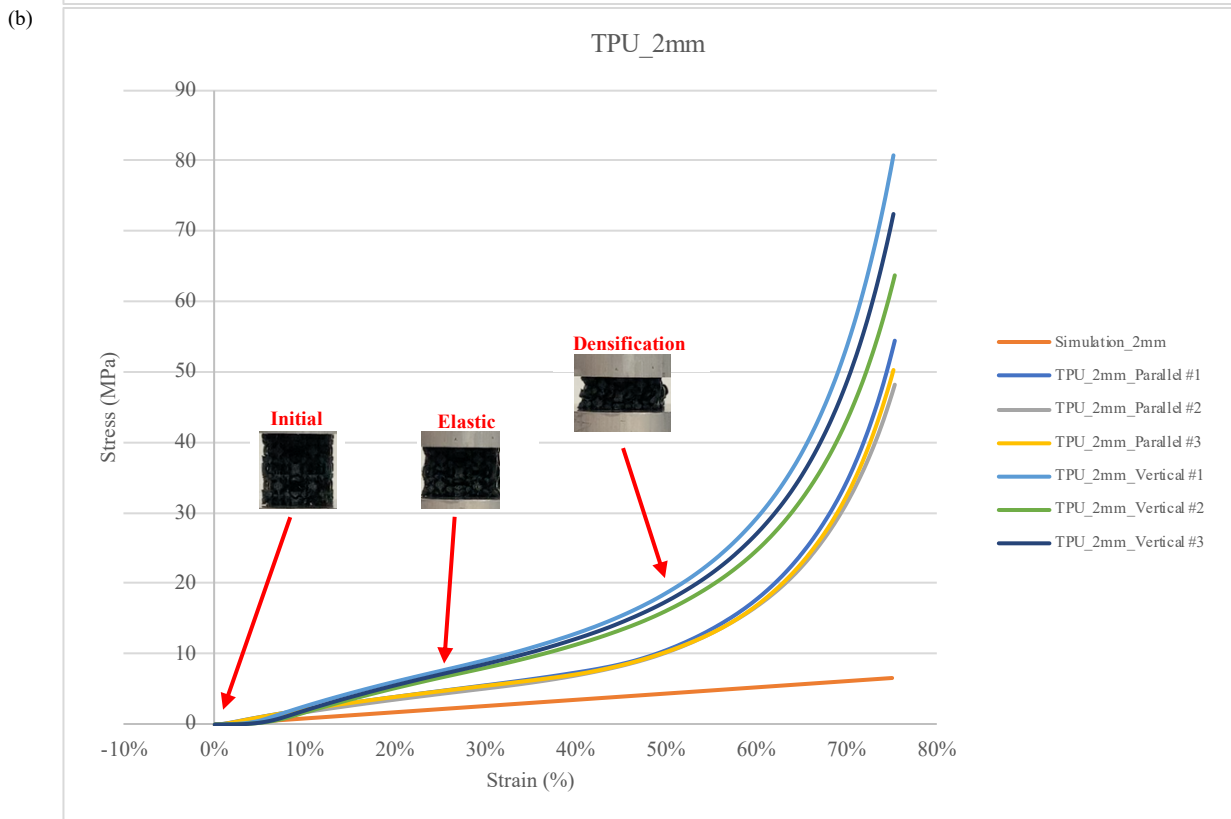
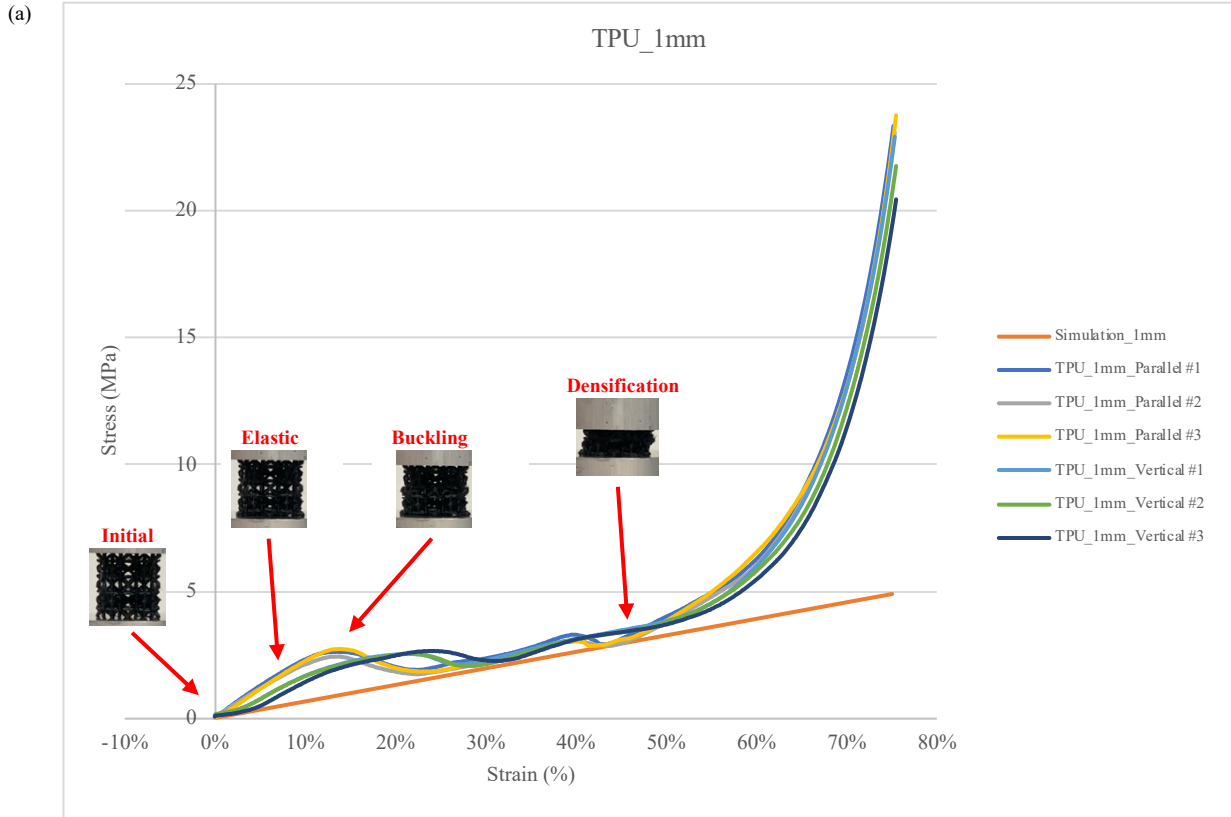


Figure 41 Cross Cube + BCC + Octahedron (TPU) - Compression Test and Simulation Results: (a) 1mm truss diameter, (b) 2mm truss diameter

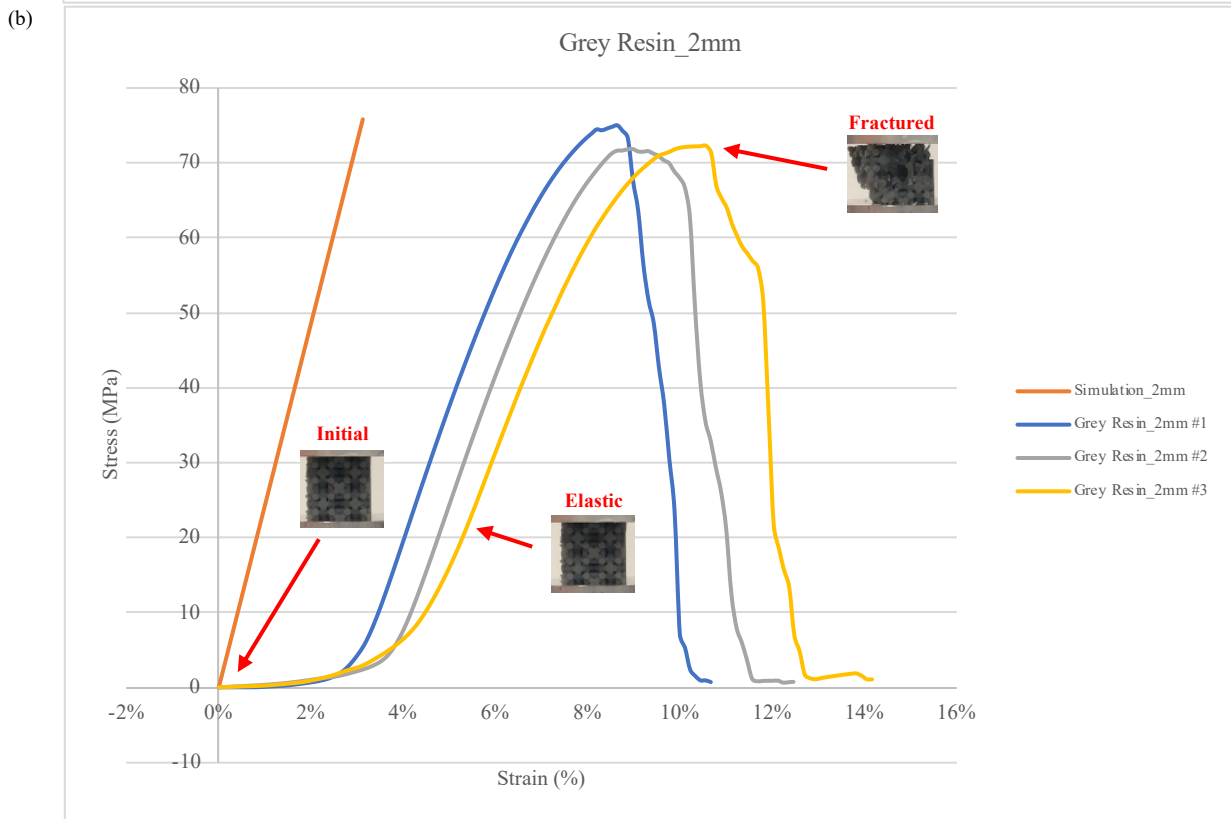
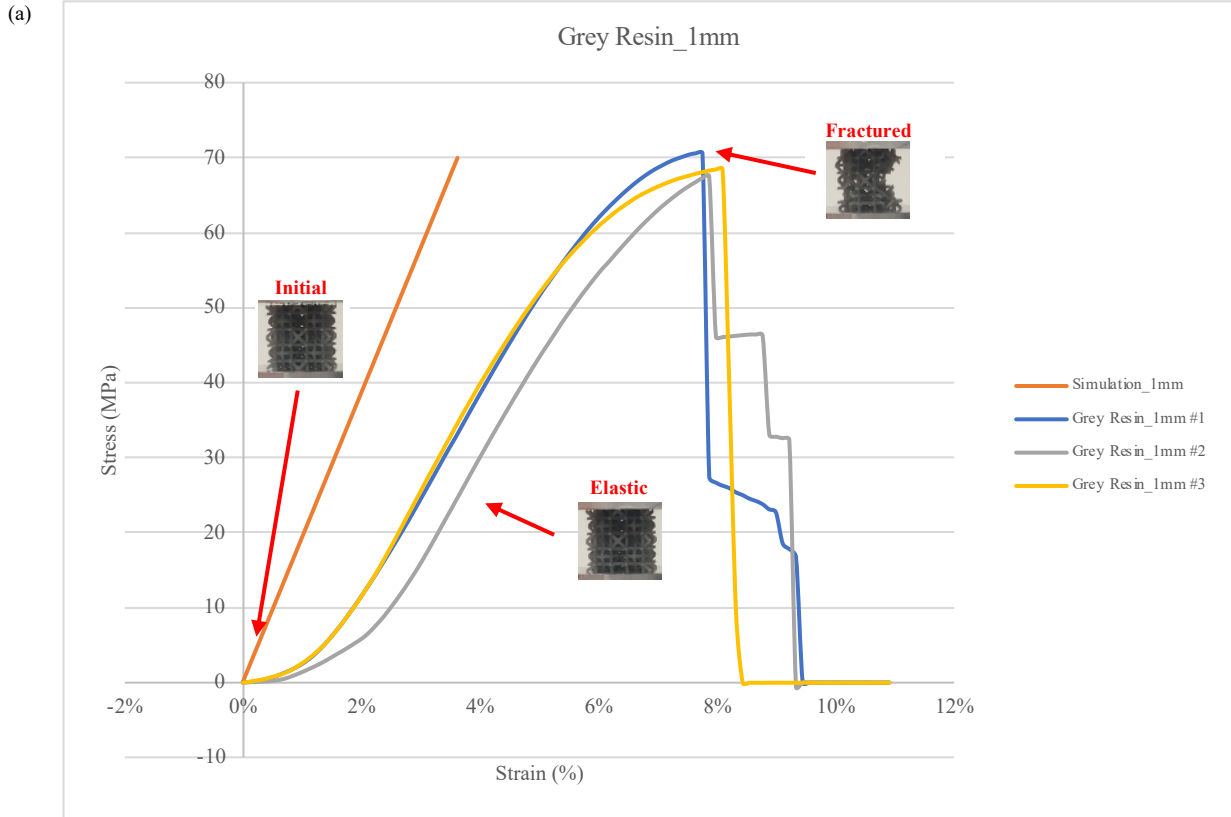


Figure 42 Cross Cube + BCC + Octahedron (Grey Resin) - Compression Test and Simulation Results: (a) 1mm truss diameter, (b) 2mm truss diameter

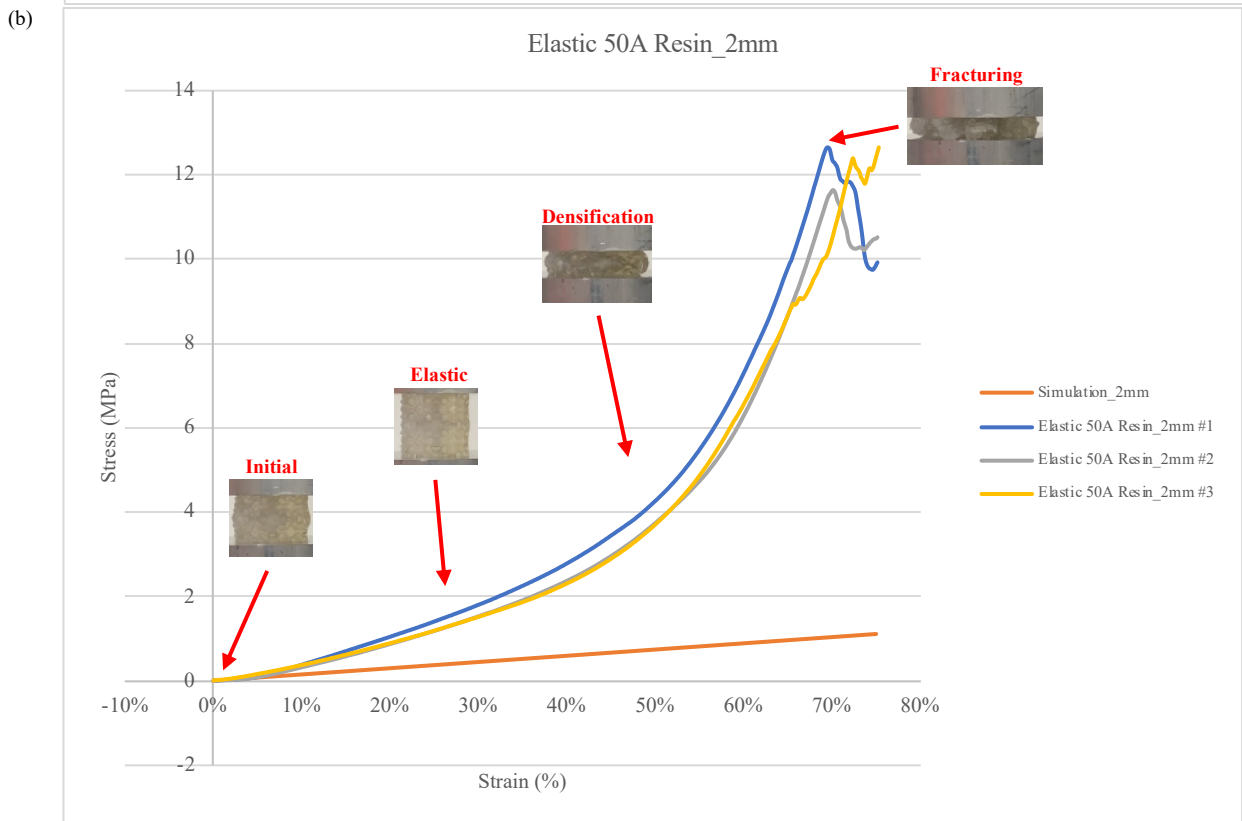
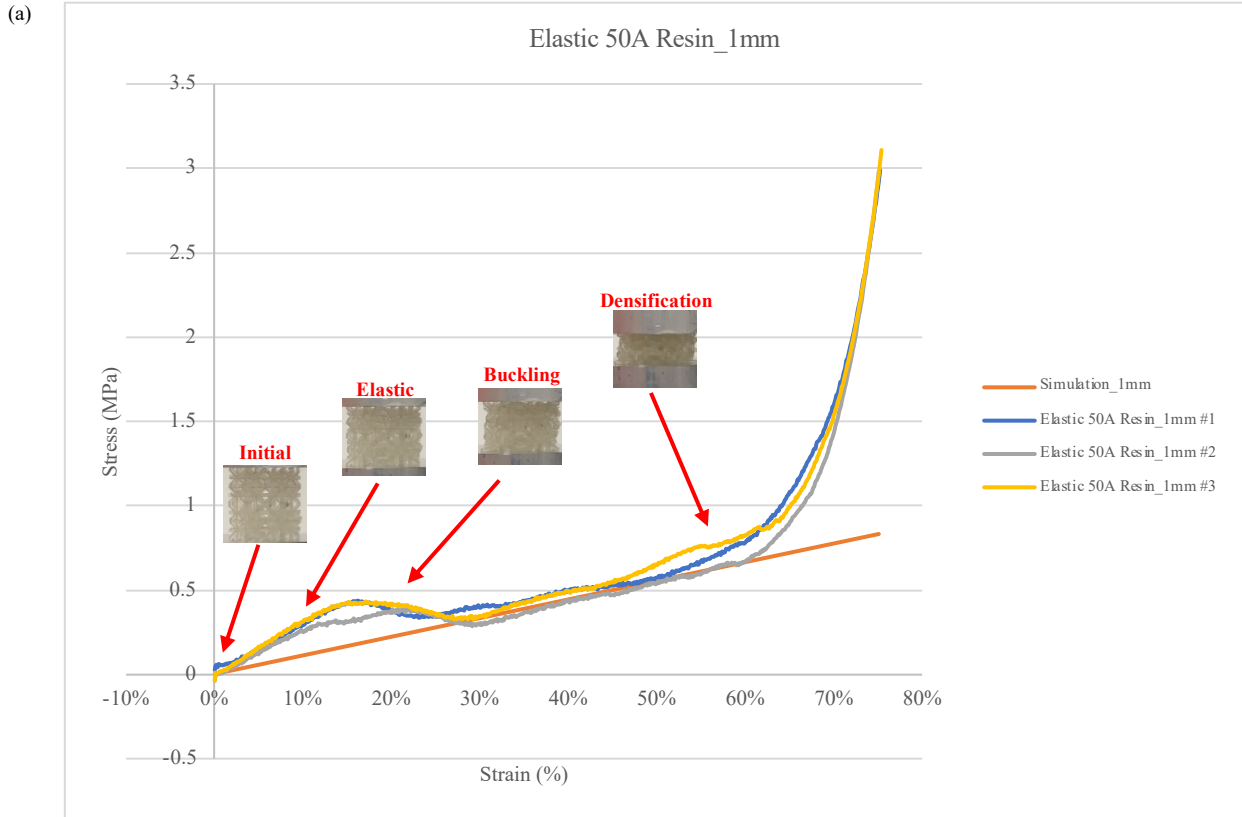


Figure 43 Cross Cube + BCC + Octahedron (Elastic 50A Resin) - Compression Test and Simulation Results: (a) 1mm truss diameter, (b) 2mm truss diameter

4 Discussion

This study aims to analyze the mechanical characteristics of different geometries of lattice structures (LS) when subjected to compressive forces. In addition to traditional LS designs such as Pure LS, Cross Cube, BCC, and Octahedron, this research also includes various geometric shapes to observe how they respond to changes in density via truss diameter modifications. The mechanical behavior of four different materials, namely PLA, TPU, Grey resin, and Elastic 50A resin, is also compared. By exploring the full range of possible geometric structures and their mechanical properties, this study aims to establish a framework that can help identify useful properties and applications for LS. The results show that the mechanical behavior of specimens with different LS types, materials, load orientations, and truss diameters can vary significantly.

4.1 Mechanical Behavior of Lattice Structure

Material selection plays a crucial role in determining the mechanical behavior of LS. Simulation results show that PLA has the highest load capacity, followed by Gray, TPU, and Elastic 50A resin. It is important to consider that material parameters may vary depending on the manufacturer and model. Therefore, experimental data are crucial for obtaining accurate material properties for design optimization. Then, the mechanical behaviors of different LS in each material with varied truss diameters are also presented with different mechanical properties and behaviors of each LS with varied truss diameter will be discussed in different materials.

4.1.1 PLA

Table 10 displays the maximum stress and strain data before buckling or yielding for each LS in PLA at different truss diameters. The stress and strain behavior of various LS made of PLA material with different truss diameters and layer orientations can be observed from the table. Fig. 43-44 illustrate the mechanical behavior of various LS made of PLA material. The following observations can be made:

Firstly, for pure LS, the Cross Cube exhibits significant buckling behavior in the 1mm sample but shows significant improvement in the 2mm sample, with an increase in stress. This suggests that buckling behavior is negatively correlated with truss diameter, while stress is positively correlated. Additionally, in the 1mm sample, the buckling behavior of parallel layer orientation is significantly

higher than that of perpendicular layer orientation, but as the truss diameter increases, this phenomenon reverses. This suggests that the increase in truss diameter is positively correlated with the supporting ability of parallel layer orientation and negatively correlated with perpendicular layer orientation. In BCC LS, the stress values are relatively low, but the strain is large. There is not much difference in mechanical properties for different layer orientations. Increasing the truss diameter increases the maximum stress value, but the strain decreases, indicating that increasing the truss diameter in BCC LS makes the structure more brittle. Additionally, it can be observed that the BCC LS specimen exhibits a very long plateau-like region after exceeding the maximum stress point, indicating that it has better mechanical behavior in terms of ductility. The stress values of the Octahedron LS fall between those of the previous two structures, and its mechanical properties differ between different directions of layer orientation, also falling between those of the previous two structures. Increasing the truss diameter leads to a slight increase in maximum stress, but the increase in strain is not significant. This indicates that for the Octahedron LS, increasing the truss diameter tends to make the structure more brittle. It can be observed that the strain of the Octahedron LS is independent of both truss diameter and layer direction, and increasing the truss diameter can make the stress tend towards independence of layer direction, exhibiting homogenizing properties. Additionally, the Octahedron LS structure exhibits a larger buckling amplitude after exceeding the maximum yield stress, indicating that it is more brittle than the previous two structures.

Then, for composed LS, For the Cross Cube + BCC LS, the variation of truss diameter results in a slight increase in maximum stress and strain in the parallel layer direction, while the stress in the perpendicular layer direction increases significantly, but the strain decreases greatly. This indicates that increasing the diameter of the truss will increase the strength of the structure, but it will also make the structure more dependent on the layer orientation. In addition, it was observed that the behavior of the Cross Cube + BCC LS in the elastic region is similar to that of the Cross Cube LS. Therefore, the Cross Cube LS is considered to be the main supporting structure for this composite LS. By adding a BCC LS on top of the Cross Cube LS, the high extensibility of the BCC LS is reflected in this composite structure. Although the maximum stress value is not as high as that of the pure LS, the buckling behavior is significantly improved, indicating that the structure has good mechanical properties in terms of ductility. For the Cross Cube + Octahedron LS, changes in truss diameter and layer direction have no significant effect on the strain, while the effect of layer

direction on stress in the 1 mm specimen is smaller than that of the 1 mm one, indicating the homogenized characteristics of the Octahedron LS are reflected in this composite structure. In addition, the behavior of the Cross Cube + Octahedron LS in the elastic region is similar to that of the Cross Cube LS and Octahedron LS. Therefore, both pure LS can be considered as the main supporting structures of this composite LS, and the mechanical behavior is not dominated by any one component but exhibits new mechanical behavior. For the BCC + Octahedron LS, layer orientation has no significant effect on the maximum stress and strain, and the maximum stress is positively correlated with truss diameter. This indicates that the properties of both BCC LS and Octahedron LS are reflected in this composite structure. Additionally, it can be observed that the 1 mm truss diameter specimens exhibit buckling after exceeding the maximum stress, while the 2 mm truss diameter specimens exhibit more of a plateau phenomenon. This suggests that the effects of BCC LS and Octahedron LS on the mechanical behavior of this composite structure are positively and negatively correlated, respectively. For the Cross Cube + BCC + Octahedron LS, the variation of truss diameter has no significant effect on stress and strain, which reflects the stress behavior of the Cross Cube LS and the strain behavior of the BCC LS and Octahedron LS. Additionally, the layer direction has an effect on stress, which is influenced by the Cross Cube and Octahedron. In terms of mechanical behavior, we can observe that the 1mm truss diameter specimens exhibit buckling behavior, similar to Cross Cube + BCC LS and Cross Cube + Octahedron LS, but with a smaller amplitude due to the influence of BCC. As the truss diameter increases, the buckling phenomenon gradually changes to plateau behavior.

Table 10 The maximum stress and strain data of LS in PLA

PLA				
LS type	Truss diameter	Layer orientation	Maximum stress (MPa)	Strain
Cross Cube	1 mm	Parallel	70	5%
		Perpendicular	50	15%
	2 mm	Parallel	80	6%
		Perpendicular	110	10%
BCC	1 mm	Parallel	8	20%
		Perpendicular	8	20%
	2 mm	Parallel	17	11%
		Perpendicular	12	11%
OCT	1 mm	Parallel	80	5%
		Perpendicular	60	5%
	2 mm	Parallel	104	7%
		Perpendicular	93	7%
Cross Cube + BCC	1 mm	Parallel	76	7%
		Perpendicular	45	20%
	2 mm	Parallel	80	10%
		Perpendicular	60	8%
Cross Cube + Octahedron	1 mm	Parallel	87	10%
		Perpendicular	65	10%
	2 mm	Parallel	102	10%
		Perpendicular	102	10%
BCC + Octahedron	1 mm	Parallel	32	7%
		Perpendicular	30	5%
	2 mm	Parallel	75	8%
		Perpendicular	75	8%
Cross Cube + BCC + Octahedron	1 mm	Parallel	78	10%
		Perpendicular	60	10%
	2 mm	Parallel	78	7%
		Perpendicular	60	9%

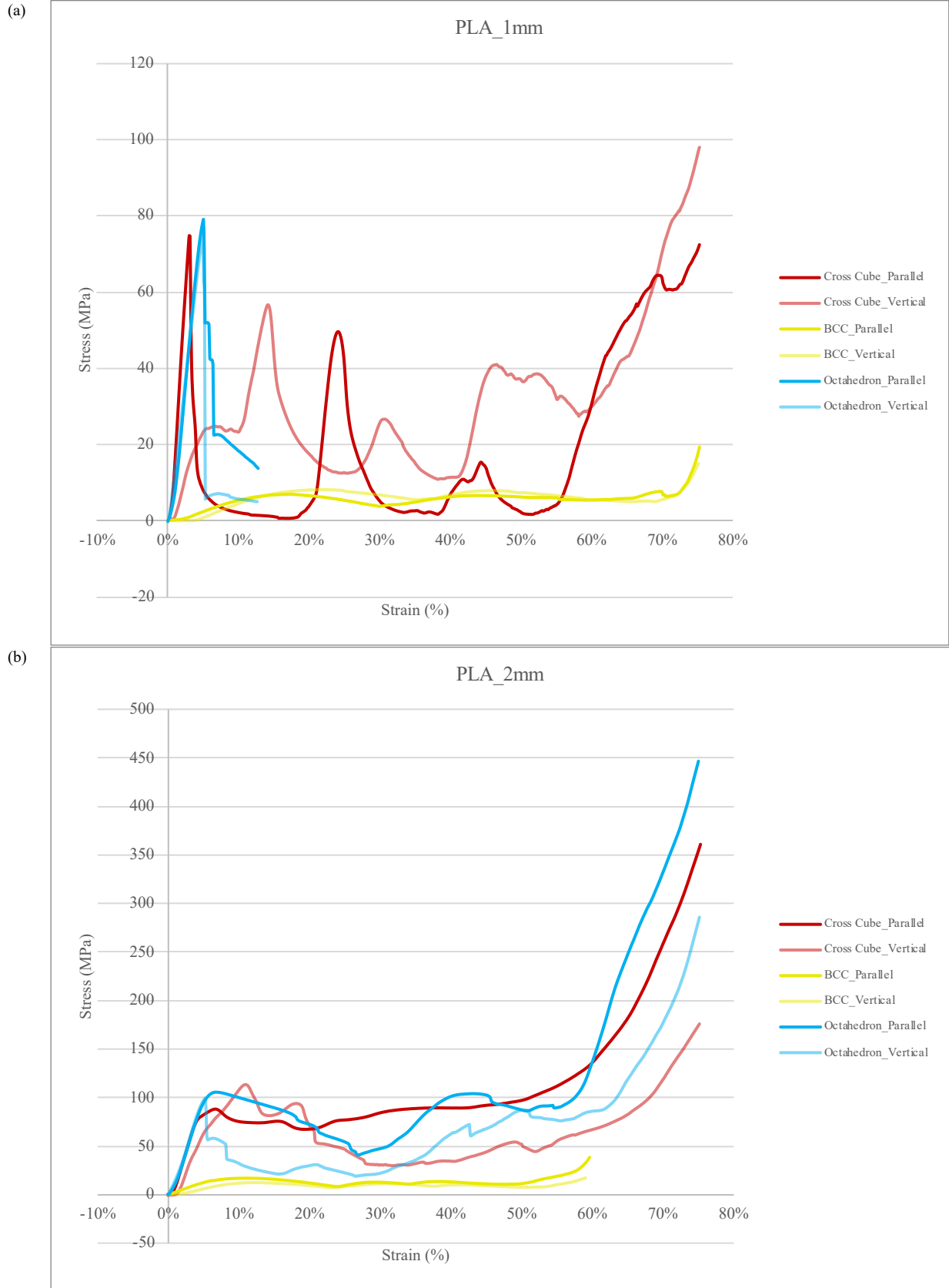


Figure 44 LS in PLA with 1mm truss diameter: (a) Pure LS, (b) Composed LS

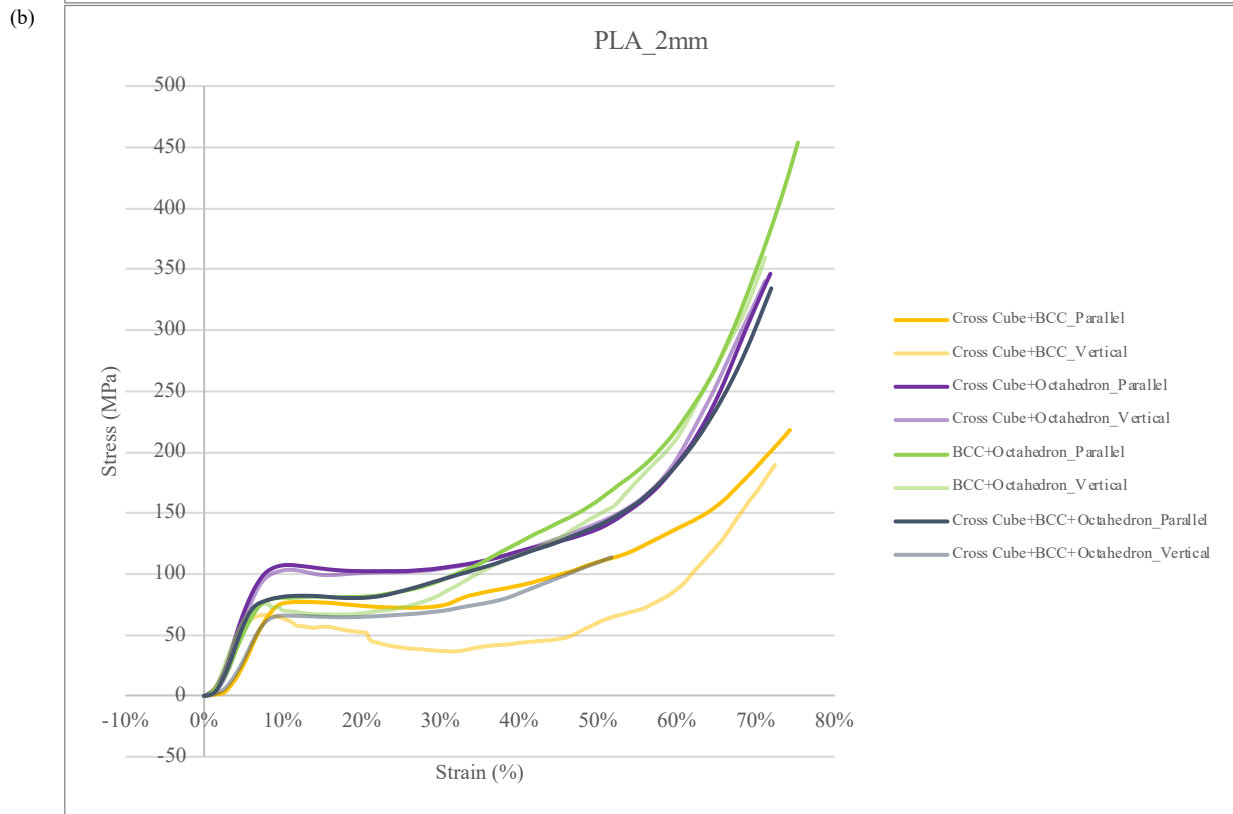
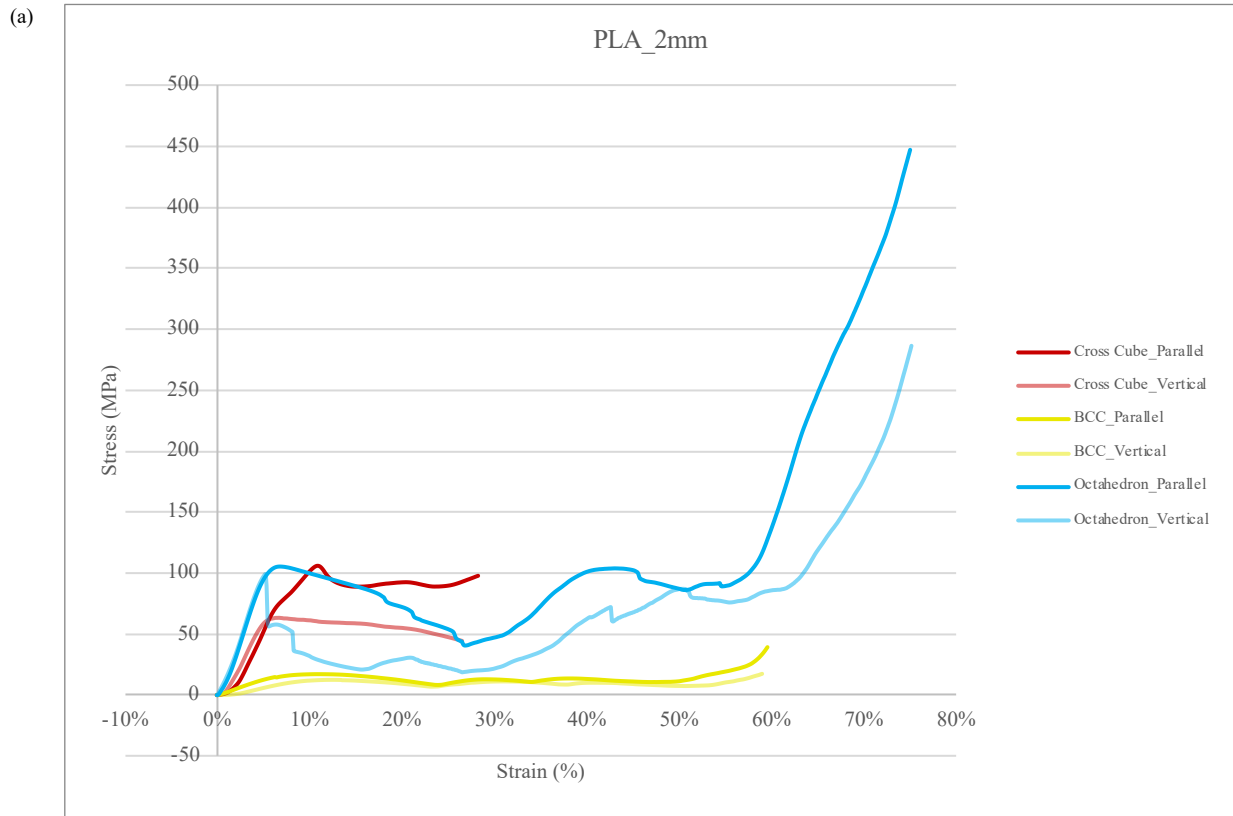


Figure 45 LS in PLA with 2mm truss diameter: (a) Pure LS, (b) Composed LS

4.1.2 TPU

Table 11 presents the stress and strain data for each TPU LS with different strut diameters prior to bending or yielding. The table allows for an analysis of the stress and strain properties of TPU LS with varying strut diameters and layer orientations. Additionally, Fig. 45-46 depict the mechanical behaviors of different LSs made of TPU, providing further insights into their behaviors.

Firstly, in pure LS, changes in layer direction have no significant effect on the strain, but their effect on stress varies depending on the LS structure. For the Cross Cube LS, stress is higher in the parallel layer direction than in the perpendicular layer direction, and increasing the truss diameter effectively increases both stress and strain. The parallel layer direction specimen with a 1mm truss diameter experiences buckling, while the perpendicular layer direction specimen undergoes plastic deformation. Both specimens exhibit similar plateau behavior thereafter, but the perpendicular layer direction specimen densifies more quickly. For the 2 mm truss diameter specimen, both directions experience buckling, but the perpendicular layer direction specimen still exhibits more plastic deformation behavior. Both specimens exhibit similar plateau behavior thereafter, but the perpendicular layer direction specimen densifies more quickly. In BCC LS, stress is relatively low, but the strain is larger. Increasing the truss diameter only slightly increases stress, and strain has no significant effect. Additionally, the BCC LS sample exhibits a long plateau region, with densification occurring only after exceeding the maximum stress point, indicating considerable elasticity in this material's structure and excellent mechanical properties in terms of ductility. For the Octahedron LS, changes in layer direction have no significant effect on stress. Observing the results, increasing the truss diameter effectively increases both stress and strain. The parallel layer direction specimen with a 1mm truss diameter experiences buckling until densification occurs. The parallel layer direction specimen with a 2 mm truss diameter exhibits plastic deformation behavior, while the perpendicular layer direction specimen experiences slight buckling until densification occurs.

For composed LS, the variation of layer direction has no significant effect on stress and strain for Cross Cube + BCC LS, while changes in the truss diameter lead to a significant increase in maximum stress and strain. Furthermore, the behavior of Cross Cube + BCC LS in the elastic region is similar to that of Cross Cube LS, indicating that Cross Cube LS is the main supporting

structure for this composed material LS. By adding a BCC LS on top of the Cross Cube LS, this composite structure exhibits high extensibility of BCC LS and effectively reduces the buckling behavior of Cross Cube LS. In addition, increasing the truss diameter reduces the plateau behavior and densifies the structure more quickly. For the Cross Cube + Octahedron LS, the orientation of the layers had a slight effect on the 1mm truss diameter specimen but less of an effect on the 2mm truss diameter specimen. This indicates that the dependence on layer orientation decreases with increasing truss diameter. However, the diameter of the truss had a significant effect on the maximum stress and strain. In addition, the behavior of the Cross Cube LS and Octahedron LS can be observed in this composed LS, with a noticeable buckling behavior in the 1mm truss diameter specimen, in addition to an increase in maximum stress, while the buckling behavior is reduced with increasing truss diameter, replaced by plastic behavior. For the BCC + Octahedron LS, the orientation of the layers had no significant effect on the maximum stress and strain, which were positively correlated with the diameter of the truss. In addition, the behavior of the BCC + Octahedron LS in the elastic region was similar to that of the Octahedron LS, indicating that the Octahedron LS is the main supporting structure in this composite LS. By adding a BCC LS on top of the Octahedron LS, this composite structure reflects the high expansibility of the BCC LS, reducing buckling behavior. For Cross Cube + BCC + Octahedron LS, the orientation of layers has an impact on the specimens with a 2 mm truss diameter, while it has less effect on the specimens with a 1mm truss diameter, indicating that the influence of layer orientation is positively correlated with truss diameter. It can be observed that the load-carrying capacity in the perpendicular layer direction becomes stronger than that in the parallel layer direction as the truss diameter increases. The variation in truss diameter also has a significant effect on stress and strain. In addition, the mechanical behavior of Cross Cube + BCC + Octahedron LS can be observed to be similar to Cross Cube + Octahedron LS, indicating that the characteristics of Cross Cube LS and Octahedron LS are reflected in this composite LS.

Table 11 The maximum stress and strain data of LS in TPU

TPU				
LS type	Truss diameter	Layer orientation	Maximum stress (MPa)	Strain
Cross Cube	1 mm	Parallel	0.9	5%
		Perpendicular	0.6	5%
	2 mm	Parallel	4.2	13%
		Perpendicular	3.4	10%
BCC	1 mm	Parallel	0.4	55%
		Perpendicular	0.4	55%
	2 mm	Parallel	0.6	55%
		Perpendicular	0.58	55%
OCT	1 mm	Parallel	1.2	9%
		Perpendicular	1.2	13%
	2 mm	Parallel	4	17%
		Perpendicular	4	17%
Cross Cube + BCC	1 mm	Parallel	1.8	9%
		Perpendicular	1.8	10%
	2 mm	Parallel	6	25%
		Perpendicular	6	25%
Cross Cube + Octahedron	1 mm	Parallel	2	10%
		Perpendicular	2	15%
	2 mm	Parallel	8	30%
		Perpendicular	8	30%
BCC + Octahedron	1 mm	Parallel	0.8	13%
		Perpendicular	0.8	13%
	2 mm	Parallel	6	30%
		Perpendicular	6	30%
Cross Cube + BCC + Octahedron	1 mm	Parallel	2.5	15%
		Perpendicular	2.5	24%
	2 mm	Parallel	8	40%
		Perpendicular	12	40%

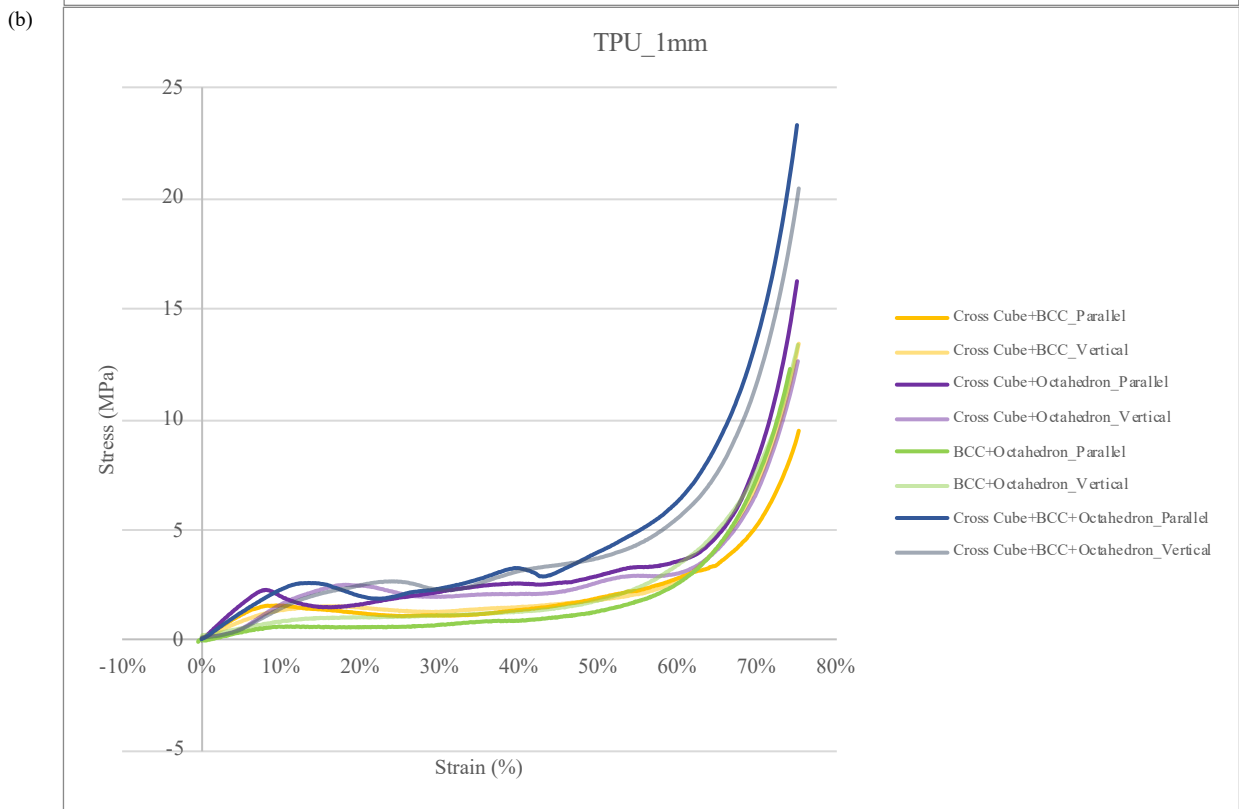
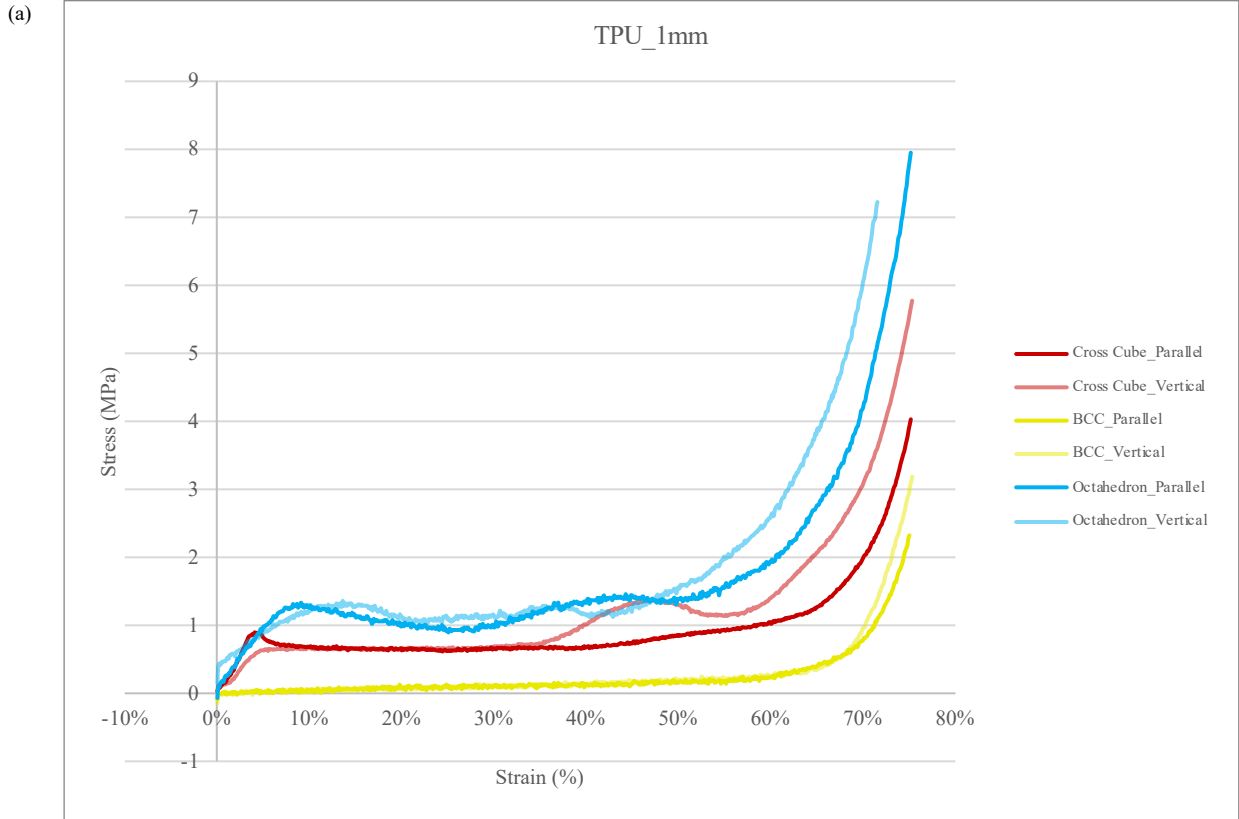


Figure 46 LS in TPU with 1mm truss diameter: (a) Pure LS, (b) Composed LS

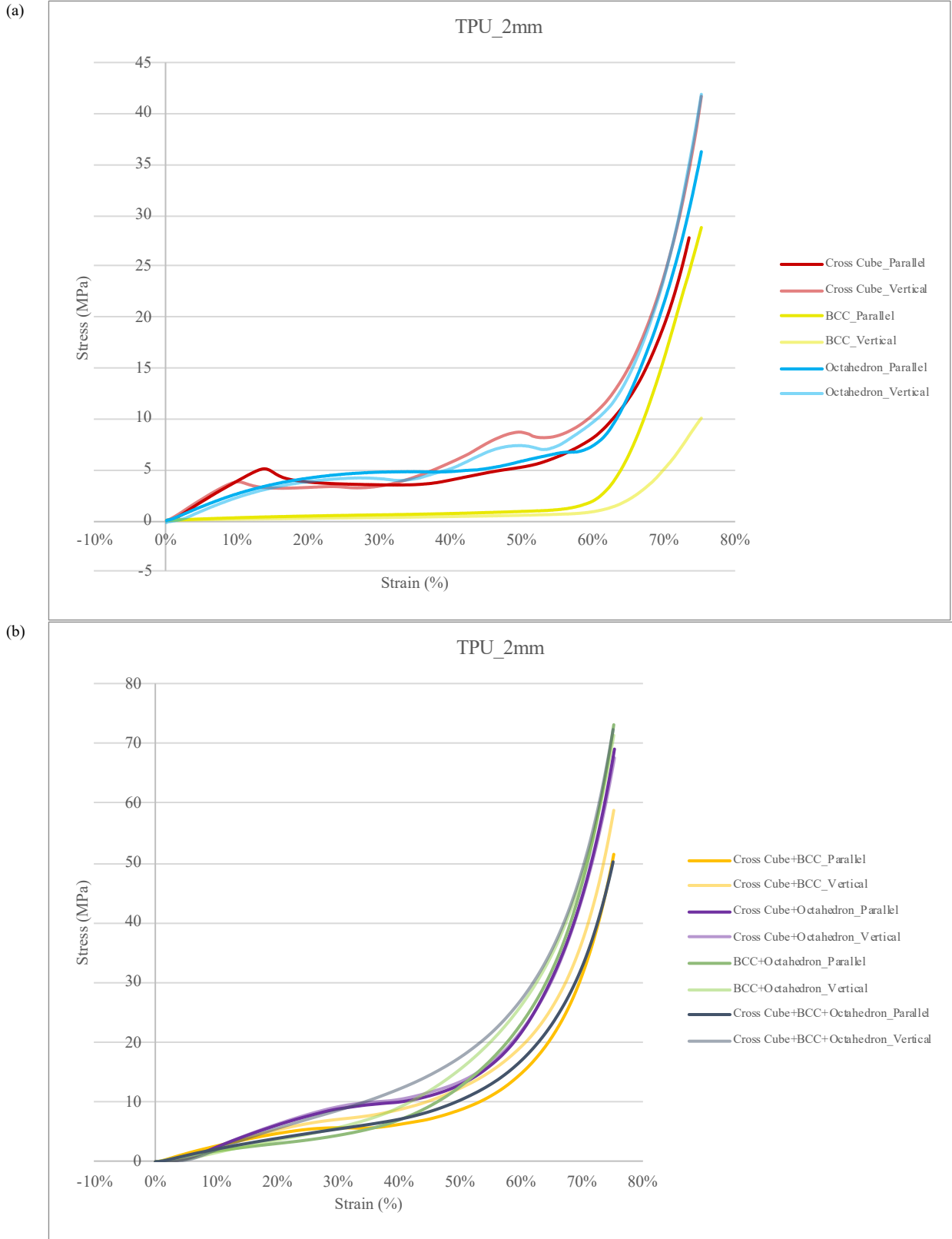


Figure 47 LS in TPU with 1mm truss diameter: (a) Pure LS, (b) Composed LS

4.1.3 Grey Resin

Table 12 presents stress and strain data for Grey resin LSs with different truss diameters prior to bending or yielding. The table provides insight into the stress and strain characteristics of Grey resin LS with varying strut diameters. In addition, Fig.48-49 reveal that Grey Resin exhibits a clear rigid behavior, indicating that LSs made from this material are brittle. The following observations can be made.

In pure LS, increasing the truss diameter of the Grey Resin LS can effectively increase the stress. In Cross Cube LS, increasing the truss diameter can increase the maximum stress, but there is no significant improvement in strain. This suggests that the stress in this structure is proportional to the diameter of the truss, while a strain is not related to the diameter of the truss. Additionally, it was observed that specimens with a 1 mm truss diameter fracture immediately after reaching the maximum stress, while those with a 2 mm truss diameter exhibit plateau behavior before fracturing. This suggests that increasing the diameter of the truss can improve the strength of the specimen and allow it to withstand higher stress. The specimen exhibits a smooth stress plateau behavior after reaching the maximum stress due to the orthogonal relationship between the truss structure and the loading surface, which allows for plastic deformation and enables the specimen to continue to bear a certain degree of stress while maintaining its shape. When the specimen can no longer withstand higher stress, it eventually fractures. In contrast, the stress in BCC LS is relatively low, and the relationship between stress, strain, and the diameter of the truss is proportional, inverse, and proportional, respectively. Although increasing the diameter of the truss can significantly increase the maximum stress, the strain capacity is also significantly reduced. This suggests that increasing the diameter of the truss can greatly stiffen BCC LS. For Octahedron LS, the variation of the diameter of the truss has no significant effect on the strain, but it can increase the maximum stress. This suggests that the rigidity of this structure is positively correlated with the truss diameter. Additionally, unlike Cross Cube LS, BCC LS, and Octahedron LS do not exhibit similar plastic behavior after increasing the diameter of the truss. This is because the truss and the loading surface in these two structures do not form an orthogonal relationship, so increasing the diameter of the truss can increase the shear force and easily lead to specimen fracture.

In composed LS, a positive correlation was observed between the diameter of the truss and the maximum stress, independent of strain. This suggests that increasing the diameter of the truss can enhance the rigidity of the structure. Additionally, it was observed that the Cross Cube + BCC LS, Cross Cube + Octahedron LS, and Cross Cube + BCC + Octahedron LS exhibited plastic behavior before fracturing, with a positive correlation between this behavior and the diameter of the truss. This indicates that the characteristics of the Cross Cube LS are reflected in these three composite structures. Furthermore, the BCC + Octahedron LS exhibited almost complete rigid behavior.

Table 12 The maximum stress and strain data of LS in Grey Resin

Grey Resin			
LS type	Truss diameter	Maximum stress (MPa)	Strain
Cross Cube	1 mm	45	5%
	2 mm	80	5%
BCC	1 mm	4.3	17%
	2 mm	9	7%
OCT	1 mm	65	6%
	2 mm	90	6%
Cross Cube + BCC	1 mm	55	8%
	2 mm	65	8%
Cross Cube + Octahedron	1 mm	50	6%
	2 mm	85	6%
BCC + Octahedron	1 mm	28	8%
	2 mm	55	7%
Cross Cube + BCC + Octahedron	1 mm	70	9%
	2 mm	75	9%

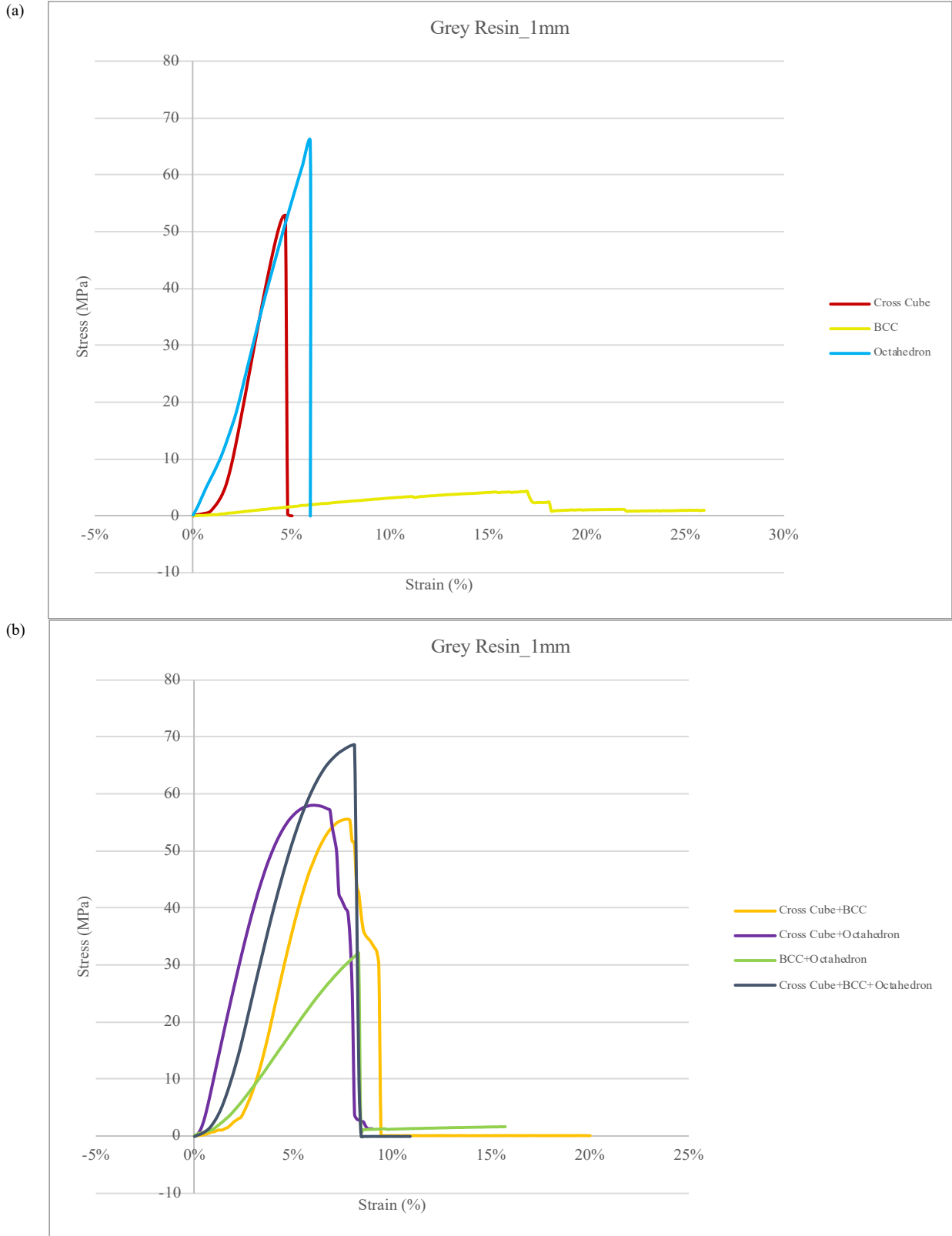


Figure 48 LS in Grey Resin with 1 mm truss diameter: (a) Pure LS, (b) Composed LS

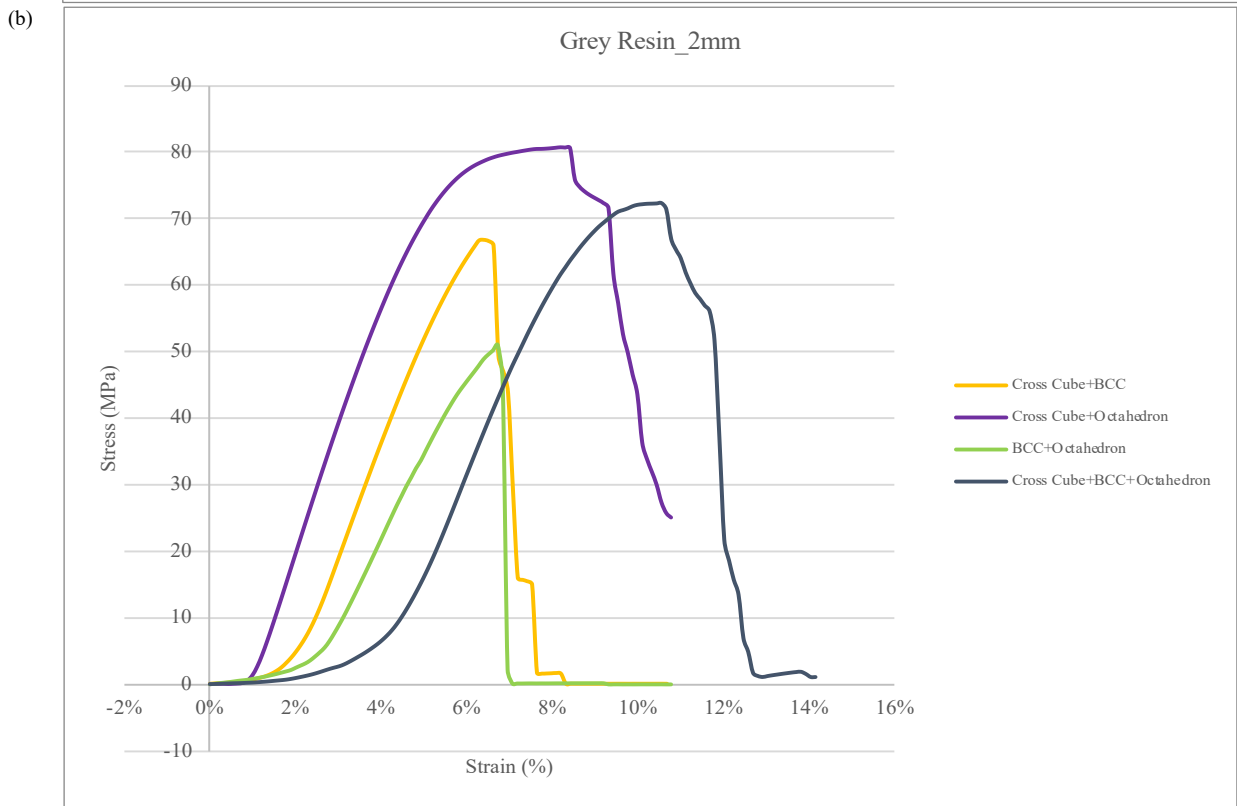
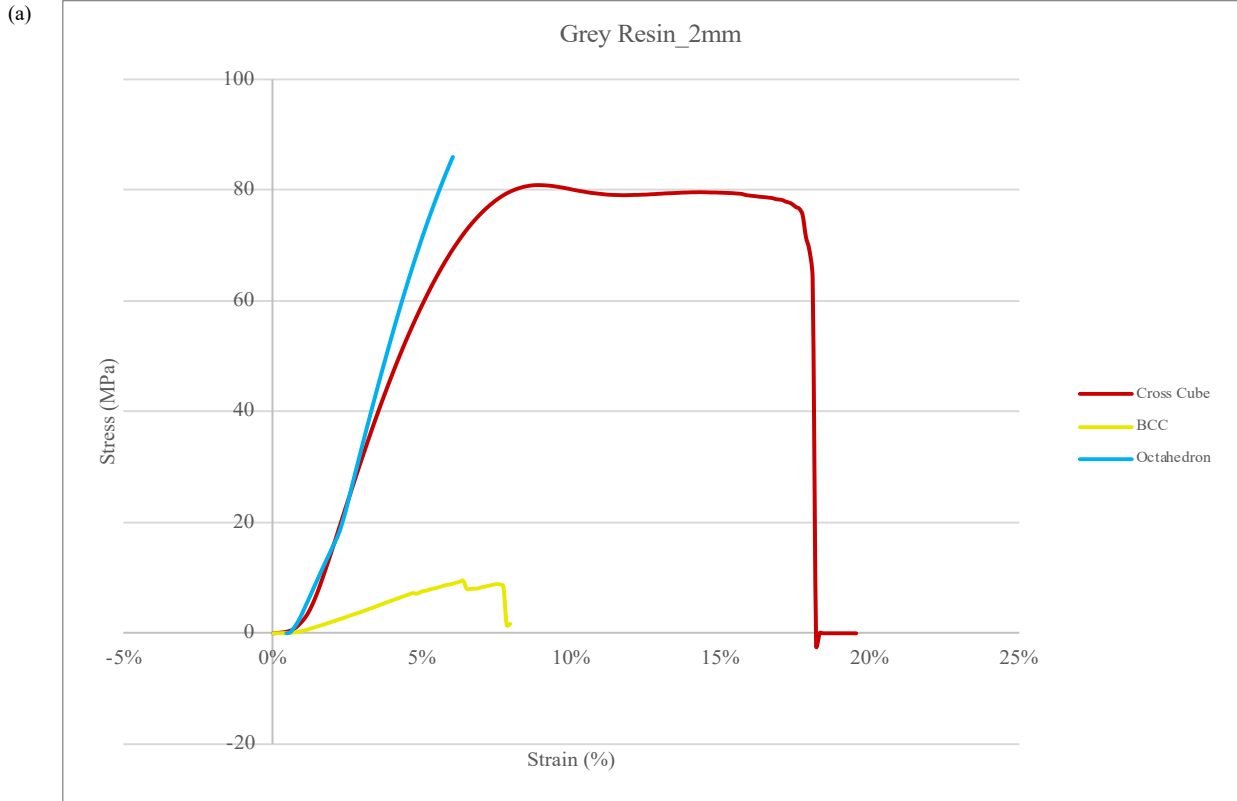


Figure 49 LS in Grey Resin with 2 mm truss diameter: (a) Pure LS, (b) Composed LS

4.1.4 Elastic 50A Resin

Table 14 presents data on the stress and strain of Elastic 50A resin LS with varying truss diameters prior to bending or yielding. This table allows for a comprehensive understanding of the stress and strain properties of Elastic 50A resin LS at different truss diameters. Additionally, the accompanying figures, Fig. 50-51, demonstrate the material's notable plastic behavior, which suggests that LS manufactured from this material possesses high ductility. From these results, the following observations can be made.

From the results, it was observed that an increase in truss diameter effectively increased both stress and strain in the Cross Cube LS and Octahedron LS structures. In specimens with 1 mm truss diameter, buckling was observed, whereas, in 2 mm truss diameter specimens, plastic and plateau behavior were observed. These findings suggest that plastic behavior in the Cross Cube and Octahedron LS structures is positively correlated with truss diameter. On the other hand, in the BCC LS, truss diameter is positively correlated with stress but negatively correlated with strain. Furthermore, the BCC LS showed a very long plateau behavior, which is indicative of better ductility. It is worth noting that in all 1 mm truss diameter pure LS specimens, serrated behavior was observed. This is due to the weak supporting capacity of the small truss diameter, leading to an unstable alternating plastic deformation phenomenon. However, this phenomenon was not observed in 2 mm truss diameter specimens, indicating that increasing truss diameter can also increase structural stability.

In composed LS structures, For the Cross Cube + BCC LS, a positive correlation between truss diameter and maximum stress and strain is observed. Additionally, specimens with a 1 mm truss diameter showed significant buckling behavior, indicating that the characteristics of Cross Cube LS are reflected in this composite structure. Similarly, the Cross Cube + Octahedron LS also exhibited a positive correlation between truss diameter and maximum stress and strain. Buckling behavior was also observed in specimens with a 1 mm truss diameter, indicating that the characteristics of both Cross Cube LS and Octahedron LS are reflected in this composite structure. The Cross Cube + BCC + Octahedron LS exhibited nearly complete plastic behavior. This means that the LS structure deformed plastically without fracturing, indicating that it can withstand larger

loads without failure. In addition, the BCC + Octahedron LS exhibited nearly complete plastic behavior.

Another interesting observation is that the serration phenomenon was reduced in composite LS specimens. This suggests that increasing the complexity of the structure can increase its stability. In summary, the results of this study provide valuable insights into the mechanical properties of LS structures and their potential applications in various fields.

Table 13 The maximum stress and strain data of LS in Elastic 50A Resin

Elastic 50A Resin			
LS type	Truss diameter	Maximum stress (MPa)	Strain
Cross Cube	1 mm	0.3	7%
	2 mm	0.5	16%
BCC	1 mm	0.15	65%
	2 mm	0.2	66%
OCT	1 mm	0.5	15%
	2 mm	0.5	20%
Cross Cube + BCC	1 mm	0.3	10%
	2 mm	0.8	30%
Cross Cube + Octahedron	1 mm	0.5	12%
	2 mm	1.3	27%
BCC + Octahedron	1 mm	0.2	10%
	2 mm	2	40%
Cross Cube + BCC + Octahedron	1 mm	0.4	15%
	2 mm	12	70%

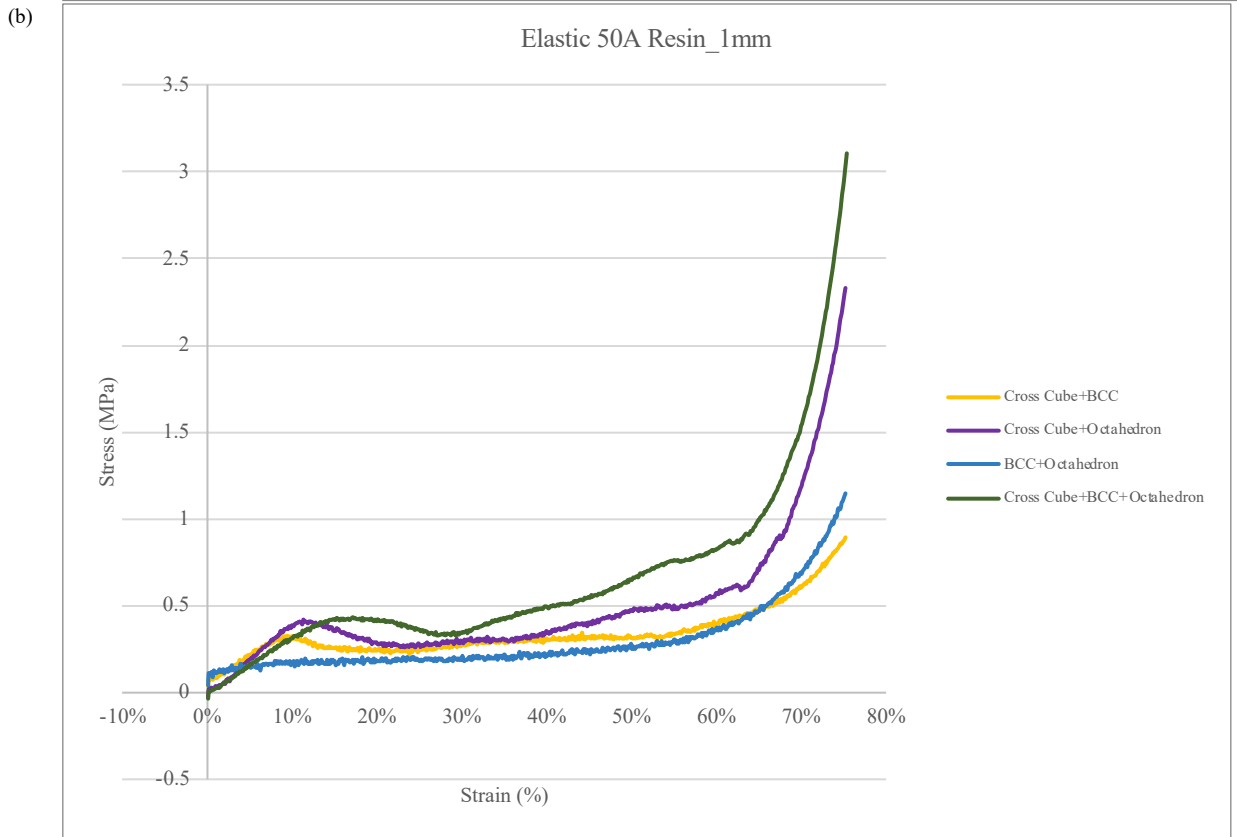
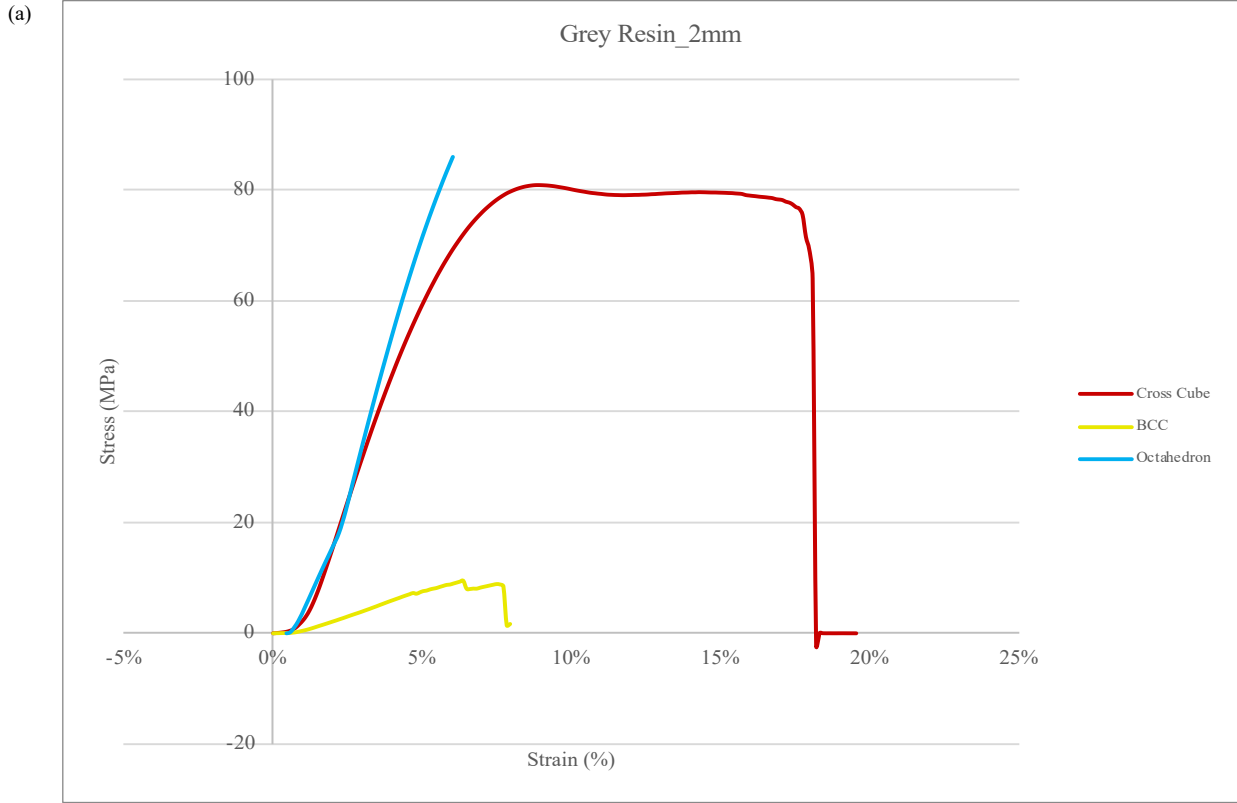
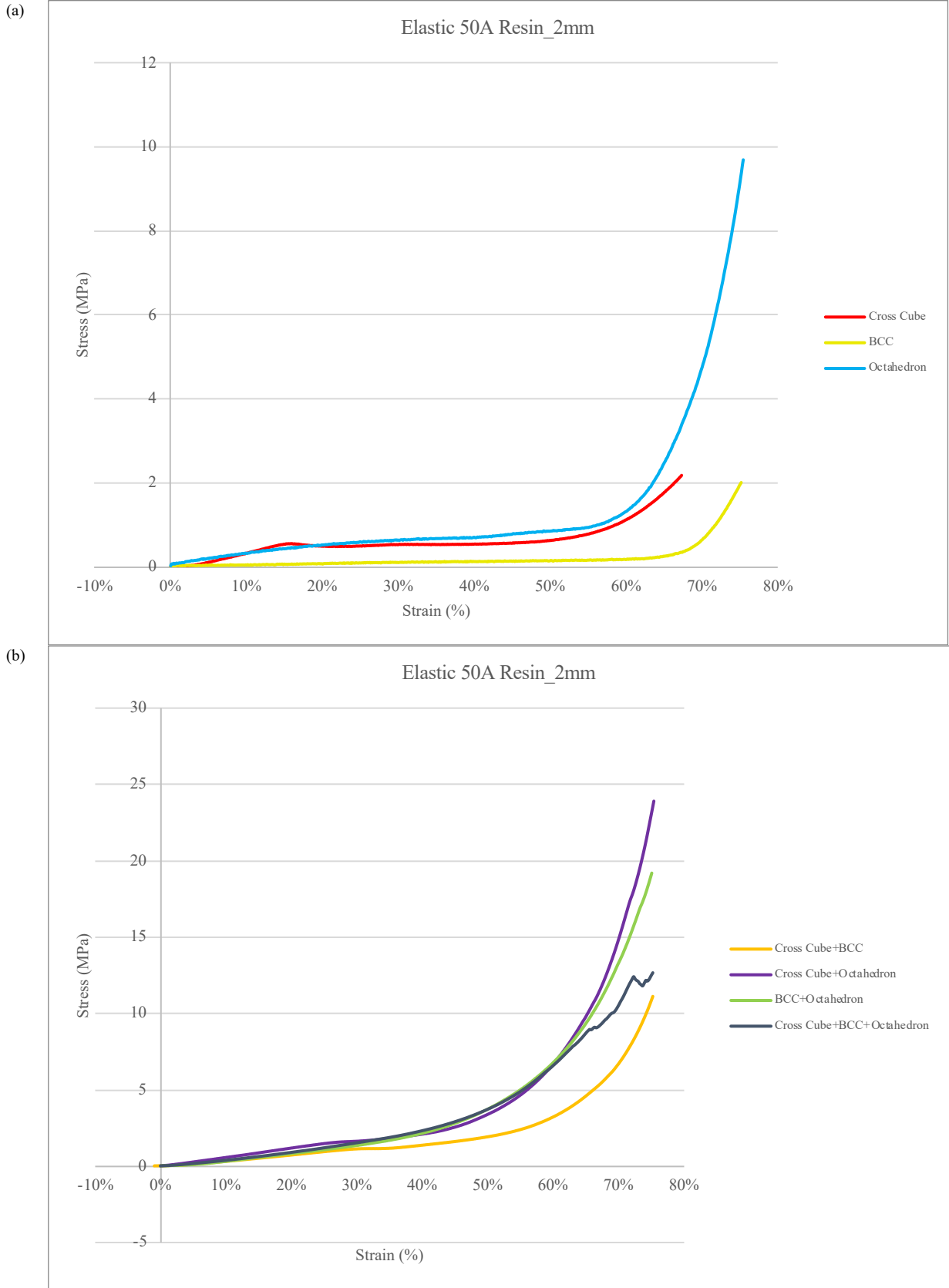


Figure 50 LS in Elastic 50A Resin with 1 mm truss diameter: (a) Pure LS, (b) Composed LS



4.2 Potential Applications of Programing Lattice Structure

LS are extensively researched for their exceptional mechanical properties, including high strength-to-weight ratio, high stiffness-to-weight ratio, and high energy absorption capacity. The development of additive manufacturing techniques such as 3D printing has made it possible to easily manufacture complex LS. However, selecting the appropriate LS, strut diameter, and material for a given application remains a challenging task. To address this challenge, this study simulated and experimented with LS made from different materials and with different strut diameters and established a basic process for selecting suitable LS, as shown in Fig. 52. The initial stage in the process is to determine the required mechanical properties of the LS for a specific application. For example, if the LS is intended for use in a load-bearing structure, high strength, and stiffness are required. On the other hand, if the LS is intended for use in energy absorption applications, high ductility, and energy absorption capabilities are required. Then, suitable materials and LS must be selected based on simulation and experimental results, taking into account the cost factor when choosing the strut diameter. Next, design and manufacturing should be carried out, and the sample's performance should be tested through experimentation. Finally, adjustments and optimizations must be made based on the testing results to ensure that the demands are met. These steps can serve as the basic process for selecting a suitable LS for a given application. The development of additive manufacturing techniques such as 3D printing has made manufacturing complex LS easy.

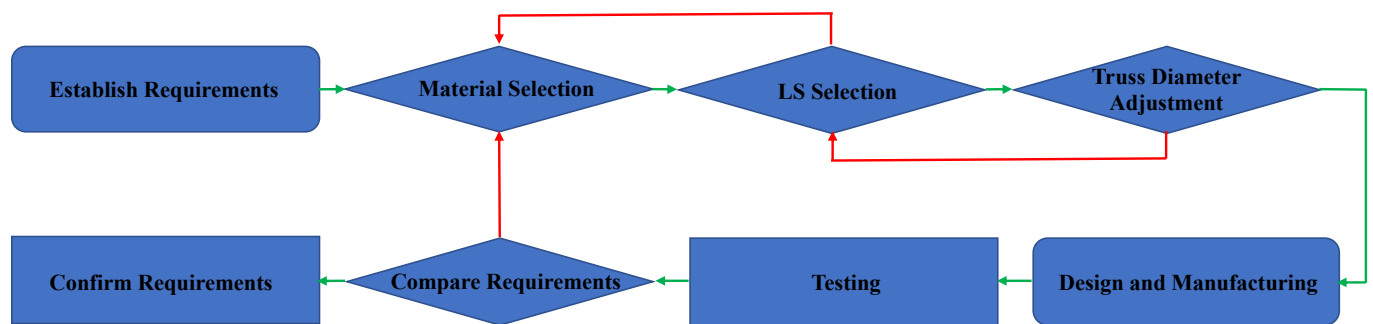


Figure 52 The process of selecting LS

5 Conclusion and Future Work

Advances in LS research and additive manufacturing techniques have led to the development of lightweight structures with exceptional mechanical properties. This study aims to further understand and develop LS by presenting experimental data on the load and extension of various LS designs with different materials and scales and by programming their mechanical behavior based on the obtained data. The study emphasizes the importance of researching the fundamental properties of LS and establishing standardization protocols to facilitate their integration into mainstream manufacturing processes. By optimizing the design of LS to achieve maximum strength while minimizing weight, this technology can be applied to various industries and applications. This research highlights the challenges and opportunities for LS in different industries and emphasizes the importance of understanding their potential applications and limitations.

However, there is still much to be explored in the field of LS research. Future work can include further research into the response of individual layers in different structural configurations under various conditions, and FEA analysis can be used to gain insight into the stress and strain experienced by LS during use. This data can then be used to program LS manufacturing, taking into account mechanical properties such as stress and strain as well as the properties of the materials used to create them.

In addition, future work can involve the use of advanced materials such as nanomaterials, composites, and 3D-printed metals to create LS with even greater mechanical properties. Research can also explore the use of LS in new applications, such as aerospace, automotive, and medical devices.

Another important area of future work is the development of a comprehensive database of LS properties and performance characteristics. This can be achieved through further research into the response of various structures under different conditions, analyzing individual layer responses through finite element analysis (FEA), and programming using data to consider the mechanical properties of LS, such as stress and strain, as well as the characteristics of the materials used to manufacture them. The analysis results can then be used to reverse engineer LS designs, informing LS design based on their response to different conditions. This approach can lead to the creation

of more efficient and effective LS that can better meet the needs of various industries. By building such a database, designers and engineers can quickly and accurately select LS for specific applications and optimize their design for maximum performance.

In conclusion, while significant progress has been made in the research and development of LS, there is still much to be done. By continuing to explore new materials, applications, and design approaches, we can unlock even greater potential in the field of LS and pave the way for a new generation of lightweight, high-performance structures.

6 Reference

- [1] B. Bhaskaran, “Additive Manufacturing: A Review DESIGN AND DEVELOPMENT OF POWER GENERATION FROM SPEED PUMP View project FABRICATION OF MECHANISED CONVEYOR USING FOUR BAR MECHANISM View project.” [Online]. Available: <https://www.researchgate.net/publication/361698547>
- [2] G. M. Shashi, M. Ashiqur, R. Laskar, H. Biswas, A. Rahman Laskar, and A. K. Saha, “A Brief Review of Additive Manufacturing with Applications Perovskite Solar Cell View project Indium Tin Oxide View project A Brief Review of Additive Manufacturing with Applications,” *BIAM Foundation*, vol. 29, 2017, doi: 10.6084/m9.figshare.12520667.
- [3] H. Alzyod and P. Ficzero, “Potential applications of additive manufacturing technologies in the vehicle industry,” *Design of Machines and Structures*, vol. 11, no. 2, pp. 5–13, 2021, doi: 10.32972/dms.2021.009.
- [4] C. Pan, Y. Han, and J. Lu, “Design and optimization of lattice structures: A review,” *Applied Sciences (Switzerland)*, vol. 10, no. 18. MDPI AG, pp. 1–36, Sep. 02, 2020. doi: 10.3390/APP10186374.
- [5] A. Seharing, A. H. Azman, and S. Abdullah, “A review on integration of lightweight gradient lattice structures in additive manufacturing parts,” *Advances in Mechanical Engineering*, vol. 12, no. 6. SAGE Publications Inc., Jun. 01, 2020. doi: 10.1177/1687814020916951.
- [6] B. K. Nagesha, V. Dhinakaran, M. Varsha Shree, K. P. Manoj Kumar, D. Chalawadi, and T. Sathish, “Review on characterization and impacts of the lattice structure in additive manufacturing,” in *Materials Today: Proceedings*, Elsevier Ltd, 2020, pp. 916–919. doi: 10.1016/j.matpr.2019.08.158.
- [7] O. Al-Ketan, R. K. Abu Al-Rub, and R. Rowshan, “The effect of architecture on the mechanical properties of cellular structures based on the IWP minimal surface,” *J Mater Res*, vol. 33, no. 3, pp. 343–359, Feb. 2018, doi: 10.1557/jmr.2018.1.
- [8] K. Raž, Z. Chval, and R. Santos, “Development of a Computational Model of Lattice Structure,” *MATEC Web of Conferences*, vol. 357, p. 02012, 2022, doi: 10.1051/mateconf/202235702012.
- [9] W. Tao and M. C. Leu, “Design of lattice structure for additive manufacturing,” in *International Symposium on Flexible Automation, ISFA 2016*, Institute of Electrical and Electronics Engineers Inc., Dec. 2016, pp. 325–332. doi: 10.1109/ISFA.2016.7790182.
- [10] K. Sathish *et al.*, “A Comparative Study on Subtractive Manufacturing and Additive Manufacturing,” *Advances in Materials Science and Engineering*, vol. 2022. Hindawi Limited, 2022. doi: 10.1155/2022/6892641.
- [11] J. Steenhuis, “Competition in additive manufacturing.” [Online]. Available: <https://www.researchgate.net/publication/365775232>
- [12] A. Abusabir, M. A. Khan, M. Asif, and K. A. Khan, “Effect of Architected Structural Members on the Viscoelastic Response of 3D Printed Simple Cubic Lattice Structures,” *Polymers (Basel)*, vol. 14, no. 3, Feb. 2022, doi: 10.3390/polym14030618.
- [13] H. Chen, W. Cao, H. Liu, W. Liu, and Z. Zhou, “Mechanical properties of cross-shaped built-in lattice circular CFST short columns after fire,” *J Constr Steel Res*, vol. 203, p. 107841, Apr. 2023, doi: 10.1016/j.jcsr.2023.107841.
- [14] J. Ye, Y. Zhang, Y. Li, and Q. Wang, “Blast shock wave attenuation in square cross-sectional truss based meso-scale lattice architectures,” *Structures*, vol. 44, pp. 755–765, Oct. 2022, doi: 10.1016/j.istruc.2022.08.020.

- [15] Y. Huang, Y. Xue, X. Wang, and F. Han, “Effect of cross sectional shape of struts on the mechanical properties of aluminum based pyramidal lattice structures,” *Mater Lett*, vol. 202, pp. 55–58, Sep. 2017, doi: 10.1016/j.matlet.2017.05.073.
- [16] Y. Liu *et al.*, “Mechanical performance of a node reinforced body-centred cubic lattice structure manufactured via selective laser melting,” *Scr Mater*, vol. 189, pp. 95–100, Dec. 2020, doi: 10.1016/j.scriptamat.2020.08.015.
- [17] Ö. POYRAZ, B. E. BİLİCİ, and Ş. C. GEDİK, “Numerical Investigations and Benchmarking of The Physical and Elastic Properties of 316L Cubic Lattice Structures Fabricated by Selective Laser Melting,” *International Journal of 3D Printing Technologies and Digital Industry*, Feb. 2022, doi: 10.46519/ij3dptdi.1034252.
- [18] K. M. Park, K. S. Min, and Y. S. Roh, “Design Optimization of Lattice Structures under Compression: Study of Unit Cell Types and Cell Arrangements,” *Materials*, vol. 15, no. 1, Jan. 2022, doi: 10.3390/ma15010097.
- [19] J. Sun, Y. Yang, and D. Wang, “Mechanical properties of Ti-6Al-4V octahedral porous material unit formed by selective laser melting,” *Advances in Mechanical Engineering*, vol. 2012, 2012, doi: 10.1155/2012/427386.
- [20] R. Hedayati, M. Sadighi, M. Mohammadi-Aghdam, and A. A. Zadpoor, “Analytical relationships for the mechanical properties of additively manufactured porous biomaterials based on octahedral unit cells,” *Appl Math Model*, vol. 46, pp. 408–422, Jun. 2017, doi: 10.1016/j.apm.2017.01.076.
- [21] E. Castro-Aguirre, F. Iñiguez-Franco, H. Samsudin, X. Fang, and R. Auras, “Poly(lactic acid)—Mass production, processing, industrial applications, and end of life,” *Advanced Drug Delivery Reviews*, vol. 107. Elsevier B.V., pp. 333–366, Dec. 15, 2016. doi: 10.1016/j.addr.2016.03.010.
- [22] S. Farah, D. G. Anderson, and R. Langer, “Physical and mechanical properties of PLA, and their functions in widespread applications — A comprehensive review,” *Advanced Drug Delivery Reviews*, vol. 107. Elsevier B.V., pp. 367–392, Dec. 15, 2016. doi: 10.1016/j.addr.2016.06.012.
- [23] Z. Li, D. Feng, B. Li, D. Xie, and Y. Mei, “FDM printed MXene/MnFe₂O₄/MWCNTs reinforced TPU composites with 3D Voronoi structure for sensor and electromagnetic shielding applications,” *Compos Sci Technol*, vol. 231, Jan. 2023, doi: 10.1016/j.compscitech.2022.109803.
- [24] B. Wittbrodt and J. M. Pearce, “The effects of PLA color on material properties of 3-D printed components,” *Addit Manuf*, vol. 8, pp. 110–116, Oct. 2015, doi: 10.1016/j.addma.2015.09.006.
- [25] M. Lay, N. L. N. Thajudin, Z. A. A. Hamid, A. Rusli, M. K. Abdullah, and R. K. Shuib, “Comparison of physical and mechanical properties of PLA, ABS and nylon 6 fabricated using fused deposition modeling and injection molding,” *Compos B Eng*, vol. 176, Nov. 2019, doi: 10.1016/j.compositesb.2019.107341.
- [26] A. Żur, P. Żur, P. Michalski, and A. Baier, “Preliminary Study on Mechanical Aspects of 3D-Printed PLA-TPU Composites,” *Materials*, vol. 15, no. 7, Apr. 2022, doi: 10.3390/ma15072364.
- [27] M. A. S. Anwer and H. E. Naguib, “Study on the morphological, dynamic mechanical and thermal properties of PLA carbon nanofibre composites,” *Compos B Eng*, vol. 91, pp. 631–639, Apr. 2016, doi: 10.1016/j.compositesb.2016.01.039.

- [28] W. Ye, H. Dou, Y. Cheng, and D. Zhang, “Self-sensing properties of 3D printed continuous carbon fiber-reinforced PLA/TPU honeycomb structures during cyclic compression,” *Mater Lett*, vol. 317, Jun. 2022, doi: 10.1016/j.matlet.2022.132077.
- [29] B. Li, S. Zhang, L. Zhang, Y. Gao, and F. Xuan, “Strain sensing behavior of FDM 3D printed carbon black filled TPU with periodic configurations and flexible substrates,” *J Manuf Process*, vol. 74, pp. 283–295, Feb. 2022, doi: 10.1016/j.jmapro.2021.12.020.
- [30] L. Cao, J. Xiao, J. K. Kim, and X. Zhang, “Effect of post-process treatments on mechanical properties and surface characteristics of 3D printed short glass fiber reinforced PLA/TPU using the FDM process,” *CIRP J Manuf Sci Technol*, vol. 41, pp. 135–143, Apr. 2023, doi: 10.1016/j.cirpj.2022.12.008.
- [31] Z. Chen, J. Li, C. Liu, Y. Liu, J. Zhu, and C. Lao, “Preparation of high solid loading and low viscosity ceramic slurries for photopolymerization-based 3D printing,” *Ceram Int*, vol. 45, no. 9, pp. 11549–11557, Jun. 2019, doi: 10.1016/j.ceramint.2019.03.024.
- [32] D. C. Aduba *et al.*, “Vat photopolymerization 3D printing of acid-cleavable PEG-methacrylate networks for biomaterial applications,” *Mater Today Commun*, vol. 19, pp. 204–211, Jun. 2019, doi: 10.1016/j.mtcomm.2019.01.003.
- [33] T. Schlotthauer, D. Nolan, and P. Middendorf, “Influence of short carbon and glass fibers on the curing behavior and accuracy of photopolymers used in stereolithography,” *Addit Manuf*, vol. 42, Jun. 2021, doi: 10.1016/j.addma.2021.102005.
- [34] M. A. Muflikhun and D. A. Sentanu, “Characteristics and performance of carabiner remodeling using 3D printing with graded filler and different orientation methods,” *Eng Fail Anal*, vol. 130, Dec. 2021, doi: 10.1016/j.engfailanal.2021.105795.
- [35] Diptanshu, G. Miao, and C. Ma, “Vat photopolymerization 3D printing of ceramics: Effects of fine powder,” *Manuf Lett*, vol. 21, pp. 20–23, Aug. 2019, doi: 10.1016/j.mfglet.2019.07.001.
- [36] Y. F. Zhong *et al.*, “Terahertz data analytics-based bonding interface damage characterization in a multilayer structural composites under cyclic loading,” *Polym Test*, vol. 116, Dec. 2022, doi: 10.1016/j.polymertesting.2022.107785.
- [37] “Fusion 360 | 3D CAD, CAM, CAE, & PCB Cloud-Based Software | Autodesk.” <https://www.autodesk.com/products/fusion-360/overview?term=1-YEAR&tab=subscription> (accessed Feb. 15, 2023).
- [38] “PLA Filament | Dremel.” <https://www.dremel.com/us/en/digilab/support/3d45-series-3d-printer/filament/pla-filament> (accessed Mar. 13, 2023).
- [39] “Overture 3D Printing Filament.” <https://overture3d.com/> (accessed Mar. 13, 2023).
- [40] “Resin Library and 3D Printing Materials.” <https://formlabs.com/materials/> (accessed Mar. 13, 2023).
- [41] H. Lee, R. I. Eom, and Y. Lee, “Evaluation of the mechanical properties of porous thermoplastic polyurethane obtained by 3D printing for protective gear,” *Advances in Materials Science and Engineering*, vol. 2019, 2019, doi: 10.1155/2019/5838361.
- [42] M. Péron, V. Sobotka, N. Boyard, S. Le Corre, and M. Péron, “Bulk modulus evolution of thermoset resins during crosslinking: Is a direct and accurate measurement possible? Bulk modulus evolution of thermoset resins during crosslinking: Is a direct and accurate measurement possible? Bulk modulus evolution of thermoset resins during crosslinking: Is a direct and accurate measurement possible?,” *J Compos Mater*, vol. 51, no. 4, pp. 463–477, 2016, doi: 10.1177/0021998316647119i.

- [43] P. D. Iedema, V. Schamböck, H. Boonen, J. Koskamp, S. Schellekens, and R. Willemse, “Photocuring of di-acrylate,” *Chem Eng Sci*, vol. 176, pp. 491–502, Feb. 2018, doi: 10.1016/j.ces.2017.11.009.
- [44] F. Mustata, N. Tudorachi, and I. Bicu, “Thermosetting resins obtained via sequential photo and thermal crosslinking of epoxy resins. Curing kinetics, thermal properties and morphology,” *Compos B Eng*, vol. 55, pp. 470–478, 2013, doi: 10.1016/j.compositesb.2013.07.023.
- [45] Z. Yang, *Material Modeling in Finite Element Analysis*. CRC Press, 2019. doi: 10.1201/9780367353216.



236K-0XUN-YC00

MIAMI UNIVERSITY

*The President and Trustees of Miami University upon approval
of the Faculty have conferred upon*

Qi-Sheng Liao

the degree of

Master of Science

*together with all the rights, privileges and honors appertaining thereto
in recognition of the satisfactory fulfillment of the requirements of this degree.*

*In Witness Whereof, we have hereunto subscribed our names and have caused the seal of the
University to be affixed at Oxford, Ohio, August eleventh, two thousand and twenty-three.*



Mary Schell
Chair of the Board of Trustees

Gregory Rantfors
President of the University

Michael W. Crowder
Dean, Graduate School